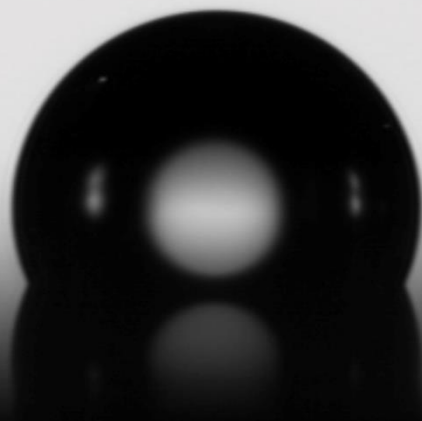# Characterization and Processing of Elastomers for Organ-on-Chip Applications

J.D. Schoonhoven

Characterization and Processing of Elastomers for Organ-on-Chip Applications

By

J.D. Schoonhoven

in fulfilment of the requirements for the degree of

Master of Science
in Biomedical Engineering

at the Delft University of Technology,

to be defended publicly on Wednesday April 6, 2022 at 13:00 PM.

Supervisors:	Dr. M. Mastrangeli
	Dr. N. Gaio
	M. Dostanic
Thesis committee:	Dr. M. Mastrangeli
	M. Mirzaali Mazandarani
	Prof. dr. R. Dekker

Contents

Abstract

The current standard for organ-on-chip substrate materials is polydimethylsiloxane (PDMS). PDMS has many beneficial properties such as biocompatibility, transparency, elasticity, and easy prototyping. The main disadvantages of PDMS are its hydrophobicity (reducing cell attachment and cell proliferation), quick hydrophobic recovery (within a few hours) after surface modification, and unselective absorption of small molecules, altering drug concentration during testing or causing cross-contamination between channels. To overcome these shortcomings, an alternative material lacking the disadvantages and retaining the advantages of PDMS is needed in the field. Ostemer 324, Ostemer 220 and a variation of PDMS (PDMS+) were characterized to determine whether they would be a suitable alternative to PDMS as substrate material. The materials were compared to PDMS and characterized for spin-coating and curing on silicon wafers, moulding, etching, surface wettability before and after surface modification (plasma treatment), stiffness, optical transparency, biocompatibility and absorption of small molecules. The results of this work show that Ostemer 324 appears to be a promising alternative, with similar characteristics to PDMS. The main advantage is its hydrophilic surface, which becomes even more hydrophilic after plasma treatment, and slow hydrophobic recovery rate. However, its curing time is longer, the material is stiffer and not easy to mould. Ostemer 220 shows very poor adhesion on Teflon coated silicon wafers, is hard to mould, and shows inconsistent results during biocompatibility testing. PDMS+ is very similar to PDMS, and improves upon the latter in terms of surface wettability after surface modification, hydrophobic recovery and small molecule absorption.

1 Introduction

1.1 Origin and Features of Organs-on-Chip

1.1.1. Drug Development

For development of new drugs, the pharmaceutical industry uses several models to test the effectiveness, toxicity and working principles of drugs on cells. Drugs discovery and development starts in the lab (pre-clinical screening stage) for the initial effectiveness and toxicity tests. After that, drugs are tested on actual patients (clinical trials stage) [1]. A complete indication of the drug development stages is provided in Figure 1. An ideal model during the pre-clinical trials should mimic human physiology and disease pathology including its proper mechanisms of action [2], [3].

Figure 1: Stages of the drug development process. Discovery and development: identification and gathering information of potential drug compounds. Preclinical research: testing in the lab on for example animals for initial effectiveness and toxicity. Clinical research: testing of drugs on people for effectiveness and safety. Review: review of the research data by a body such as the food and drug administration (FDA). Post-market safety monitoring to keep confirming drug safety once they are on the market [1].

Two-dimensional (2D) cell culturing is used as a method to test cell function during pre-clinical trials. However, 2D cell culture models rely on cells cultured on flat rigid substrates under static conditions. This is not an accurate representation of the three dimensional cell environment, as these cells are only affected by one plane and lack influence of mechanical stimulation [4].

Another pre-clinical testing method makes use of animals. However, the results of animal models have been shown to be inaccurate due to physiological differences between humans and animals [5]. Results obtained regarding drug efficacy in animal and other currently existing 2D models do not always translate to humans in the subsequent human clinical trials, thereby limiting drug development [2]. Therefore, improved, more accurate drug testing models are needed that better mimic human physiology in a 3D environment.

1.1.2 Organ-on-Chip

The challenges mentioned above are addressed by developing 3D *in vitro* models including human cells. Microfluidic systems can be employed to actively supply drugs and nutrients to the 3D tissues by mimicking a blood vessel. These microchannels help to simulate the mechanical and physiological environment of vessels present in an organ tissue [6].

The combination of a 3D tissue and a microfluidic device is often referred to as an organ-on-chip (OoC). The OoC devices are used to test tissue function, cell behaviour, disease mechanisms, drug efficacy and toxicity [3], [7], [8]. OoC models have a wide field of application, as mentioned for drugs but also for food, cosmetics and the chemical industry [7]. By testing drugs for efficacy before the clinical trial, OoC technology has the potential to improve safety for the clinical trial itself and can cut cost, by preventing investment in clinical trials for ineffective or unsafe drugs [9].

OoCs are commonly used in combination with human-induced pluripotent stem cells (hiPSCs), from which different cell types can be derived. iPSCs can for example develop into immune cells or lung cells [3]. The chip affects properties of the microenvironment in which the cells are cultured, altering the stiffness, pressure, pH, nutrients, toxins and microfluidic flow [10].

Several types of OoC models are being developed, such as for brain, kidney, liver, lung, heart, intestine, blood-brain barrier and immune system [10], [11]. Previous work has also focused on developing complex multi-organ systems in OoC such as lymph node models, endothelial vascular models, breast cancer, kidney, and cancer development models [9], [12]. Moreover, OoCs have been used to develop disease models. Examples are neurological diseases such as Alzheimer, Parkinson, motor neuron disease but also rheumatoid arthritis, diabetes, heart failure and infectious diseases [3]. The current thesis will focus on a heart tissue model.

1.1.3 Heart-on-Chip

One of the biggest problems in drug development is cardiac toxicity of drugs, even when developed for treating non-heart related diseases, which results in for example cardiac arrhythmias [5], [13], [14]. Moreover, many people suffer from heart related diseases, and to better understand these and develop treatments, accurate models of the workings of heart tissue are necessary.

The contracting part of the heart is called the myocardium, and consists of cardiomyocytes. The cardiomyocytes are arranged in a parallel fashion, composing the so-called myocardial fibres. Other, specialized, cardiomyocytes are for example pacemaker cells and Purkinje fibres, which are the conductors of the electrical signals through the heart. Approximately 50-60% of the heart cells are cardiac fibroblast, which form the extracellular matrix (ECM) of the heart [13].

The heart is one of the organs that can be modelled with OoC technology. This kind of OoC can be called a heart-on-chip (HoC). A HoC model should at least include the cardiomyocytes, the important functional cells of the heart, and environmental factors of these cells. When allowing cardiac cells to self-assemble under the influence of environmental factors such as ECM-proteins, so-called engineered heart tissue (EHT) is formed. The assembled cardiac cells form beating cardiac muscle strands around flexible anchoring points; for example two elastic pillars [15]. Various HoC platforms have been designed that support the formation of EHT.

A HoC model has the potential to solve the problem of cardiomyocyte maturation (see next section) by developing adult cardiomyocytes in a three dimensional structure. One example of a three dimensional structure that provides maturation is the model by Eder *et al.* [14]. The model is formed by seeding the cells in an ECM-like gel. The substrate contains two flexible pillars. After 10 days the tissue starts to beat rhythmically and the contractile forces can be measured by measuring pillar deflection [14]. Unlike conventional 2D models, this particular 3D model allows for optical measurement of force, frequency, contraction and relaxation of the beating cardiac cells. Measurements can also be performed

Figure 2: A miniaturized heart on chip platform. PDMS in blue with tissue in brown assembled around two pillars. The platform fits in the well of standard 96-well culture plates. Modified from [15].

by direct integration of for example capacitive sensors or strain gauges into the substrate that can measure non-invasively [13], [14]. Dostanic *et al.* created a similar model on a miniature scale (Figure 2). This miniature platform only requires 50.000 cells [15], compared to 1 to 2 million cells for the larger model [14]. The model by Dostanic *et al.* will be used as reference in this thesis to test and compare different substrate materials.
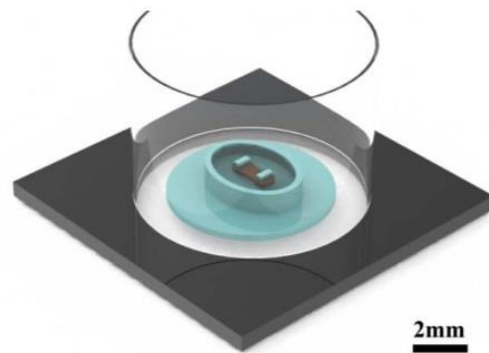
1.1.4   Mechanotransduction

Properly mimicking the *in vivo* microenvironment of cells in an OoC model is a critical aspect partly because of the concept of mechanotransduction, which plays a critical role in cell development and cell behaviour. Mechanotransduction is defined as all the molecular processes that contribute to transform physical cues into a biological response [16], [17]. This process is present in both the human body and in an engineered environment like an OoC. It starts by activation of proteins on the cell surface that are able to sense mechanical signals. These sensing proteins include integrins, stretch-activated ion channels and g-protein coupled receptors. The activated proteins are the start of a signalling cascade towards the nucleus of the affected cell [16], [18]. The signal that arrives in the nucleus of the cell activates different genes by which the cell responds to the stimulus. The cell thereby alters its phenotype by adjusting features such as its stiffness, alignment or protein expression in response to its physical environment.

A clear example of the effects of mechanotransduction is in seen in the maturation of cardiomyocytes derived from hiPSCs. Cultured hiPSC-derived cardiomyocytes in HoC models lack cell maturation in comparison to *in vivo* adult human cardiomyocytes [5], [19]. These underdeveloped cardiomyocytes are smaller and have less structural organization in terms of cell alignment and protein expression than matured cardiomyocytes. Improvement of the HoC model to improve cardiomyocyte maturation is important as underdevelopment of the cells results in a different electrical potential, lower cell contractile forces and in the end a different cell response to drugs [14]. Cardiomyocyte maturation can be improved by passive stretching [20], electrical cyclic stimulation (pacing), and co-culturing with other cardiac cells [21], [22]. Finally, a 3D structure and substrate material stiffness can affect maturation of the cells, therefore material selection for HoC is important.

1.2   Substrate Material

The effects of mechanotransduction are modulated by properties of the substrate material, for example the material stiffness. Currently, the majority of OoCs are made of polydimethylsiloxane (PDMS), a transparent, silicone-based elastomer [23]. PDMS has been used since the 1990's and is still the most used polymer in prototyping of microfluidic and OoC devices [24]. Many properties of PDMS are beneficial for the field of OoC, such as its biocompatibility, optical transparency, gas (oxygen, carbon dioxide) permeability, and flexibility. PDMS is one of the substrate materials that has the right stiffness properties for the aforementioned mechanotransduction and cardiomyocyte development. Tissue stiffness can range from 1kPa to 1 GPa, where heart tissue falls within a range of about 50 kPa. The stiffness of PDMS ranges from 1 to 3 MPa [25], [26]. However, the material has a few disadvantages. Disadvantages of PDMS are its hydrophobicity and resulting unselective absorption of molecules (including drugs), its incompatibility with organic solvents, and its limited compatibility with large-scale production methods such as injection moulding and hot embossing [7]. Due to these disadvantages, there is a need for an alternative material to be used for OoC substrates.

1.1.2   Alternative Material Selection

When looking for a suitable alternative, several material properties need to be taken into account. These properties include low bulk cost, easy production, a modifiable surface, gas permeability, optical transparency in at least the visible spectrum, appropriate stiffness, easy bonding, ease of processing, achieving target feature size, and biocompatibility [27]–[29]. Most importantly, to overcome the current disadvantages of PDMS, an alternative material should be compatible, or at least potentially compatible with mass production, chemically resistant, have low hydrophobicity, long surface hydrophobic recovery rate, and have low absorption rates of small molecules.

An extensive literature review (see Appendix A) discusses alternative material options, based on these aforementioned properties. Table 1 summarizes the properties of the most promising materials resulting from this literature review and compares them to PDMS. The table indicates, for example, that all of the selected materials show a reduced absorption of small molecules compared to PDMS; the wettability is also improved for most materials. Particularly, cyclic olefin co-polymer (COC) shows many beneficial properties. However, the material is only available as solid pellets and therefore only suitable for large-scale fabrication techniques such as injection moulding.

Ostemer is a very promising material as PDMS replacement. It is a UV curable, thermoset, off-stoichiometric thiol-ene polymer [30], [31]. Ostemer is produced by combining 2 monomers, one with thiol active groups and the other with allyl functional groups [29]. When the thiol and allyl groups are balanced, the material is stoichiometric [29]. In an off-stoichiometric mixture, one of the monomers is in excess, with functional groups of either the allyl or thiol remaining.

Ostemer is reportedly biocompatible, has good binding properties, is transparent and the stiffness is tuneable by altering the mixing ratio of its components. Most advantageous is that it has lower absorption of molecules and is more hydrophilic compared to PDMS [29], [32]–[36]. Disadvantages might be its reduced gas permeability, oxygen scavenging properties and increased cost [29]. Scavenging consumes the oxygen and reduces the oxygen concentration, while a reduced gas permeability would only block oxygen molecules. Reduced gas permeability could cause a problem if cells in an OoC platform are provided with oxygen trough material membranes. Specifically, Ostemer 324 and Ostemer 220 (Mercene labs) are interesting. According to datasheets, Ostemer 324 has a better chemical resistance than Ostemer 220, and is more stiff compared to Ostemer 220. The stiffness according to literature ranges from 10 to 30 MPa, which could potentially be suitable for HoC applications [37], [38]. Both Ostemers are commercially available.

Table 1: Material properties of selected alternatives to PDMS. Advantageous and disadvantageous material properties of PDMS in the first column. The other materials have their material properties indicated as better (+), equal (~) or worse (-) than PDMS (see legend). PFPE: Perfluoropolyether, COC: cyclic olefin co-polymer, LSR: liquid silicone rubber, SEBS: styrene ethylene/butylene styrene block copolymer.

	PDMS	PFPE	COC	LSR	SEBS	Flexdym	Versaflex CL30	Ostemer (322)
Production	~	+	~	+	+	+	~	+
Absorption	-	+	+	+	+	+	+	+
Wettability	-	-	+	-	+	+	+	+
Casting	+	+	+	+	+	+	-	+
Transparency	+	+	+	+	+	+	+	+
Chemical compatibility	-	+	+	+	+	?	?	~
Adhesion	+	+	+	+	?	?	?	+
Min. feature size	+	+	+	+	+	+	+	+
Stiffness	+	+	~	+	+	+	+	~
Gas permeability	+	+	+	?	-	-	-	-
Cost	+	-	+	+	+	+	+	-

+	Advantage	+	As good as or better than PDMS
-	Disadvantage	-	Worse than PDMS
~	Depending on application	~	Depending on application
		?	No information available / unknown

Four materials were selected based on the literature review to try to obtain and test them: Perfluoropolyether (PFPE, Fluorolink AD1700, Solvay), Flexdym (FlexaSpin, Eden tech), Ostemer 324 and Ostemer 220 (Mercene labs). Unfortunately, PFPE and Flexaspin turned out not to be available in sample quantities (minimum 100kg) and not commercially available respectively, and are therefore not included in this thesis. PDMS (Sylgard-184) was used as the control.

Moreover, during this project, we were provided with an additional and non-commercially available polymer designed by Philips Research, department Remote Patient Management & Chronic Care. The compound is a modified PDMS. The added compound changes the surface functional groups, meant to improve cell adhesion and proliferation. Tests in this thesis were conducted to assess whether the properties of PDMS changed or remained the same under the influence of the addition. In the remainder of the thesis this material will be referred to as PDMS+.

1.2   Thesis Goal and Outline

This master project will focus on testing and validating the material properties of Ostemer 324, Ostemer 220 and PDMS+ in the lab to confirm whether these materials are a suitable PDMS replacement for OoC applications and in particular HoC. PDMS will be used as a control. Tests with selected fabrication processes will provide clarity on the ease and possibilities of fabrication of OoC devices with these materials. Stiffness and wettability measurements indicate the effect of the material on cell proliferation. Optical transparency measurements will indicate compatibility with optical imaging techniques. Finally, biocompatibility in terms of toxicity and cell proliferation and absorption of small molecules is tested to form a complete picture of the material characteristics based on which a possible alternative material can be selected.

First, Chapter 2 will describe the testing of the selected materials for compatibility with fabrication processes for OoC, such as, spin-coating, moulding, photolithography and etching. We also tried to use injection moulding with PDMS.

Then, Chapter 3 will describe the mechanical characterization of the materials based on contact angle measurement to determine the hydrophobicity, uniaxial tensile test to determine the Young's modulus, and transmittance measurements to determine optical transparency.

Chapter 4 describes the biological characterization of the materials. Biocompatibility will be determined in terms of toxicity, cell adhesion and cell proliferation. And finally, by a newly designed method incubating Nile Red dye with the material, the absorption of the materials will be analysed.

2 Processing of Elastomers

This chapter will introduce fabrication methods currently available for processing polymers on silicon wafers. Moreover, it presents my applications of these methods to the selected alternative materials (PDMS, Ostemer 324, Ostemer 220 and PDMS+) in the clean room 100 of the Else Kooi Laboratory located at Delft University of Technology. Industrial injection moulding was also considered for this work and preliminary results are included in Appendix B.

2.1   Microfabrication

The selected fabrication methods of spin-coating, curing and moulding are based on the fabrication process of the EHT platform of Dostanic *et al.*, as described in Section 1.1.3. The elastomer platform consists of an elliptic well with two pillars and is fabricated by soft lithography. First, a mould is made by deep reactive ion etching of a silicon wafer. Before moulding, the mould is covered with a non-adhesive layer. PDMS is spin coated on top of the mould. Degassing under vacuum is performed to remove all trapped air from the mould. After curing the material, the polymer can be peeled off from the mould, revealing the moulded EHT platform. To check whether the EHT platform can be fabricated with the alternative materials, the materials will be spin coated and cured (Section 2.1.1) before performing the actual moulding process (Section 2.1.2).

2.1.1   Spin-Coating and Curing

The selected materials consist of multiple liquid components that are mixed together, spin coated on a coated (Figure 3a) silicon wafer and then cured (Figure 3b). Cross-linking of the resulting polymers is performed by UV curing, thermal curing or both depending on the material. Afterwards, if the substrate is coated with a non-adhesive layer, the patterned elastomer can be peeled from the mould, as illustrated in Figure 3c [7]. This method is referred to as casting when the substrate is patterned [23], [39], [40].
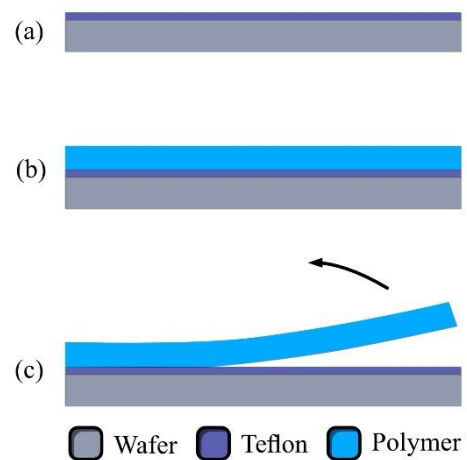

Figure 3: Spin-coating and curing a polymer on a silicon wafer. (a) Non-adhesive Teflon layer. (b) Spin coated polymer. (c) Peeling off of polymer membrane.

The materials were all deposited on silicon wafers and cured. The silicon wafers used were either coated with a SiO_2 layer to improve adhesion or with a Teflon layer to reduce adhesion (Figure 3a). The SiO_2 layer (2 μm thickness) was made by plasma-enhanced chemical vapour deposition (PECVD) at 400°C. Radio frequency induces plasma formation of precursor gasses, which in turn induce a chemical reaction that results in SiO_2 deposition [41]. A Teflon layer of 300 nm was produced by C_4F_8 deposition at 20°C for 60 sec. The wettability of these surfaces are specified in Section 3.1.1.1.

The materials were first spun on Teflon-coated wafers. If Teflon coating did not work properly the material was spun on a SiO_2 coated wafer. After initial characterization of the spin coating and curing process, the materials were in general spun on Teflon-coated wafers when loose polymer membranes were needed for testing (tensile test, biocompatibility), and spun on SiO_2 coated wafers when the polymer could or had to remain on the wafer during the test (etching).

PDMS consists of two components (elastomer and curing agent) which were mixed in a 10:1 weight ratio using a speedmixer (Thinky ARE-250 mixing and degassing machine; 30 s 500 rpm followed by 90 s 2000 rpm), to improve mixing and reduce bubble formation. The PDMS was spin coated for 30 s using a Brewer Science Manual Spinner (Figure 4a). The thickness of the resulting polymer layer depends on the viscosity of the liquid, the rotation speed of the spinner and the spin duration (spin coating profile). PDMS can be cured at room temperature, but to speed up the process the wafers were cured thermally at 90°C for 60 minutes in a Memmert UM 200 oven (Table 2).

The Ostemer 324 and Ostemer 220 also consist of two components (hardener A and base B) mixed in a 1.24:1 and 1.86:1 ratio respectively. After mixing, the Ostemers were spin-coated on a silicon wafer and cured. Ostemer 324 was spun for 60 seconds to ensure proper spreading of the material. Ostemer 220 was spun for 30 s. The curing mechanism is different for each Ostemer. Ostemer 324 was cured under UV light of 365 nm for 20 to 60 seconds (Figure 5) in a SUSS MicroTec MA/BA8 mask aligner (4.6 mWatt/cm^2 light intensity) and subsequently cured thermally in a Memmert UM 200 oven for 2.5 hours at 100°C (Figure 6). The Ostemer 220 was cured only with UV curing, also under 365 nm for 20 to 60 seconds. Throughout this thesis the samples of both Ostemers were UV-cured for 60 seconds unless stated otherwise.
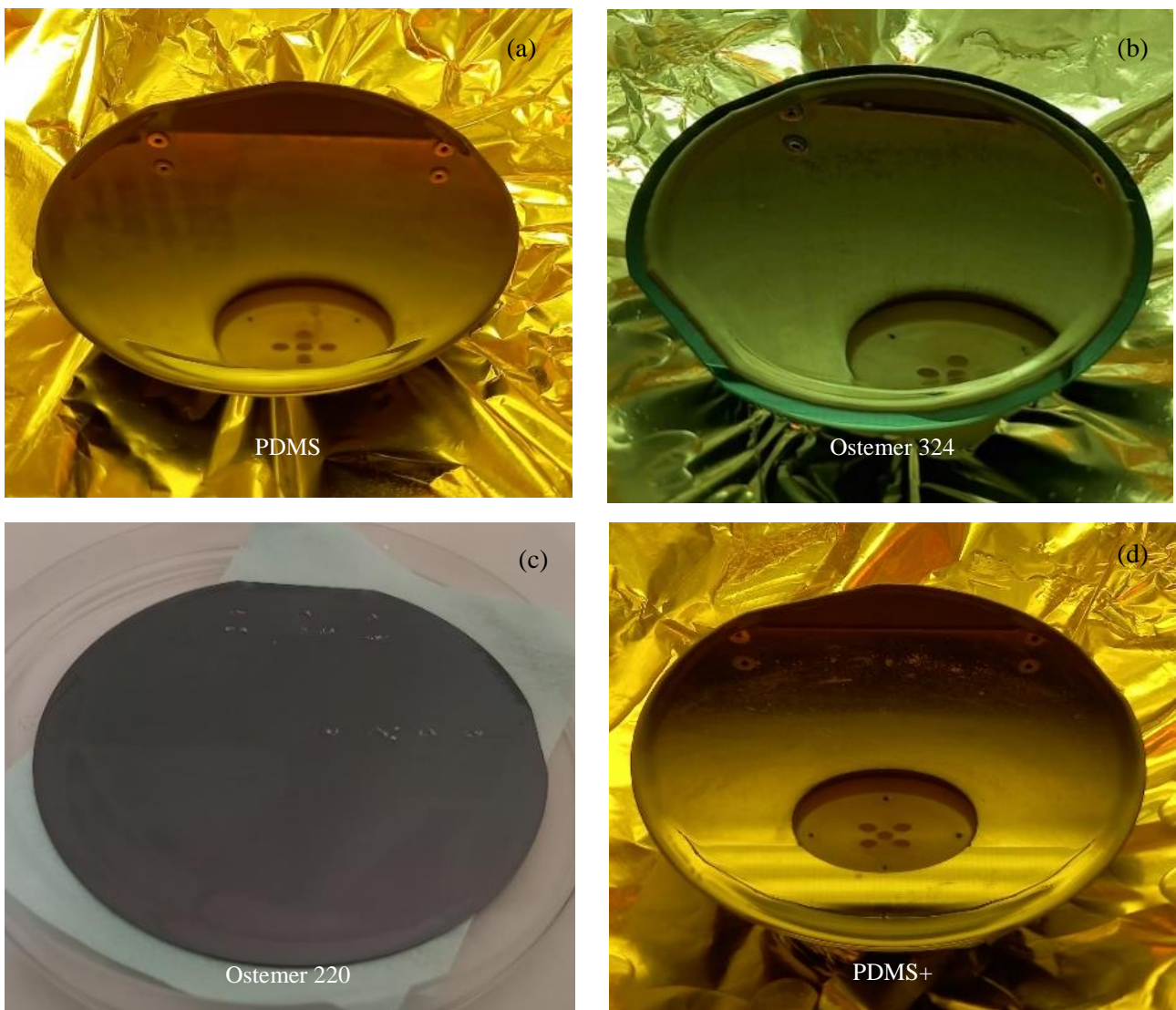

Figure 4: (a) PDMS spin coated on Teflon coated wafer, before curing. (b) Ostemer 324 spin coated on Teflon coated wafer, before curing. (c) Ostemer 220 spin coated on SiO₂ coated wafer after curing, including measurement points for thickness measurement. (d) PDMS+ spin coated on Teflon coated wafer before curing.

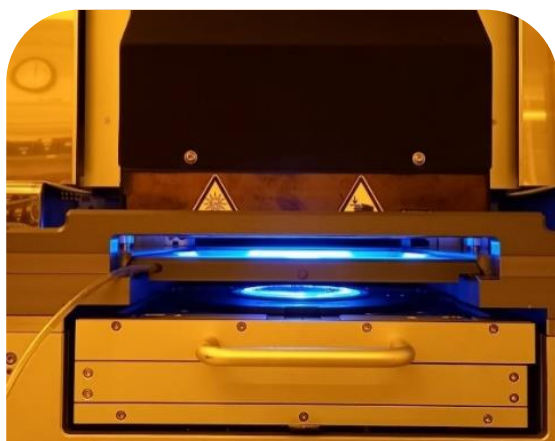| Material	Spin time [s]	Spin speed [rpm]	UV curing [s]	Thermal curing
PDMS	30 - 50	300 - 4000	-	90°C 1 hour
Ostemer 324	60	300 - 4000	60	100°C 2.5 hours
Ostemer 220	30	300 - 4000	60	-
PDMS+	30	300 - 6000	-	120°C 1.5 hours

Figure 5: SUSS MicroTec MA/BA8 Mask aligner during UV exposure of the polymers.

Figure 6: Oven for thermal curing of the polymers.

PDMS+ is a modification of PDMS. The details of the modification is proprietary information and therefore not shared. The mixture is poured on a silicon wafer and spun for 30 seconds. The samples are left out for at least 1 hour before thermally curing the samples for 1.5 h at 120°C in the oven (Memmert UM 200).

Ostemer 324 and PDMS+ compare to PDMS for the spin coating procedure (Figure 4a, Figure 4b, Figure 4d). The materials spread uniformly on the silicon wafers when spin coated and could be peeled off from the Teflon coated wafer after curing. Spinning on a SiO_2 coated wafer worked properly for these three materials; the materials spread uniformly.

When Ostemer 220 was poured on a wafer, the adhesion between the liquid polymer and the Teflon coated wafer was insufficient for spin coating. During spinning, the material on a Teflon coated wafer did not adhere and spun off from the wafer (Figure 7a). The remaining liquid pulled together due to the surface tension of the liquid and low chemical affinity with the non-adhesive substrate, leaving only a small drop of material remaining on the wafer (Figure 7b). When spin-coated on SiO_2 the Ostemer 220 adhered properly and spread without any problems (Figure 4c).
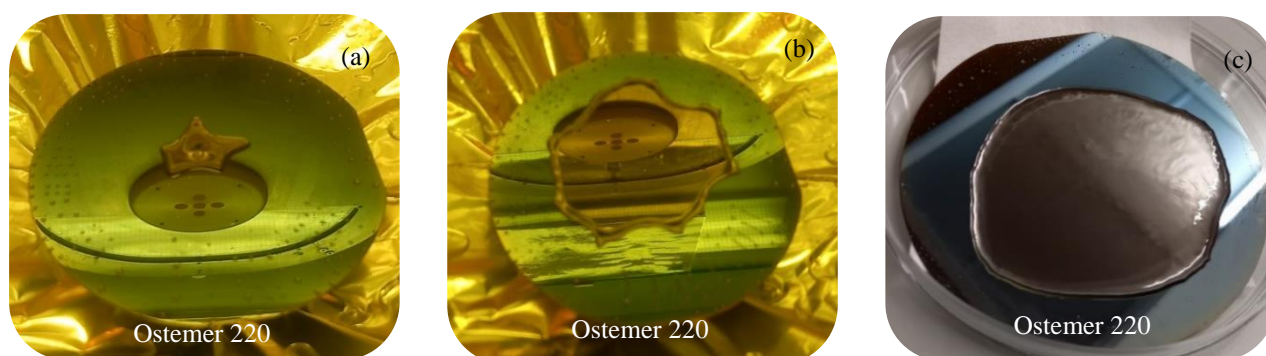
2.1.1.1 Peeling Off of Ostemer 220

Figure 7: (a) Ostemer 220 spin coated on Teflon coated wafer before curing. (b) Ostemer 220 spin coated on Teflon coated wafer before curing, 30 seconds after (a). (c) Ostemer 220 tilted on Teflon coated wafer after curing.

Some of the characterization required the polymer layers to peel off from the silicon wafer. For PDMS, PDMS+ and Ostemer 324 this was not a problem as they spun and cured on Teflon coated wafers, and could be peeled off afterwards. However, it was a problem for Ostemer 220 due to poor adhesion. In a first effort to fabricate loose samples of Ostemer 220, the polymer was deposited on a Teflon coated wafer and tilted by hand to cover the wafer (Figure 7c). The Ostemer properly cured but the resulting layer was thick (~632 µm; measured by a single measurement with Dektak 8 stylus profiler as described in the next section) and had a visible non-uniform surface and was therefore not optimal for further testing.

To obtain better and thinner samples, an alternative deposition method was devised whereby photoresist was used as sacrificial release layer, similar to the method used in Quirós-Solano *et al.* [42]. A SiO$_2$ coated wafer was first coated with a 4 µm-thick layer of photoresist (AZ ECI 3027) (Figure 8). The photoresist coated wafer was baked for 2 minutes at 90 degrees and then the Ostemer 220 was spin coated (300 rpm 30 seconds) on top of the photoresist layer an cured for 60 seconds under UV light.

Figure 9a shows the polymer 5 minutes after curing, and shows that air bubbles have formed underneath the polymer. A theory for the bubble formation is poor adhesion between the Ostemer 220 and photoresist layer. The bubbles started to form immediately after curing and continued for a few days at least. Figure 9b shows the bubble formation 4 days after curing. After curing the Ostemer 220, the photoresist layer was dissolved to release the polymer membrane from the substrate. First, acetone was used to dissolve the photoresist. However, Ostemer 220 swells when in contact with acetone. The material then tore into small pieces (less than 1x1cm)
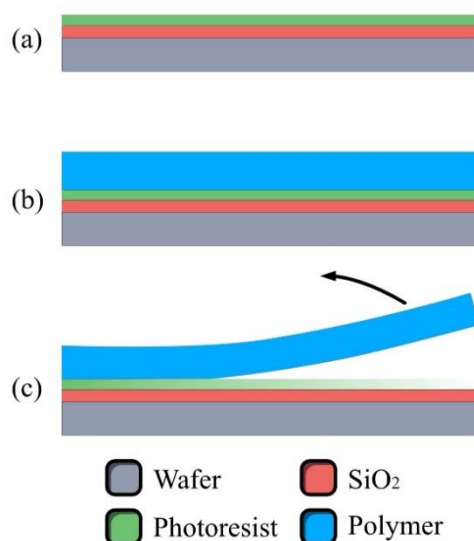

Figure 8: Illustration of the method using a sacrificial photoresist layer before spinning Ostemer 220 to facilitate peeling off of the material from the wafer. (a) SiO₂ coated wafer with a photoresist layer. (b) Ostemer 220 spin-coated on top. (c) Dissolving photoresist with isopropanol to release the polymer membrane.

when pulled from the wafer. To try and obtain larger samples, the entire wafer was left submerged in acetone for 10 minutes (Figure 9c). The acetone dissolved the photoresist and the polymer came loose from the wafer; however, the membrane also showed tears spread across the surface. The tears were probably a result from the swelling of the material, which caused ripples in the materials as seen in Figure 9c.

In a second effort, IPA was used to dissolve the photoresist. This solvent did not appear to affect the material but detached the material from the wafer more slowly. Submerging the wafer for 10 minutes had no beneficial effect. Cutting the polymer up while on the wafer and carefully pulling off small samples between a finger and knife worked. This way samples of the Ostemer 220 were successfully obtained for tensile, transparency and biocompatibility testing with the desired thickness. The cut samples of Ostemer 220 were cleaned properly by submerging and flushing them in IPA to remove all trace of photoresist off the surface and then rinsing them with DI water to remove the IPA. The samples were left to dry at room temperature.

2.1.1.2 Spin curve

After spinning and curing the samples, the thickness of the resulting polymer layer was determined using a stylus profiler (Dektak 8). The layer thickness was determined by removing a small section from a cured material layer on a silicon wafer and then measuring the material thickness at 7 points on the material edge, respectively 4 points on the centre axis and 3 points on a line closer to the edge of the wafer (Figure 10). The Dektak machine performs contact based topography measurements by tracking the height of a diamond tipped stylus across the material surface. The stylus deflection is measured and can thereby measure a change in height between the material and the exposed silicon wafer surface. The seven measurements were averaged. Based on the spinning speeds used during spin-coating (300, 500, 1000, 2000, and 4000 rpm) related to the thickness of the resulting layer, the spin-coating curve of each material was determined and is shown in Figure 11. The spin curve for PDMS was not fully determined. Indications from literature and existing recipes were used to prepare the samples. An often used spin coating recipe for PDMS throughout this thesis is 800 rpm for 50 seconds, used to create a 70.8 ± 1.8 µm-thick layer of polymer.

The spin curve is comparable for each of the four materials (Figure 11). Even though Ostemer 324 is the most viscous material in its liquid form, the curve falls below PDMS and PDMS+ due to the increased spin time (60 s compared to 30 s). PDMS+ is slightly less viscous than PDMS. Of each material, thin layers down to about 6 µm to 9 µm were made. The thickest layers achieved range from about 75 µm to 175 µm.
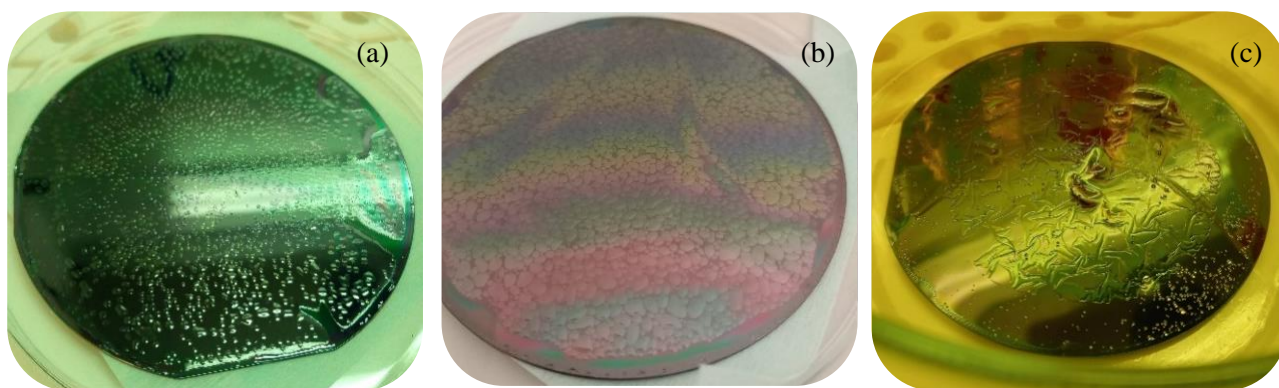

Figure 9: Ostemer 220 spin coated (300 rpm 30 seconds) on a 4000 nm layer of photoresist on a SiO$_2$ coated wafer and cured, in three different conditions. (a) About 5 minutes after curing showing bubble formation. (b) Four days after curing showing increased bubble formation and (c) submerged in acetone.
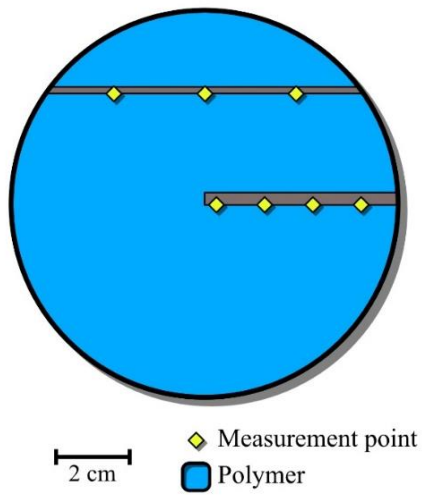
Figure 10: Schematic indication of measurement points for polymer layer thickness on a wafer. Two strips of polymer are cut away and the step height between the remaining polymer layer and wafer is measured on the measurement points.
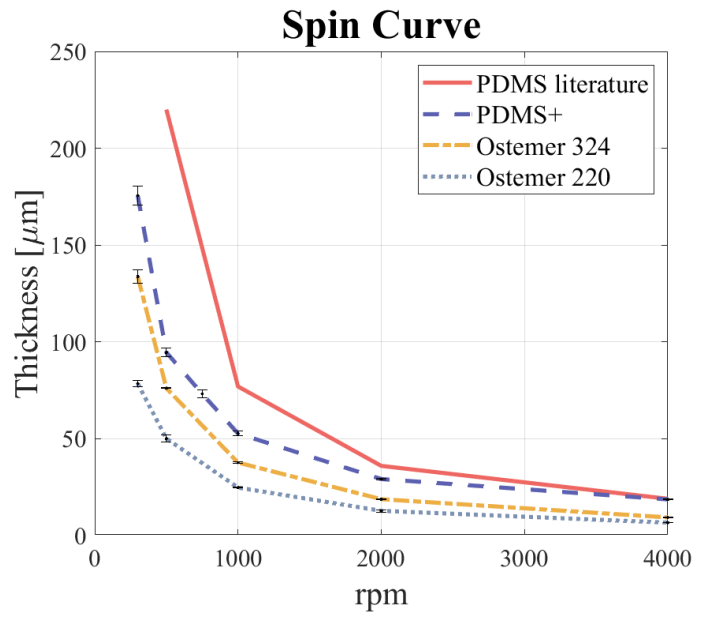

Figure 11: Spin curve of all materials. Ostemer 220 and PDMS+ spun for 30 seconds and Ostemer 324 for 60 seconds. PDMS data from literature is spun for 60 seconds from [110], [111].

2.1.2 Moulding

A parameter that should be taken into consideration is the size of the features that are possible to create with a material. Feature size depends on the manufacturing method in combination with material properties. Many OoCs have nanometre scale features, and micrometer scale channels, therefore the selected fabrication method should be able to create nano- or micrometer features with the selected material.

To test whether the materials are suitable for moulding, they were used to mould the EHT platform of Dostanic *et al*., described in Section 1.1.3 [15]. The mould was a silicon wafer wherein the platform shapes were etched by dry etching using a SiO_2 layer as a hard mask (shown in Figure 12a and b). The platform size was 2.8 mm along the major axis of the elliptic well and had a pillar height of ± 370 μm. The mould was covered with an anti-adhesive layer, deposited by evaporation of perfluorooctyl-trichlosorsilane (silane) in a vacuum chamber, to facilitate removal of the polymer from the mould (Figure 12c) [15]. The polymer was spin-coated on the mould and subsequently degassed under vacuum for about 20 minutes to remove the trapped air bubbles that remained inside the cavities of the mould (Figure 12d). Then the polymer was cured according to the associated curing procedure. After curing, the polymer could be peeled off from the mould, as illustrated in Figure 12e. The resulting platforms were imaged with a Keyence VK-X250 laser microscope.
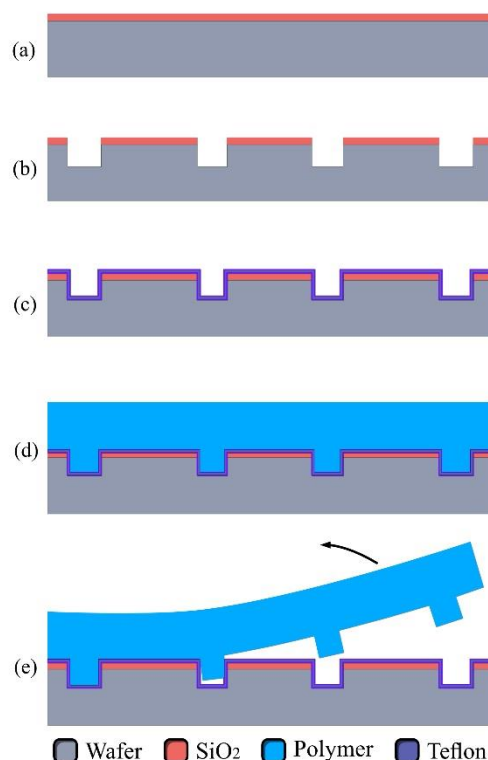

Figure 12: Illustration of polymer moulding. (a) SiO_2 coated wafer. (b) Deep reactive ion etching to form the mould. (c) Non-adhesive coating of Teflon (or silane). (d) Spin-coating, degassing and curing polymer layer. (e) Peeling the shaped substrate from the mould.

PDMS, Ostemer 324, Ostemer 220 and PDMS+ were moulded using the same mould. No problems occurred during moulding of PDMS, the resulting platform is shown in Figure 13a. The mould was coated with silane to reduce adherence after curing. However, on the initial try with Ostemer 324, the adhesion to the mould was insufficient with the liquid material. The material spread poorly and pulled together into a droplet due to the surface tension of the material, similar to spin coating Ostemer 220 on a Teflon coated wafer. To fully cover the mould, an excess of material was used. Unfortunately the excess and viscosity of the material prevented bubbles to exit the liquid during degassing, resulting in poorly shaped platforms.

Since spin coating Ostemer 324 worked properly on Teflon coated wafers, the mould was recoated with Teflon. This indeed improved the adherence of Ostemer 324 making it possible to cover the mould without an excess of material. However, due to the viscosity of the material, bubbles still exited the material poorly during degassing (Figure 14a). On areas where the layer was thin, the air bubbles did exit the material layer. However, the exiting bubbles pushed away the material and thereby left spots on the mould without material. The layer thickness turned out to be essential: too thin or too thick layers resulted in problems with degassing. After degassing for 2 hours in increments of 15 minutes, spreading the material again in between, the material was cured. After curing, the material could be pulled from the mould. This needed to be done carefully to prevent tearing of the stiff material. Some of the shapes did tear off and remained inside the mould. Complete platforms were formed as shown in Figure 13b.
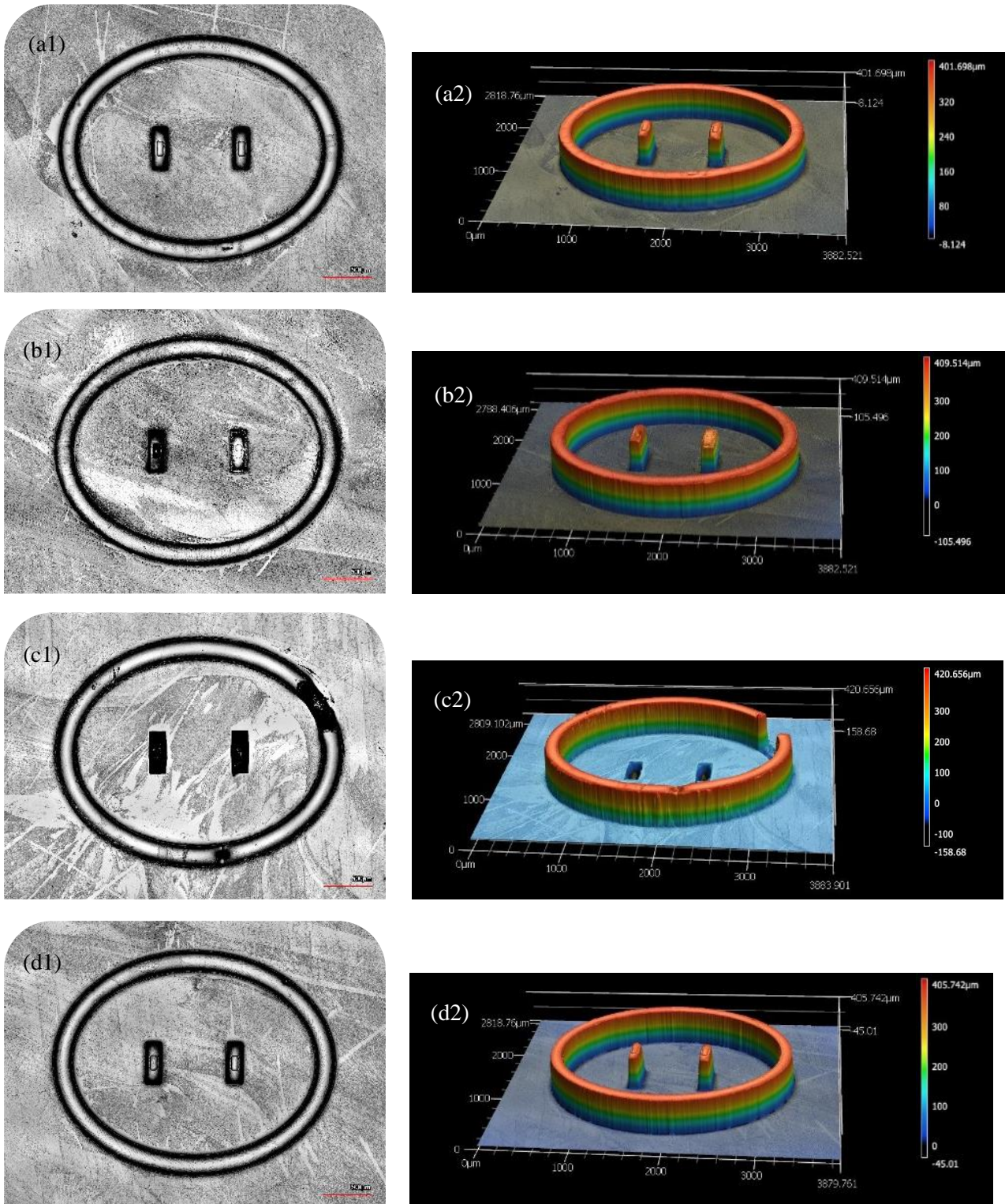
Figure 13: Moulded engineered heart platform under 10x enlargement. (a) PDMS. (b). Ostemer 324. (c) Ostemer 220. (d) PDMS+. Left column (1) confocal laser microscopy image, scale bar indicates 500 µm. Right column (2) 3D image based on confocal laser microscopy.

The adherence problems on non-adhesive layers were expected to be worse for Ostemer 220 compared to Ostemer 324. Moulding the material indeed showed poor adhesion between the liquid and the Teflon-coated mould. Degassing of the material showed the same problems as for Ostemer 324, bubbles did not clear from the material (Figure 14b), or locally removed the material when they did clear (Figure 14c). The wells and pillars only formed partially, as seen in Figure 13c.

Moulding the PDMS+ material went without any problems, equal to PDMS. During degassing no bubbles appeared (Figure 14d). The reduced viscosity compared to PDMS explains the improved ability of the material to enter the holes in the mould. The resulting platform is shown in Figure 13d. The substrate surface surrounding the well in Figure 13 shows a patterning. The pattern is transferred from the mould surface, which is scratched slightly during cleaning of the mould after each moulding session.

Conclusion

The engineered heart tissue platform was successfully moulded with Ostemer 324. Ostemer 324 can thus be moulded, taking into account the thickness of the poured layer. Based on observations during re-distributing of the material during the degassing process, excess material prevents bubbles from exiting the mould, while insufficient material limits entry of material into the mould shapes. Moulding with Ostemer 220 was unsuccessful, only a few partially shaped platforms were created. The PDMS+ material behaves as PDMS, and was successfully moulded.
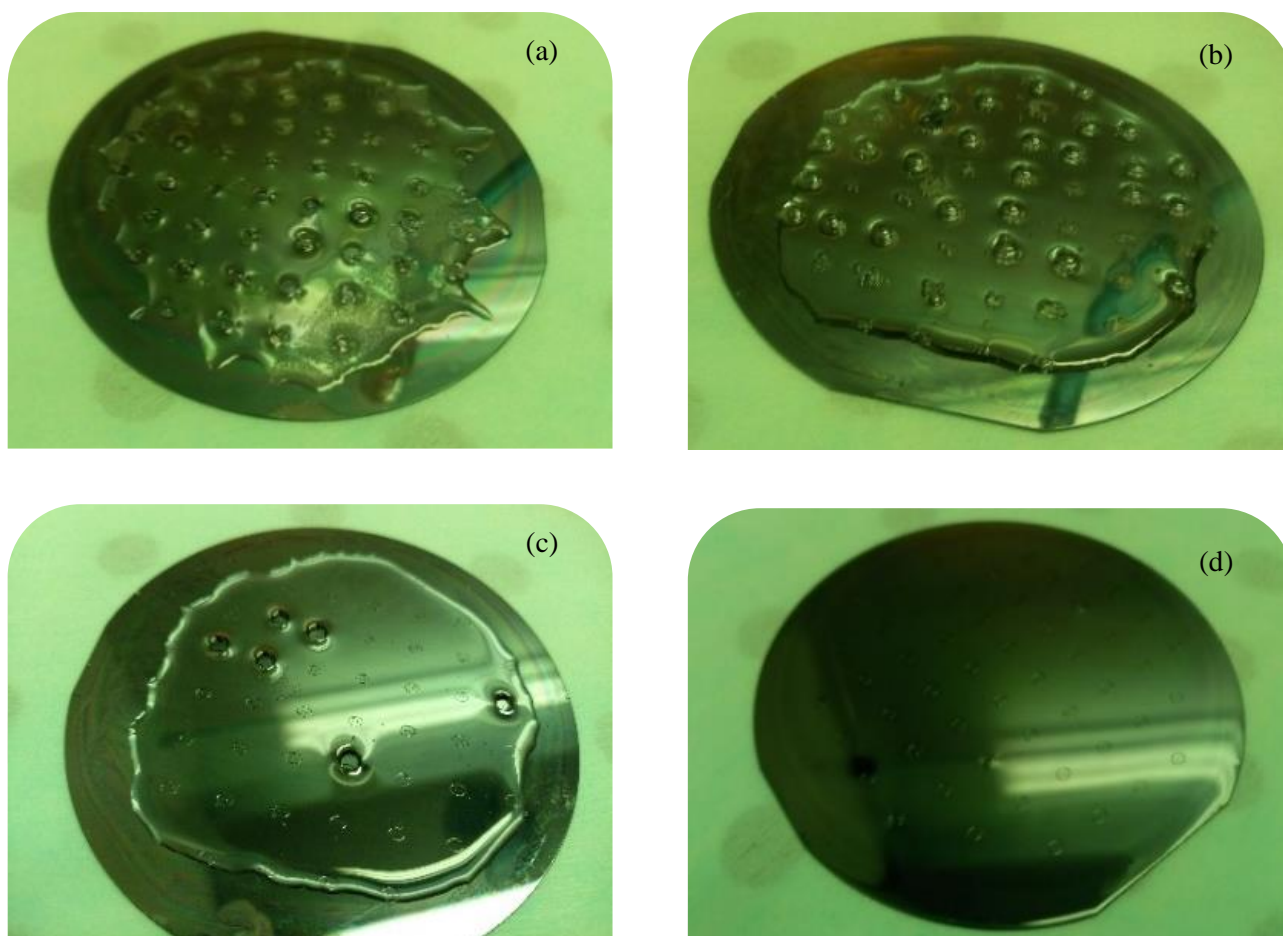

Figure 14: Wafer mould with polymer during the degassing process. (a) Ostemer 324 during degassing. (b) Ostemer 220 during degassing (c) Ostemer 220 after degassing. (d) PDMS+ during degassing.

2.1.3 Sputtering and Etching

Microfluidic systems can be produced by several existing technologies. For example microfabrication techniques such as photolithography, wet and dry etching [23]. These microfabrication techniques can be applied to PDMS. To see whether the techniques are also applicable to Ostemer 324, Ostemer 220 and PDMS+, lithography and etching of a pattern of small holes was performed on thin polymer layers. Dr. N. Gaio from Bi/ond aided in the etching processing.

2.1.3.1 Degassing test

The degassing rate of a material determines whether a material is suitable for processing steps under vacuum, such as etching and vapour deposition. To make sure the selected materials are suitable for lithography and etching, a test was performed to determine the degassing rate of the materials.

Ostemer 324, Ostemer 220 and PDMS+, spin coated and cured on SiO_2 coated wafers in different thicknesses, were tested with the Leak-up-rate test (LUR) in a Trikon Sigma 204 deposition system. The LUR test determines the amount of degassing from the material, for example the curing agent from the polymer [43]. The amount of degassing from the material is tested by putting the sample in a vacuum chamber and measuring the change in pressure. After 10 minutes the final leak rate is calculated based on the starting pressure and final pressure (Torr), depending on the time (seconds), and corrected for the chamber volume (46) according to Equation (1).

$$Leak\ rate = \frac{(p_{end} - p_{begin}) \times 46}{time} \qquad (1)$$

The calculated value determines whether or not the sample passed or failed the test [43]. The test is failed when the leak rate is higher than $2 \times 10^{-6} \frac{Torr \times L}{sec}$ at the time point of 10 minutes. Table 3, Table 4 and Table 5 show the layer thickness and result for the LUR test.

Table 3: LUR test for Ostemer 324.

Ostemer 324

Rotation speed	Thickness	Leak rate [$\frac{Torr \times L}{sec}$]	Result
500 rpm	76.1 ± 0.2 μm	4.21×10^{-5}	**failed**
2000 rpm	18.8 ± 0.3 μm	1.6×10^{-6}	**passed** after 70 min degassing
4000 rpm	9.1 ± 0.1 μm	1.95×10^{-6}	**passed** after 20 min degassing

Table 4: LUR test for Ostemer 220.

Ostemer 220

Rotation Speed	Thickness	Leak rate [$\frac{Torr \times L}{sec}$]	Result
300 rpm	78.8 ± 2.0 μm	3.91×10^{-4}	**failed**
2000 rpm	12.8 ± 0.6 μm	7.15×10^{-7}	**passed** immediately
4000 rpm	6.7 ± 0.0 μm	5.52×10^{-7}	**passed** immediately

PDMS+

Rotation Speed	Thickness	Leak rate $[\frac{Torr \times L}{sec}]$	Result
300 rpm	175.6 ± 5.0 μm	6.08×10^{-6}	**passed** immediately
750 rpm	73.2 ± 2.1 μm	5.99×10^{-6}	**passed** immediately
4000 rpm	18.7 ± 0.3 μm	5.93×10^{-6}	**passed** immediately

Ostemer 324 and Ostemer 220 are only suitable for deposition with thin layers (up to at least 18 μm), while the PDMS+ material is suitable for much thicker layers (at least 175.6 μm). If the sample is left in vacuum for a certain amount of time before starting the measurements, this initial time of degassing reduces the leak rate. This was necessary for the Ostemer 324: the samples only passed the test after initial degassing of 70 and 30 minutes before the actual 10 minute test. These results confirmed that the next processing steps of sputtering and etching could be performed.

2.1.3.2 Sputtering and Etching

Three samples were prepared for each material. SiO_2 was deposited on three silicon wafers by PECVD. Then Ostemer 324 was spin coated on top of the SiO_2 layer at 4000 rpm for 60 seconds and cured for 60 seconds under UV light and subsequently 2.5 hours at 100°C, resulting in a layer of 9.1 μm thickness. Three more SiO_2 coated wafers were made and Ostemer 220 was spin coated on top at 4000 rpm for 30 seconds (cured for 60 seconds under UV light) resulting in a 6.7 μm-thick layer (Figure 15b). Three more SiO_2 coated silicon wafers were made for PDMS+, which was deposited at 6000 rpm for 30 seconds to obtain a 10.7 μm layer. The degassing test (see Section 2.1.3.1) determined that layers of these thicknesses for these materials are suitable to start the etching process.

A layer of 250 nm aluminium was sputtered on top of the polymer layer (Figure 15c) using a Trikon Sigma 204 sputter machine at low power (1kW) and low temperature (25°C). The aluminium layer functions as a protecting layer (hard mask) for the etching of the polymer layer underneath. Deposition of the aluminium occurs under vacuum. The wrinkles seen within the resulting aluminium film, as shown in Figure 16, are caused by a deformation mismatch between the metal film and the polymer layer. The wavelength of the wrinkles is affected by the layer thickness and elasticity of the aluminium film and of the substrate. Deformation is mainly due to the thermal expansion and compression during the deposition process as well as compression by the vacuum environment [44], [45].
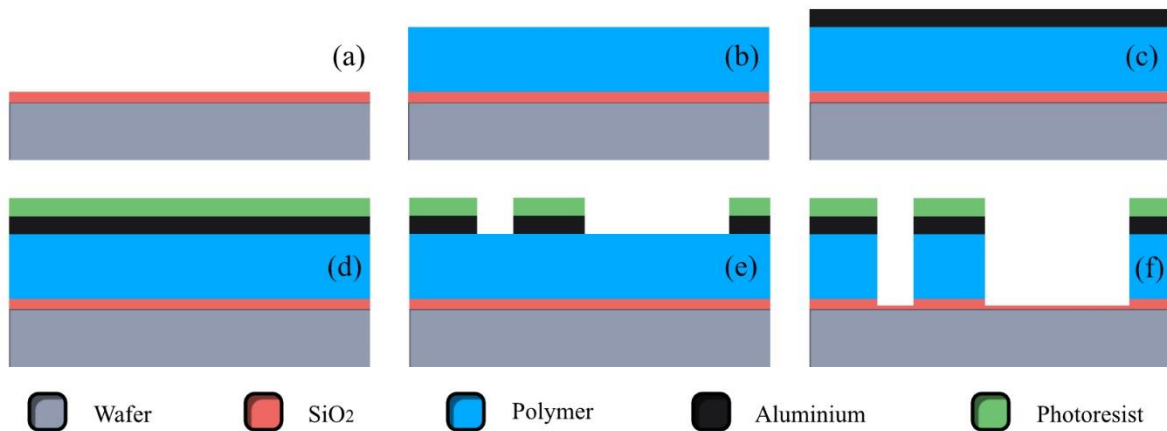

Figure 15: Schematic view of the etching process. (a) Wafer. (b) Wafer with spin coated polymer. (c) Additional sputtered layer of 250 nm aluminium. (d) Additional photoresist layer. (e) Patterned photoresist layer and etched aluminium layer. (f) Etch result.

Interestingly, the different materials indeed showed a different size of the wrinkle pattern, visualized with an Olympus MX61L optical microscope at 50x magnification (Figure 16). Additional images using a SEM Hitachi Regulus 823 are shown in appendix C. Different stiffness of the materials affects the deformation during the deposition process. The much stiffer Ostemer 324 indeed shows much smaller wrinkles compared to the less stiff other three materials. The differences between PDMS, Ostemer 220 and PDMS+, even though they have a similar stiffness, can be explained by the difference in layer thickness.
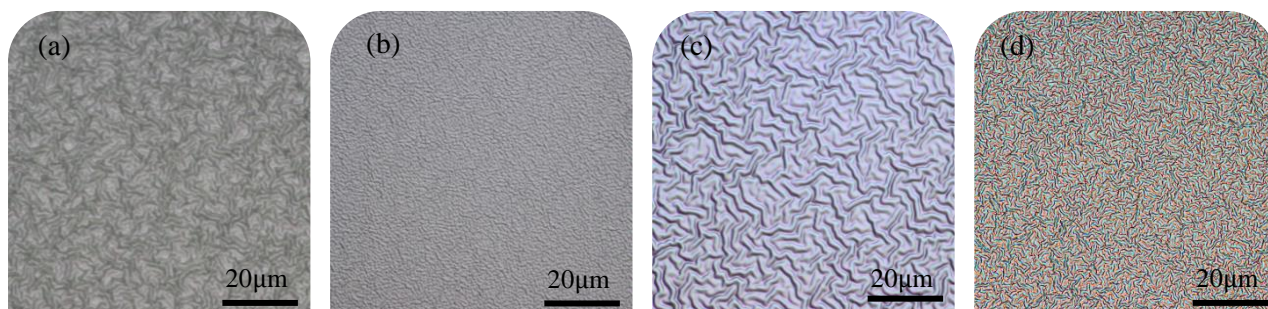

Figure 16: 250nm Aluminium sputtered on top of a polymer layer at 50x magnification. (a) 7.0 µm layer PDMS, (b) 9.1 µm layer Ostemer 324, (c) 6.7 µm layer of Ostemer 220 and (d) 10.7 µm layer PDMS+.

On top of the aluminium layer, a photoresist layer was deposited (Figure 15d), the photoresist layer was exposed in the mask aligner with a mask. The used mask pattern contained small circles of two different sizes, 600 µm and 4 µm in diameter (Figure 17). The photoresist was then baked for 90 seconds on 115 degrees and subsequently developed.
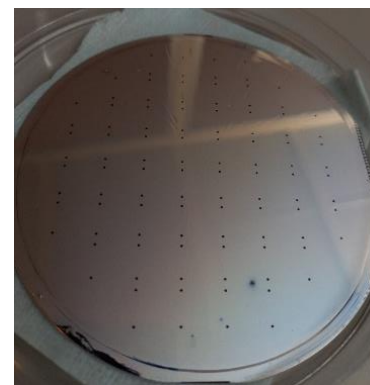
After photoresist development (Figure 15e), the aluminium in the exposed areas was etched (Trikon Omega 201 etcher; CL:HB, 1:1.3, P: 5 mTorr, RIE Bias: 50 W, ICP Power: 500W [43]), creating circular holes. Additional reactive ion etching used the patterned aluminium as a mask to etch the polymer layer (CH_4:SF_6:O_2,1:1:1, P: 20mTorr, RIE Bias: 20W, ICP Power: 500W [43]; illustrated in Figure 15f). After 25 minutes of etching the holes reached down onto the SiO_2. This is similar to the time it takes for holes to be fully etched in PDMS.

Figure 17: Image of an etched wafer. SiO_2 coated silicon wafer with Ostemer 324, patterned and etched with two different sizes of holes. The large holes are visible on the image.

To check whether the material was completely etched, the holes were imaged using an Olympus MX61L microscope (Figure 18) and scanning electron microscope (SEM Hitachi Regulus 823) (Figure 19, Figure 20 and Figure 21). For some holes the polymer on top was cut away to reveal the underlying SiO_2 layer. If the pattern of the hole is visible in this SiO_2 layer, this indicates the hole was fully etched trough, landing on the silicon oxide.

The images show that etching of Ostemer 324, Ostemer 220 and PDMS+ was successful on the first try with the same procedure used for PDMS. The holes are fully formed with sharp edges. The hole pattern is still visible even when the polymer layer is scratched away showing that the polymer layer is etched all the way through to the SiO_2 layer (Figure 19, Figure 20 and Figure 21). The landed pattern for PDMS+ is less clear in Figure 21d but visible in Figure 21f.

These results show that the three new materials can be patterned with etching technology. Reactive ion etching can be used to produce small features on all three of the tested materials, down to at least 4µm scale holes. Additional processing is needed to optimise the etching procedure for each of the materials, and to see which other types of structures can be achieved.
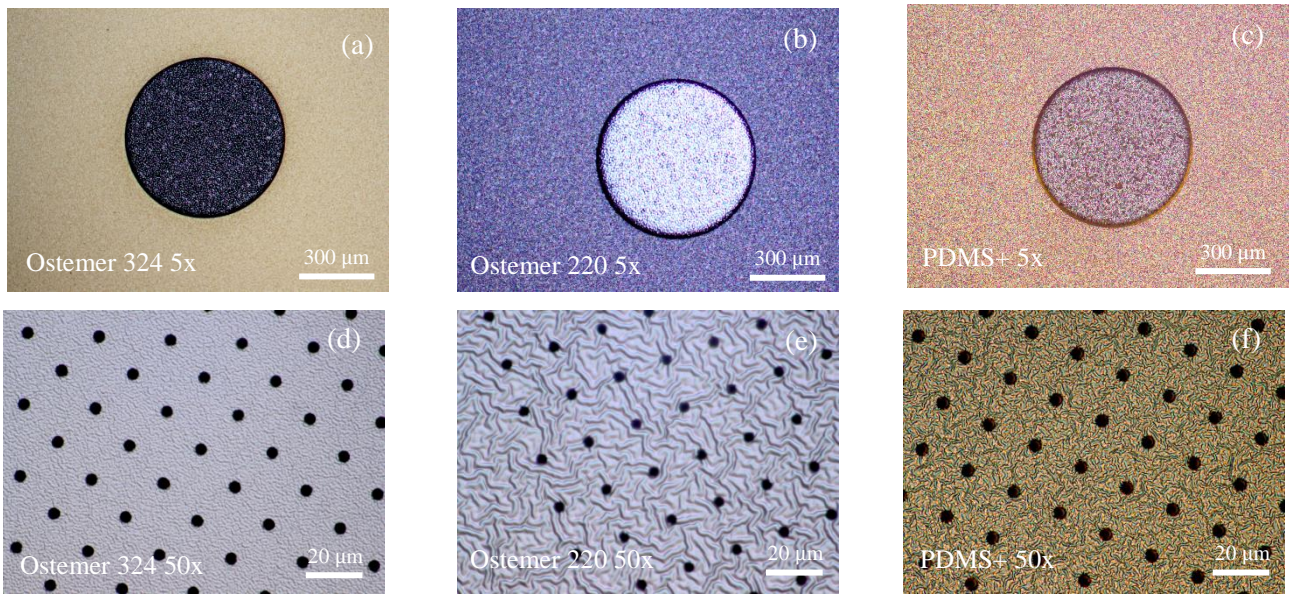
Figure 18: Etching of Ostemer 324, Ostemer 220 and PDMS+. (a-c) under 5x magnification showing the larger hole (600 μm diameter). (c-f) under 50x magnification showing the smaller holes (4 μm diameter).

Figure 19 SEM imaging of the etched holes in Ostemer 324. (a) Tilted (45°) top view of the larger hole. (b) Top view of the larger hole with scratching in the polymer showing the over-etched area. (c) Tilted side view of the edge of the larger hole, showing the different layers. (d) Top view of the smaller holes with scratching in the polymer. (e) Tilted top view of the smaller hole. (f) Tilted top view of the smaller holes, showing the pattern on the SiO$_2$ layer in the lower left corner of the image where the polymer is scratched away, as well as the etched holes in the top right corner.
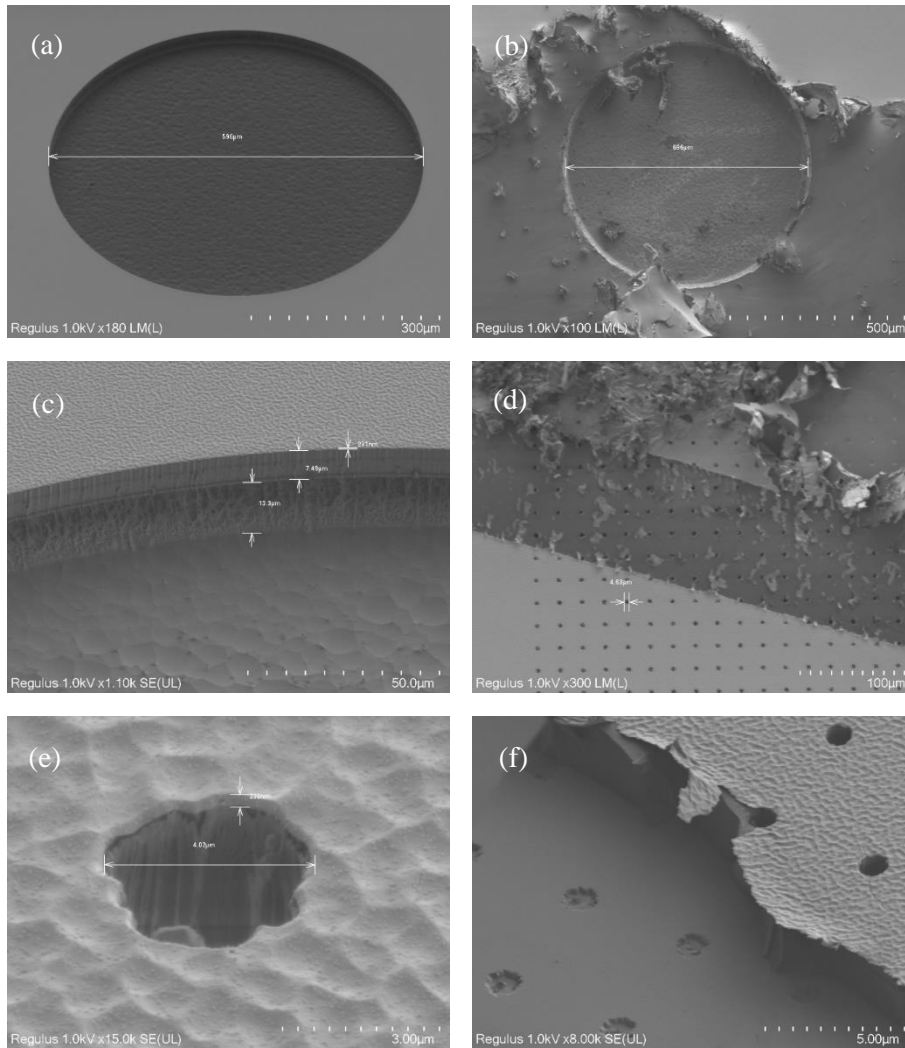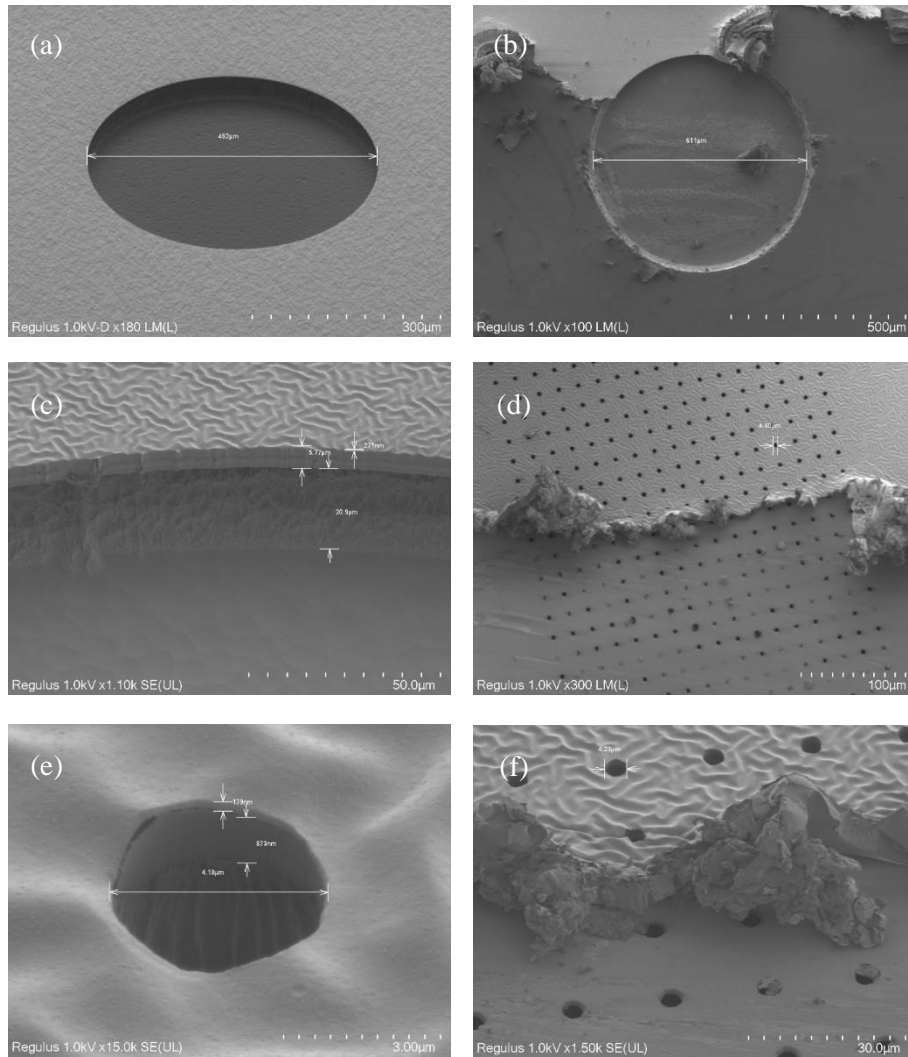
Figure 20 SEM imaging of the etched holes in Ostemer 220. (a) Tilted (45°) top view of the larger hole. (b) Top view of the larger hole with scratching in the polymer showing the over-etched area. (c) Tilted side view of the edge of the larger hole, showing the different layers. (d) Top view of the smaller holes with scratching in the polymer. (e) Tilted top view of the smaller hole. (f) Tilted top view of the smaller holes, showing the pattern on the SiO_2 layer in the lower halve of the image where the polymer is scratched away, as well as the etched holes in the top half.
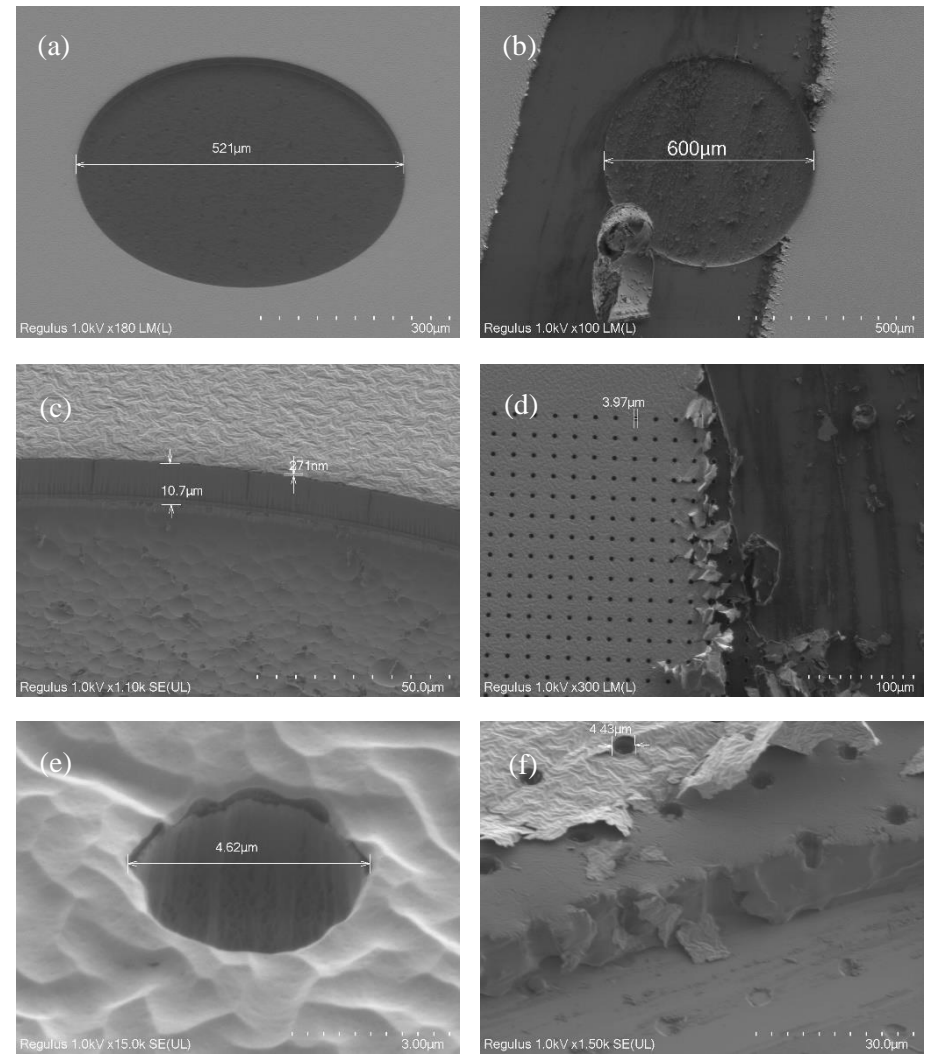
Figure 21: SEM imaging of the etched holes in PDMS+. (a) Tilted (45°) top view of the larger hole. (b) Top view of the larger hole with scratching in the polymer showing the over-etched area. (c) Tilted side view of the edge of the larger hole, showing the different layers. (d) Top view of the smaller holes with scratching in the polymer. (e) Tilted top view of the smaller hole. (f) Tilted top view of the smaller holes, showing the pattern on the SiO_2 layer in the lower right halve of the image where the polymer is scratched away, as well as the etched holes in the top left half.

3 Mechanical Characterization

This chapter shows the results of mechanical characterization of the materials based on several tests. These tests are performed after curing of the material and can help to determine whether the materials are suitable for fabrication of OoC devices. The tested characteristics are: surface properties before and after plasma treatment, stiffness and optical transparency. The samples prepared for these tests were cured according to the method defined in Chapter 1.

3.1   Wettability

Wettability refers to the affinity of a material surface with another material in liquid form. With respect to water, possibly the most common liquid used to quantify wettability, the material surface can either be hydrophobic or hydrophilic. The wettability of the material affects the ability of cells to adhere to the material and the interaction of the material with added fluids such as cell culture medium. Cells adhere better to hydrophilic materials, hence the importance of this parameter.

Hydrophilic materials are polar materials, which means the molecules of the material have partial positive and negative charges. Negatively charged proteoglycans on a cell surface attach to the positively charged hydrophilic material surface. Wettability also affects flow rate of for example the cell culture medium through a microfluidic channel [46]. Hydrophilicity can be measured by the contact angle of water droplets on the surface of the material, as shown by α in Figure 22. The preferred contact angle for cell adherence is 20° to 40° for fibroblasts [47]. Lee *et al.* showed an optimal cell adhesion for endothelial cells on a polymer surface with contact angle of 55° under fluid shear stress conditions [48]. Ikonen *et al.* in turn showed that a (hydrophilic) hydrogel surface supported cadiomyocyte growth, without quantifying the contact angle [49], indicating that there is no exact contact angle for the optimal condition.

Treatments with oxygen plasma or ultraviolet light can alter the wetting properties of a material surface, [5], [27], [50]. Other options are salinization, chemical vapour deposition or the use of coatings such as acrylic acid [50]. PDMS can also be coated to make it more hydrophilic. However, these coatings can affect cell response and the test result and are therefore not always desirable [51]

A surface modification technique for increasing hydrophilicity used in the field, not just on PDMS, is plasma treatment. Plasma is a partially ionized gas, where electrons are free instead of bound to an atom. These free electrons react with the material surface, creating so-called chemical functional groups [27]. This surface treatment oxidizes the material, by including more oxygen in the functional groups on the surface (Figure 23). Since oxygen is a polar molecule, the surface becomes more polar and thus more hydrophilic. This treatment makes the surface permanently or temporarily hydrophilic. After some time, the surface of the polymer can become hydrophobic again, a process known as hydrophobic recovery [28]. During this recovery the untreated molecules from inside the material move towards the surface, or the surface molecules turn towards the inside [52]. It depends on the material whether this happens and how long the recovery takes. Surface modifications on thermoplastics can give hydrophilicity for up to a few years, while on elastomers the time range is a few days
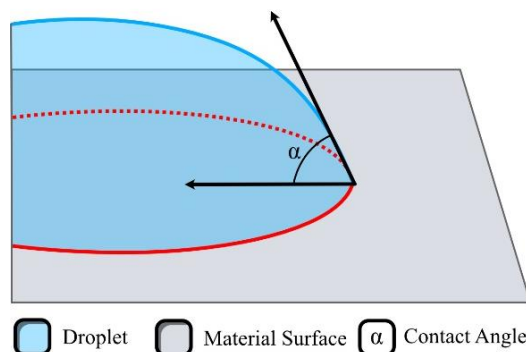

Figure 22: Illustration of contact angle measurement on a droplet of water on a solid material surface, adapted from [112].

PDMS Surface

CH₃   CH₃   CH₃

$$-\text{Si}-\text{O}-\text{Si}-\text{O}-\text{Si}-$$

CH₃   CH₃   CH₃

Plasma Treatment →

Oxidized PDMS Surface

OH   OH   OH

$$-\text{Si}-\text{O}-\text{Si}-\text{O}-\text{Si}-$$
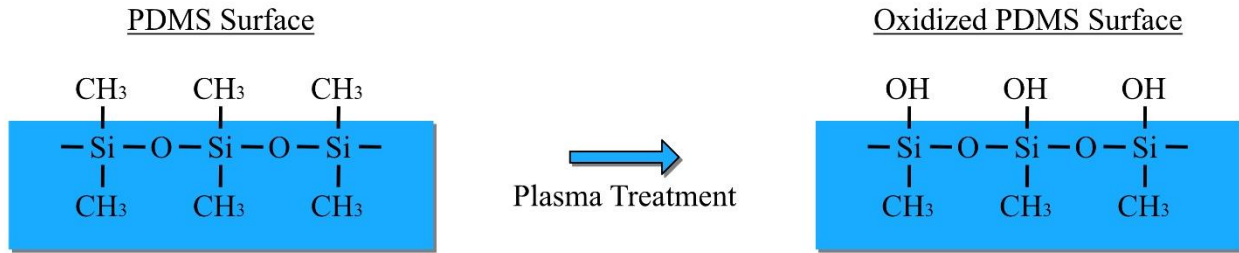
CH₃   CH₃   CH₃

Figure 23: schematic representation of change in functional groups on the surface of PDMS after plasma treatment. Adapted from [43], [60].

up to a few weeks [53]. The disadvantage of PDMS is that the recovery happens quite rapidly (within 24 hours), making it less convenient for long-term cell testing as the tests need to be performed directly after the plasma treatment to ensure the highest hydrophilicity.

3.1.1 Contact Angle Measurements

3.1.1.1 General wettability

The wettability of the materials was determined based on water contact angle measurements and measured after curing, after plasma treatment and over time after the plasma treatment. The contact angle α is the angle composed by a droplet on a the material surface, as illustrated in Figure 22. For a contact angle $\alpha < 90°$, the surface is formally considered to be hydrophilic, while a contact angle $\alpha > 90°$ indicates a hydrophobic surface [54]. However, there is no clear data for this split to be at 90°, so hydrophilicity is somewhat open to interpretation. The focus is mainly on obtaining the values of wettability.

Contact angle measurements were performed on cured PDMS, Ostemer 324, Ostemer 220 and PDMS+ with a DataPhysics Instruments contact angle system OCA-20 (Figure 24). A water droplet of 3 µl was positioned on the material and the angle of the static droplet surface with the material surface was measured (Figure 22). Four individual measurements on four different materials are shown in Figure 25. For PDMS, both the mixing ratio of 10:1 and 5:1 were tested. Ostemer 220 was tested for two processing types: cured on a SiO₂ wafer and cured on a layer of photoresist to check whether the photoresist and IPA process described in Section 2.1.1.1 affected the wettability of the material.

Contact angles of the materials, calculated as an average of six or more measurements, outliers excluded, are shown in Table 6. These indicate that the wettability of PDMS in mixing ratio 10:1 and 5:1 are similar (106.6 ± 0.4° and 105.8 ± 0.4°). Both Ostemers are more hydrophilic than PDMS, with contact angles of 62.2 ± 3.6° (Ostemer 324) and 64.2 ± 3.2° (Ostemer 220). The contact angle of the Ostemer 220 obtained from the method with photoresist and dissolving in IPA appears to have increased slightly compared to the material untreated with IPA, but is still very similar (64.2 ± 3.2° compared to 68.3 ± 5.0°). Based on a two-tailed t-test, equal variance, this difference is significant (p = 0.03).
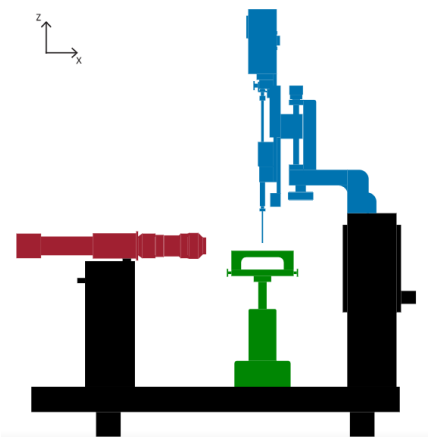
Figure 24: Schematic representation of Optical Contact Angle system. (red) optics, (blue) liquid dosing, (green) sample positioning platform. From [112].
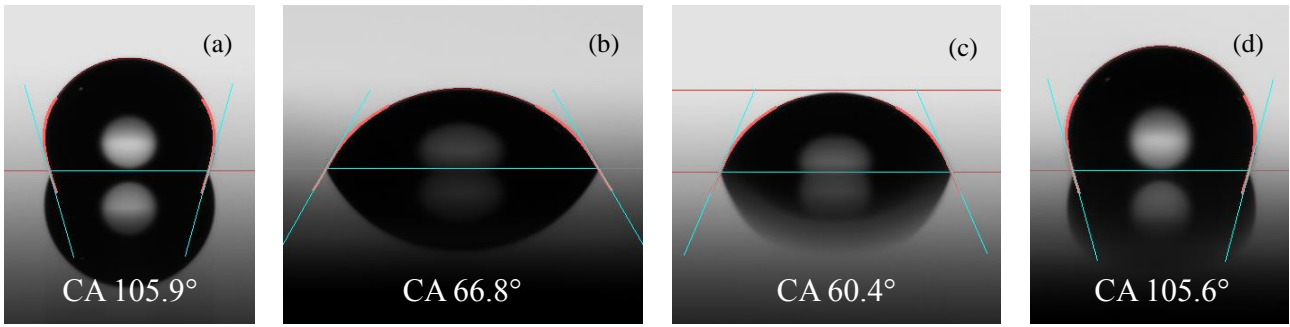
Figure 25: Contact angle measurements of a 3 µl droplet of DI water on (a) PDMS 10:1, (b) Ostemer 324. (c) Ostemer 220 and (d) PDMS+. After curing without any surface treatment.

Table 6: Contact angle measurements in degrees, measured after curing.

Material	n	Contact angle [°]
PDMS 10:1	6	106.6 ± 0.4
PDMS 5:1	7	105.8 ± 0.4
Oste 324	11	62.2 ± 3.6
Oste 220	11	64.2 ± 3.2
Oste 220 IPA	14	68.3 ± 5.0
PDMS+	8	106.1 ± 0.5

The increased hydrophilicity of Ostemer 324 and Ostemer 220 has the potential to greatly improve cell attachment and cell proliferation in OoC devices compared to PDMS.

Surface Coating Characterization

Spinning Ostemer 324 and Ostemer 220 on Teflon, Silane or SiO_2 coated wafers showed differences in adhesion. The wettability of these surface coatings was therefore determined. Table 7 shows the wettability of three surface treatments of silicon wafers, without any additional material spun on top. The values clearly show that Teflon ($102.2 ± 0.2°$) and Silane ($95.2 ± 0.8°$) are more hydrophobic than SiO_2 ($16.7 ± 2.3°$).

Table 7: Contact angle measurements of wafer coatings.

Coating	n	Contact angle [°]
Teflon	5	102.2 ± 0.2
SiO_2	5	16.7 ± 2.3
Silane	5	95.2 ± 0.8

3.1.1.2 Surface modification: Plasma treatment

The wettability of PDMS, Ostemer 324, Ostemer 220 an PDMS+ was tested with 3 different plasma treatment settings using a Diener low power oxygen plasma system (ATTO-BL-PCCA). The goal was to quantify the time it takes for the materials to return to their original wettability, not necessarily to optimize the process. The samples were cured polymer layers still attached to the wafer. The performed plasma treatments were 3 minutes at 20 W, 1 or 2 minutes at 74 W and 18 minutes at

20 W, respectively. The first and second settings are standard recipes used to reduce the contact angle of PDMS towards zero. In the third setting the time of the plasma treatment for 20 W was elongated to try to lower the contact angle of the Ostemer 324. Contact angle measurements were repeated after the plasma treatment over time and are visualized in bar plots, with standard deviation as error bars. Outliers were excluded from the data. Almost all measurements were done using the accompanying software of the optical contact angle system. However this software could not detect contact angles $< 10°$, therefore these measurements were done manually using ImageJ software.

The first setting treated the material for 3 mins in the plasma machine on a power setting of 20 W (10% of the maximum machine power). The graph (Figure 26) shows the contact angle of PDMS was, as expected, lowered to $3.8 \pm 1.3°$ (a reduction of 102.7°), Ostemer 324 was only lowered by 10.5° to $51.7 \pm 2.2°$, Ostemer 220 was significantly lowered by about 45.9° degrees to $18.3 \pm 0.3°$ and PDMS+ was, similarly to PDMS, reduced from $106.1 \pm 0.5°$ to $6.8 \pm 1.9°$. After 72 hours the contact angles returned towards the original values. Notably the contact angle of PDMS+ did not return as quickly towards the starting value compared to PDMS. The droplets are visualised in Figure 29 for PDMS and Figure 30 for Ostemer 220.

The second setting was a plasma treatment for 1 minute at 74 W (37% of the maximum machine power). This hardly affected the Ostemers, hence Ostemer 324 and Ostemer 220 were subjected to another minute of treatment, for a total of 2 mins at 74 W. Figure 27 shows the contact angle over time from 1 hour until 4 weeks. 2 data points for PDMS+ were not measured due to logistical problems (2 and 4 weeks).

In the final setting (Figure 28) the plasma treatment was at 20 W for 18 mins to reduce the contact angle of Ostemer 324. This seemed to work, however it was a less suitable setting for the Ostemer 220 and PDMS as their contact angle was not reduced as much as in the earlier settings. The graph shows the contact angle over time, from 24h until 6 weeks.

For the 1 or 2 minute plasma treatment test at 74 W, PDMS was already back to the original contact angle after 24 hours, Ostemer 324 and Ostemer 220 both took 5 days. The contact angle of PDMS+ reduced comparably with PDMS, and yet the window of hydrophilicity is 5 times longer for PDMS+, as the contact angle returned towards the original angle after 5 days.

The results for the 18 minute treatment show a slightly longer recovery time for PDMS of somewhere between 24 and 72 hours. Ostemer 324 underwent a large reduction of the contact angle after the treatment ($17.1 \pm 1.4°$) and recovery time was 2 to 3 weeks. The measurements for Ostemer 220 are less clear, and also less relevant as the initial reduction of contact angle was only to $38.5 \pm 2.0°$.
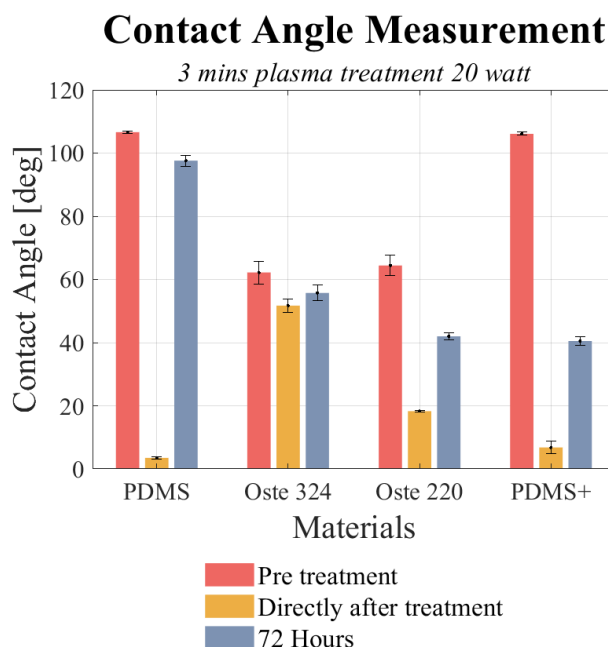

Figure 26: Contact angle measurement of PDMS, Ostemer 324, Ostemer 220 and PDMS+ before, directly after and 72 hours after a 3 minute plasma treatment on 20 W. Error bars indicate standard deviation.

Contact Angle Measurement
1 or 2 mins plasma treatment 74 watt

Legend:
- Pre treatment
- Directly after treatment
- 1 hour
- 2 hours
- 24 hours
- 5 days
- 8 days
- 2 weeks
- 3 weeks
- 4 weeks
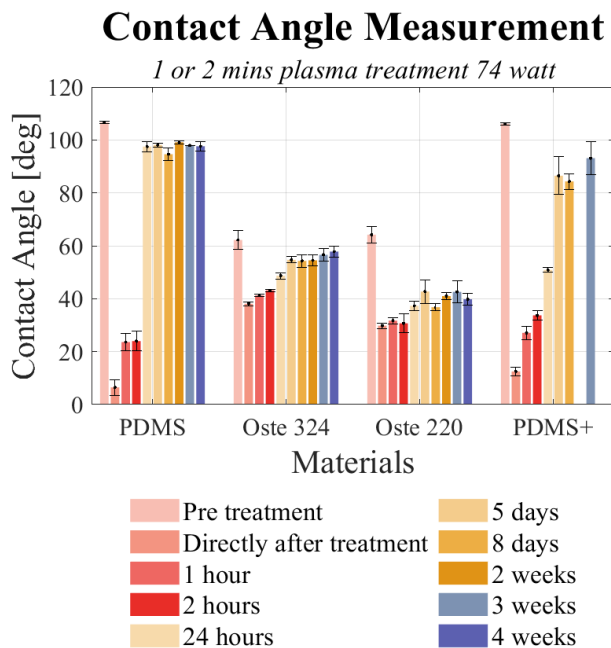
Figure 27: Contact angle measurement of 4 materials before, directly after and on several time points after a 1 or 2 minutes plasma treatment at 74 W.

Contact Angle Measurement
18 mins plasma treatment 20 watt

Legend:
- Pre treatment
- Directly after treatment
- 24 hours
- 72 hours
- 1 week
- 2 weeks
- 3 weeks
- 4 weeks
- 5 weeks
- 6 weeks
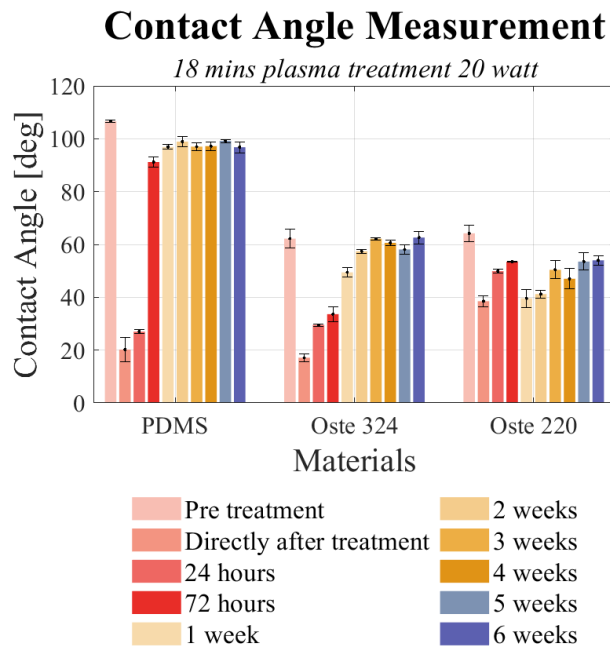
Figure 28: Contact angle measurement of 4 materials before, directly after and on several time points after a 18 min plasma treatment at 20 W.
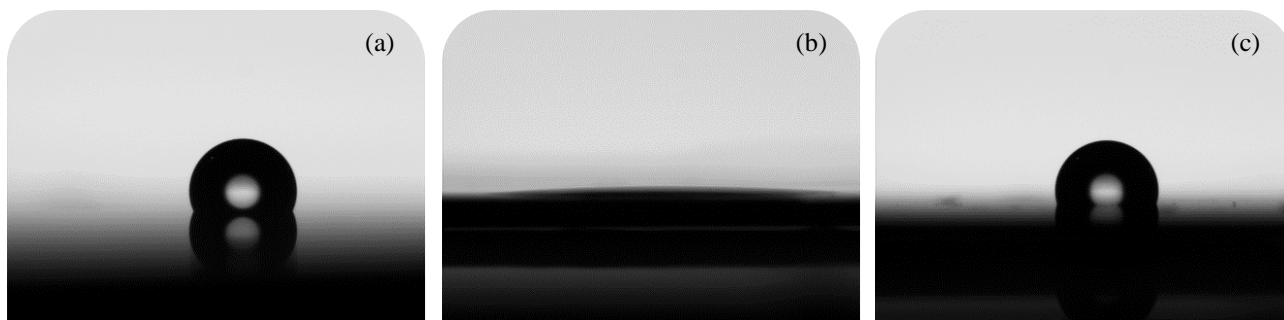
Figure 29: Water droplet of 3 µl on PDMS surface for contact angle measurement, (a) before plasma treatment (b) directly after plasma treatment of 3 minutes at 20 W and (c) after 72 hours.

Figure 30: Water droplet of 3 ul on Ostemer 220 surface for contact angle measurement, (a) before plasma treatment (b) directly after plasma treatment of 3 minutes at 20 W and (c) after 72 hours.

Conclusion

Ostemer 324, Ostemer 220 and PDMS+ show good results in terms of wettability after plasma treatment. For the Ostemers the initial contact angle is already less than that of PDMS. Plasma treatment does not reduce the contact angle as strongly as for PDMS and PDMS+, but does reduce the contact angle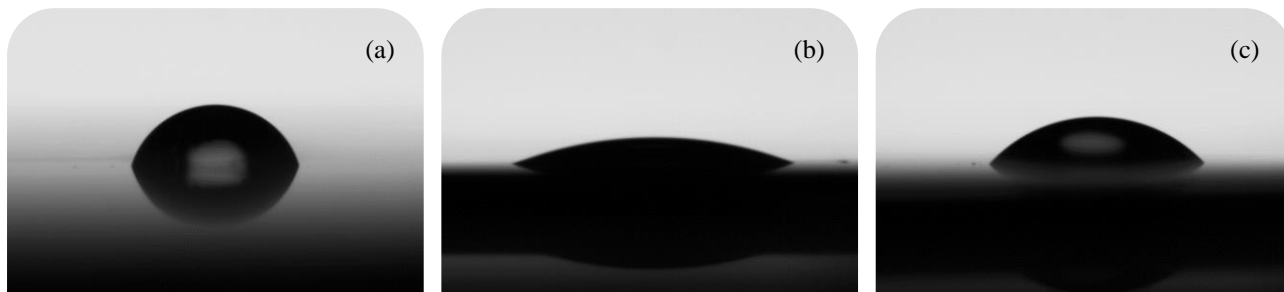 towards the optimal wettability of 20 to 40°. The hydrophobic recovery of both Ostemers and PDMS+ are better compared to PDMS, as the window of hydrophilicity is much longer.

3.1.1.3 Wettability depending on UV curing time

In a separate test, dependency of wettability to UV curing time of Ostemer 324 and Ostemer 220 was checked (Table 8). The contact angle of Ostemer 324 is not affected by UV curing time, the difference is not significant, determined by a one-way ANOVA test. The difference between the contact angle for Ostemer 220 is significant (one-way ANOVA, $p<0.01$). More specifically, the contact angle of Ostemer 220 with curing time of 20 s is increased more significantly (vs 60 s) than for 20 s vs 40 s curing, $p=0.0002$ and $p=0.016$ respectively (two-tailed t-test, equal variance for 20 vs 60 seconds, unequal variance for 20 vs 40 seconds).

Table 8: Contact angle measurement of Ostemer 324 depending on UV curing time, including 2.5 hours of thermal curing at 100 ℃ and contact angle measurement of Ostemer 220 depending on UV curing time.

Ostemer 324		Ostemer 220	
UV curing time	Contact angle	UV curing time	Contact angle
60 sec	62.2 ± 3.6	60 sec	64.2 ± 3.2
40 sec	62.5 ± 0.7	40 sec	64.7 ± 0.6
20 sec	64.0 ± 1.0	20 sec	75.1 ± 2.2

3.2 Stiffness

Different tissues require different substrate stiffness for optimal cell and tissue development. Additionally, material stiffness is important in dynamic OoC systems, for example platforms with an inflatable membrane. Tissue stiffness itself differs greatly, for example brain tissue has a Young's modulus of 1kPa and bone of 1 GPa [16]. The stiffness of healthy heart tissue ranges below 50 kPa, while damaged heart tissue ranges above 100 kPa [25]. PDMS has a stiffness of 1 to 3 MPa, while that of glass is 50 GPa, and thermoplastics used for petri-dishes such as polystyrene have a stiffness of 3 GPa [26].

The stiffness of the material should mimic the stiffness of the natural tissue environment. A material with tuneable stiffness would be preferable. The stiffness of all four materials can theoretically be tuned by altering the mixing ratio of the components and altering the curing process. The next experiment will determine the stiffness of the four materials.

3.2.1 Uniaxial Tensile Test

To determine the Young's modulus of the materials, strips of the polymers were tested with an uniaxial tensile test using a Dynamic mechanical analyser (DMA), TA instruments Q800 at the Precision and Microsystem Engineering department of TU Delft. The samples were cut and peeled off a wafer after curing. The samples where approximately 80 μm thick, 8 mm wide and 20 mm in length. Within the testing setup the length of the tested sample was only 5 to 10 mm as the rest of the sample was clamped in the system (Figure 31).
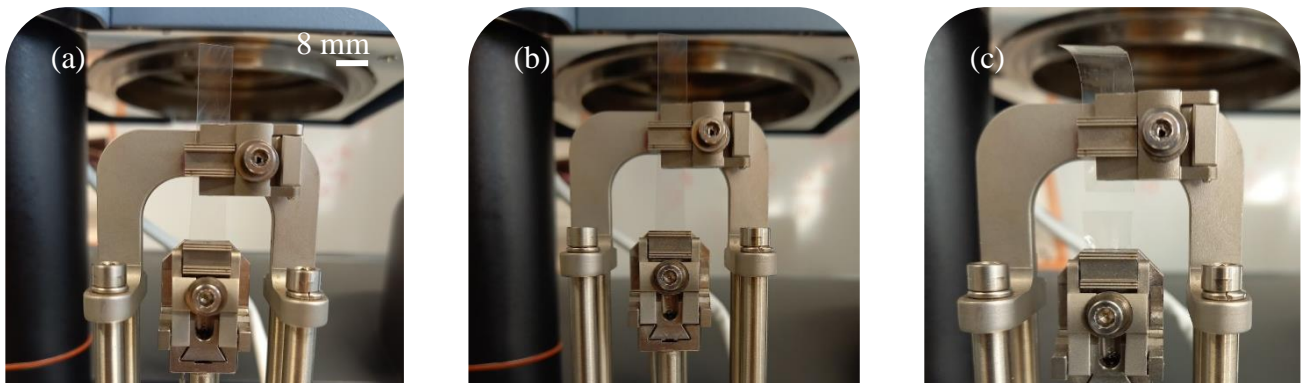
Figure 31: Tensile test of Ostemer 324 sample. (a) At the start of the experiment, (b) during stretching of the sample and (c) after fracture of the sample.

The setup clamps the samples on each end and slowly pulls them apart, increasing the pulling force over time at a rate of 3 N per minute up to 15 N. The measurement stops when the maximum stretched length of 25 mm is reached or when the sample fractures. The outcome is a stress-strain curve (Figure 32), from which the Young's moduli of the materials were determined by calculating the slope of the graphs. Other parameters such as the yield and fracture point were also determined from the graph (Table 9). All outliers were excluded from the data and the standard deviation is shown. The yield point for Ostemer 324 in UV curing time of 40 and 20 seconds could not be determined from the graph, as no clear yield point was visible in the measurements.

Table 9: Mechanical properties of PDMS, Ostemer 324, Ostemer 220 and PDMS+ based on tensile test including standard deviation. The stiffness for Ostemer 220 is not expected to be but possibly affected by the use of isopropanol (IPA) in the sample preparation.

Material	Thickness (µm)	UV curing time (sec)	Young's modulus (MPa)	Yield point (MPa)	Fracture point (MPa)	Strain until break (%)
PDMS 10:1	70.8 ± 1.8	-	1.1 ± 0.2	2.3 ± 0.6	4.4 ± 1.8	262.4 ± 103.6
PDMS 5:1	76.7 ± 0.1	-	2.4 ± 0.5	2.7 ± 0.4	8.3 ± 1.6	209.0 ± 47.7
Oste 324	76.1 ± 0.2	60 sec	5.2 ± 1.3	4.2 ± 0.9	4.8 ± 1.2	89.3 ± 3.4
Oste 324	76.1 ± 0.2	40 sec	4.6 ± 0.3	-	4.7 ± 0.9	88.3 ± 9.2
Oste 324	76.1 ± 0.2	20 sec	4.9 ± 0.7	-	3.7 ± 0.3	70.1 ± 12.7
Oste 220 *IPA*	78.8 ± 2.0	60 sec	1.4 ± 0.2	1.0 ± 0.3	1.1 ± 0.2	82.4 ± 7.8
PDMS+	94.6 ± 2.2	-	2.3 ± 0.5	2.8 ± 0.3	8.1 ± 1.0	254.7 ± 85.3

As expected, the PDMS 5:1 mixing ratio of elastomer and curing agent was stiffer (2.4 ± 0.5 MPa) than the 10:1 mixing ratio (1.1 ± 0.2 MPa). The Young's modulus of PDMS+ (2.3 ± 0.5 MPa) is a bit stiffer than PDMS 10:1 and just as stiff as PDMS 5:1. The difference between PDMS+ and PDMS 10:1 can be explained by the different curing procedure. The thermal curing of PDMS+ is longer and at a higher temperature, resulting in a higher stiffness. Ostemer 324 (5.2 ± 1.3 MPa) is stiffer than PDMS 10:1. Ostemer 220 (1.4 ± 0.2 MPa) compares well to PDMS 10:1, and is as expected based on the material data sheet lower than Ostemer 324 [38].

For Ostemer 324, the Young's modulus was determined for 3 different UV curing times (60, 40 and 20 seconds), to determine whether there is a relation between curing time and Young's modulus. From the data (Table 9) can be concluded that there is no significant difference between the Young's modulus and UV curing time for Ostemer 324 based on a one way ANOVA test. However the sample size is small (n=4, n=3, n=3 for 60 s, 40 s and 20 s respectively). A larger sample size is needed to really confirm these results.

The yield point on the stress strain curve indicates the limit of the elastic range of the material. Below the yield point the material will return to the original shape and above the yield point the material is deformed permanently. The yield point for PDMS 10:1, PDMS 5:1 and PDMS+ are similar (2.3 ± 0.6,
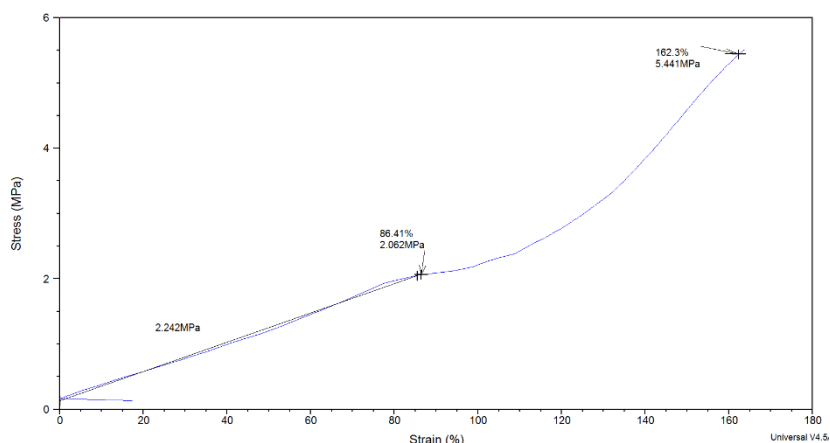

Figure 32: Stress-strain curve output from the DMA showing a single measurement for PDMS 5:1.

2.7 ± 0.4 and 2.8 ± 0.3 MPa). The yield point for Ostemer 324 is almost twice as large (4.2 ± 0.9 MPa) while the yield point for Ostemer 220 (1.0 ± 0.3 MPa) is about half compared to PDMS and PDMS+.

The fracture point is the point where the material breaks and separates into two pieces. Notable is that PDMS 10:1 and Ostemer 324 have very similar values (4.4 ± 1.8 and 4.8 ± 1.2 MPa) and the point is much lower for Ostemer 220 (1.1 ± 0.2 MPa). The values are again very similar for PDMS 5:1 and PDMS+ (8.3 ± 1.6 and 8.1 ± 1.0 MPa).

Finally the strain until break shows the percentage of change in length between the starting length and the length at the breaking point. Here both Ostemers have lower values in the range of 80 to 90% compared to the other materials with a 200 to 260% range.

According to the data provided by the company supplying the Ostemers (Mercene Labs), for Ostemer 220 the Young's modulus is 10-30 MPa [38], compared to 1.4 ± 0.2 MPa in our measurements. For Ostemer 324 the Young's modulus is provided as 30 MPa and the strain until break as 30% [37]. Our measurements show a lower Young's modulus of 5.2 ± 1.3 MPa and strain until break of 89.3 ± 3.4%. This difference between the reference data and the current measurements can be explained by the sensitivity of the material to the mixing ratio, layer thickness and intensity of curing, both UV light intensity and the thermal curing temperature. The reference data used much larger samples for their stiffness measurement. The company confirmed that curing intensity and time combined with a different size of material sample can result in differences during the curing process and therefore result in differences in the resulting stiffness of the material compared to the reference data. Furthermore, Ostemer 220 is possibly affected by the use of isopropanol in the sample preparation.

Conclusion

The stiffness measurements for the materials provides important data for future use of the materials. The overall differences between the materials are not large and falls within a range of 1 to 5 MPa. The stiffness of the new materials does not differ greatly from PDMS, and the materials could therefore in terms of stiffness be compatible with similar applications of PDMS. Further testing with tissues or moving components is needed to see whether the materials are suitable for more specific applications.

3.2.2 Nano-Indentation test

To determine the stiffness of the moulded pillars (Chapter 2.1.2), nanoindentation was performed on moulded pillars of each material using a FemtoTools Nanomechanical testing system (FT-NMT03). The tool uses a silicon-tip sensing probe to apply force and measure displacement of in this case the elastic pillars (Figure 33). Single pillars were cut out from the moulded substrate. The dimensions (*L, w, h)* of each micropillar were first determined with a Keyence VK-X250 laser microscope. The pillars were then mounted on a sample holder

Figure 33: Setup of the nanoindentation tool. The image shows the circular sample platform with the silicon sensing probe touching one of the pillars.

of the nanomechanical system next to the sensing probe. The probe was positioned at a predetermined height halfway the width of the pillar. During the measurement, the probe applied force to the micropillar until a set force value was met (Figure 34). The displacement of the tip was measured continuously by a piezo-scanner. After reaching a set displacement or set force, the tip stops applying

force and is pushed back by the micropillar moving back to its original position [15]. This force was also measured. The slope of the resulting force-displacement curve of the returning pillar movement represents the stiffness of the pillar k. Multiple measurements were performed along the height of three pillars for each material.

Equation 2 for cantilever beam displacement y at position x along a beam with a load F on position a along the beam, was rewritten for E (Young's modulus). The measured stiffness k [N/m] was corrected for the 15° angle of the probe to obtain the horizontal vector of F. Using the measured pillar dimensions and horizontal vector k, the average Young's modulus for the micro pillars was calculated. The results are shown in Table 10.

$$y = \frac{Fx^2}{6EI}(3x - a)$$ (2)

$$E = k\frac{2x^3}{0.5wh}$$ (3)

Table 10: Young's moduli of materials based on nanoindentation of moulded micro-pillars.

Material	Young's Modulus [MPa]
PDMS	0.80 ± 0.25
Ostemer 324	4.46 ± 1.98
Ostemer 220	1.15 ± 1.24
PDMS+	1.25 ± 0.64

The measurements for Ostemer 220 were challenging as the pillars were not fully formed and the pillar substrate was slightly tilted for some of the samples. The variability of the overall data is quite large. More measurements are needed to confirm the results. The current results do compare well to the results from the uniaxial tensile test, where Ostemer 324 is also the stiffest material, followed by PDMS+, Ostemer 220 and PDMS.
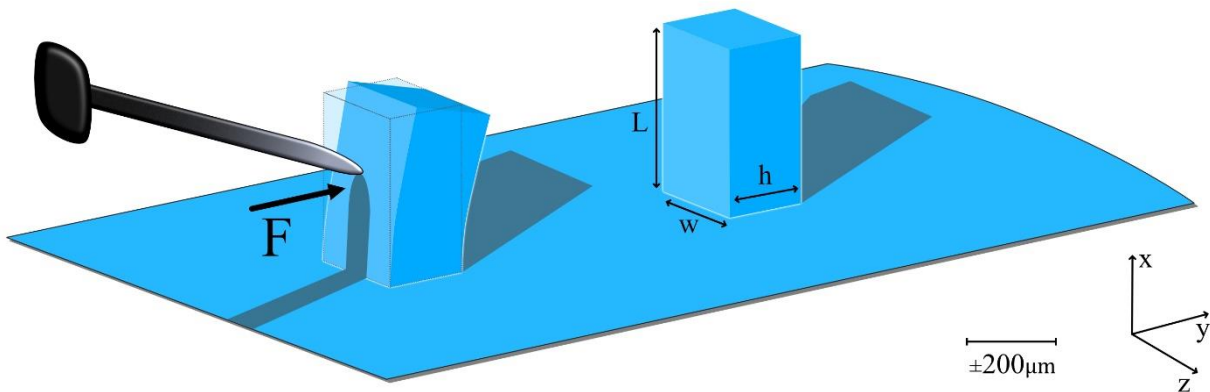

Figure 34: Illustration of bending micro pillars from an EHT under applied load during nanoindentation. The probe applies a force under 15° angle, measuring displacement of the pillar and the backwards pushing force of the elastic pillar during the returning movement of the probe.

3.3 Optical Transparency

The material used as a substrate in an OoC should be transparent enough to be compatible and not interfere with microscopy and other monitoring techniques. The material should also have a low amount of auto fluorescence and low absorbance of light. For example when using fluorescent microscopy, light absorption by a material decreases the sensitivity of the fluorescence assays, by reducing the total fluorescence. Not only absorption of light, but also auto fluorescence of the material decreases sensitivity of fluorescence assays, as it increases the total fluorescence [46], [55]. The transparency and fluorescence of the material are thus important properties as they affect the data quality of visualization and monitoring techniques.

Transparency of a material is important for imaging of the samples or devices. This can pertain to imaging of material structures, or imaging of cells on top or within the material. For biological imaging, the visible light spectrum is the most important. Imaging can be done either by regular bright field microscopy, or, to increase resolution, with fluorescent microscopy. In fluorescent microscopy, fluorescent dyes are used to stain sample structures. Each component of a cell reacts best to a specific dye, and in turn each dye has its own emission spectrum. For example, cell nuclei can be imaged with a yellow dye, and the actin of the cell with a red dye, to give a high resolution image where the structures can be seen in detail. A light source in the microscope excites the dye within the sample, to which the dye emits light back into a detector [56], [57]. This measured emission spectrum is a specific wavelength or range of wavelengths depending on the dye and is referred to as a channel. The wavelengths 405 nm (blue), 488 nm (green), 594 nm (orange) and 647 nm (red) are frequently used channels for fluorescent imaging [58]. These wavelengths are indicated as vertical lines within the shown measurement results (Figure 36). This section will show the result of a transparency test, measuring the transmittance of light through the material.

3.3.1 Transmittance Measurement

The transparency of PDMS, Ostemer 324, Ostemer 220 and PDMS+ was tested by transmittance measurements using a PerkinElmer Lambda 1050+ UV/VIS/NIR spectrometer at the Photovoltaic Materials and Devices department of TU Delft. The machine transmits a beam of light through the sample towards a detector to determine the percentage of incident light that passes through the material and reaches the detector, depending on its wavelength. The tested samples were four membranes each for all four polymers, 3x3 cm^2 in size with a thickness of approximately 70μm. The transparency was measured for wavelengths between 350 and 750 nm in increments of 5 nm. Figure 35 shows me positioning a sample in the clamp of the spectrometer. Figure 36 shows the measurement results.
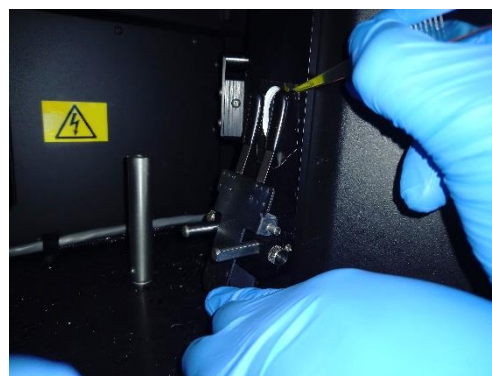

Figure 35: Sample of Ostemer 324 placed in the clamp of the spectrometer

The materials have a transparency ranging from 90% to 94% in the visible light spectrum (~400 to 700 nm) measured at 400 to 750 nm, where PDMS is the most transparent. PDMS is also the most transparent in the UV light spectrum (10 to 380 nm), measured at 350 to 400 nm, while the transparency for the Ostemers drops in the UV spectrum to around 85%. The datasheet provided by the Ostemer company indicates a transparency of 97% from 370 nm to 1200 nm for Ostemer 324 [37], which is higher than the measured values. The performed test only measured up until 750 nm. The datasheet also indicates an absorption of light below 380 nm, which corresponds to the measured

data. This difference between the reference data and the current measurements can be explained by the sensitivity of the material to different mixing ratio and intensity of curing, for both UV light intensity and thermal curing temperature and time.

Conclusion

As Figure 36 shows, the materials are all transparent for the indicated commonly used channels for fluorescent dyes, as well as in the visible light spectrum and are therefore suitable for bright field microscopy and fluorescent imaging. Additional testing can provide more information on the possible auto-fluorescence and absorption spectrum of the materials. The current transparency is suitable for the biocompatibility test and fluorescent measurements in the upcoming absorption test.
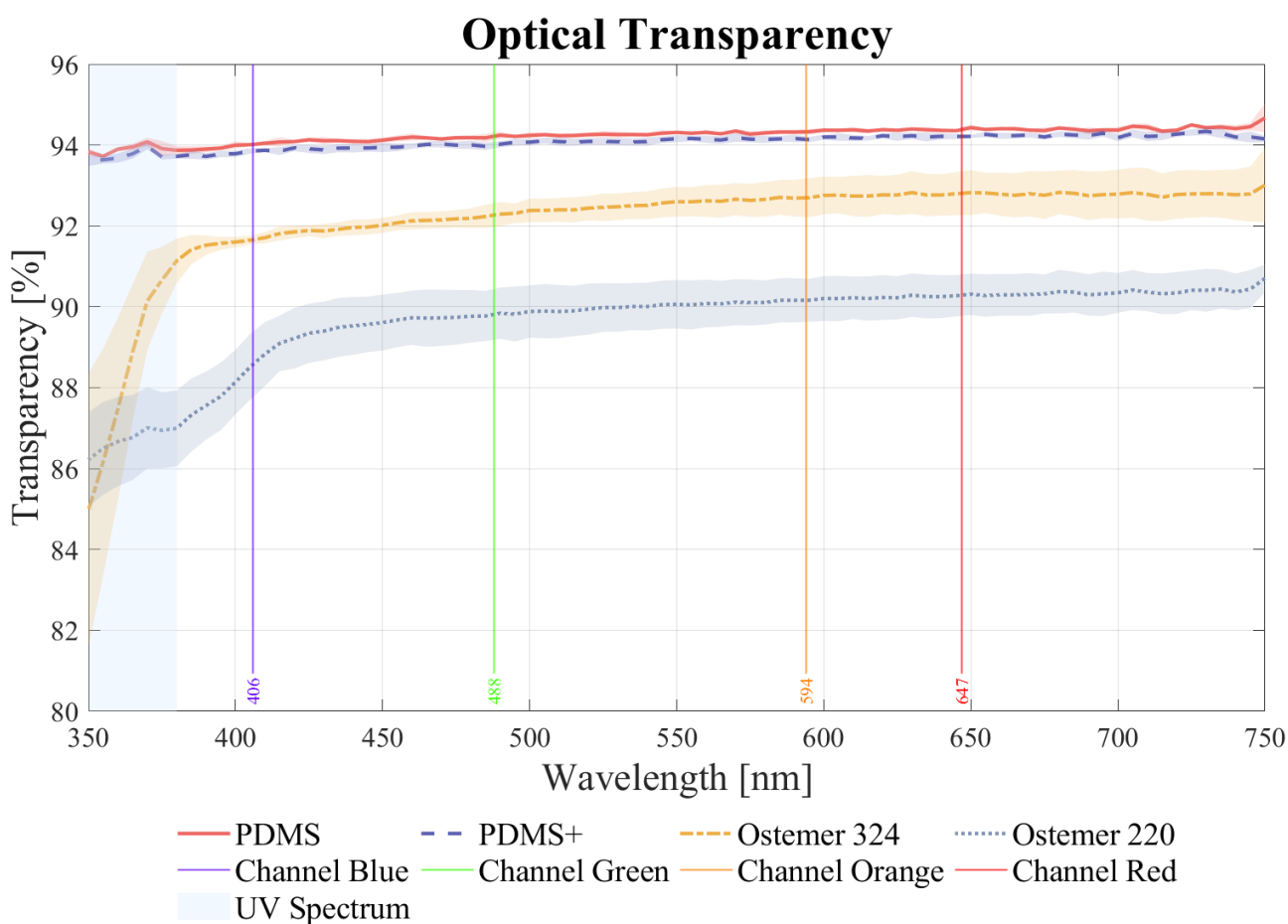

Figure 36: Transparency measurement of the materials, by percentage of light that passes through the sample depending on wavelength. Vertical lines roughly indicate the channels commonly used in fluorescent microscopy. The shaded area indicates the UV light spectrum below 380nm. The x-axis shows a representation of the corresponding colour to the wavelength.

4 Biological Characterization

This chapter will examine the biocompatibility of PDMS, Ostemer 324, Ostemer 220 and PDMS+ in terms of cytotoxicity and cell morphology directly; by seeding cells on material samples and indirectly; by incubating the cells with medium that was conditioned by the material samples. Biocompatibility tests were performed by A. Othman, biologist at Bi/ond. Absorption of small molecules by the materials will be tested as well using a fluorescent dye and fluorescent imaging techniques. The absorption test was performed at the Bionanoscience Department of the faculty of Applied Science (TU Delft) and executed by Dr. J. Capoulade.

4.1 Biocompatibility

Biocompatibility of the material is important when cells are used in OoC devices for testing. Biocompatibility is a general term, relating to the interaction between the material and a biological system. For this thesis, the relevant factors for biocompatibility are considered to be non-cytotoxicity and the effect on cell morphology. The material should ideally be non-toxic and improve cell adhesion between the cells and the material, as well as between cells. Cell adhesion can be adjusted by surface hydrophilicity and surface morphology (roughness). The tests performed in this thesis are not set to optimise the cell adhesion, rather to give a first indication of toxicity and the effect of the new materials on cell morphology. Other examples of factors for biocompatibility are for example non-immunogenic, non-thrombogenic and non-carcinogenic [59].

4.1.1 Biocompatibility Tests

Biocompatibility of the materials was determined with two tests, both performed twice. First round of tests included PDMS, Ostemer 324 and Ostemer 220. The layer thickness of the materials were 70.8 ± 1.8 μm (800 rpm 50 sec), 76.1 ± 0.1 μm (500 rpm 60 sec) and 632 μm (tilted by hand) respectively. The second round of the tests included PDMS, Ostemer 324, Ostemer 220 and PDMS+. The layer thickness of the materials were 70.8 ±1.8 μm (800 rpm 50 sec), 76.1 ± 0.1 μm (500 rpm 60 sec), 78.8 ± 2.0 μm (300 rpm 30sec) and 73.2 ± 2.1 μm (750 rpm, 30 sec) respectively.

Biocompatibility and specifically cell morphology is affected by surface energy, hydrophilicity, topography and surface functional groups [60]. Therefore, the tests were performed with a non-plasma treated sample set and a plasma treated sample set. As discussed in Chapter 3, plasma treatment increases surface hydrophilicity of the materials, which is beneficial for cell attachment.

4.1.1.1 Polymer Preparation

Squares of 1x1 cm^2 were prepared for this test. These squares were sterilized by submerging them for 10 mins in 70% ethanol solution and subsequently cleaned for 10 mins submerged in DI water. For each material two samples were tested. One sample of each material was plasma treated in Diener low pressure plasma system (ATTO-BL-PCCA) for 3 mins at 20 W to improve hydrophilicity. A second round of testing included twelve samples for each material, for which six samples were plasma treated for 6 mins at 20 W and six samples were not plasma treated. The samples were brought to the lab for the biocompatibility test directly after plasma treatment to minimize the effect of hydrophobic recovery.

4.1.1.2 Cell Preparation

Human dermal microvascular endothelial cells (HMEC-1, cat# CRL-3243™) were commercially acquired (ATCC, USA). Cells were grown in MCDB131 basal medium (without L-Glutamine; Life Technologies cat# 10372019) containing 10 ng/mL Epidermal Growth Factor (EGF; Thermofisher cat# PHG0314), 1 µg/mL Hydrocortisone (Sigma cat# H0396), 10 mM Glutamine (ATCC 30-2214), and Fetal Bovine Serum (FBS; ATCC 30-2020) to a final concentration of 10%. Cells were passaged upon reaching 80-90% confluency using Trypsin-EDTA solution (ATCC 30-2101).

HMEC-1 cells were harvested from their culture flasks by trypsinisation and centrifuged at 125 g for 6 minutes. The pellet was re-suspended in MCDB131 full growth medium at a concentration of 2x105 cells/mL.

4.1.1.3 Conditioned Cell Culture Medium Biocompatibility Test

The first test was an indirect and qualitative measurement of biocompatibility. The material samples were incubated in MCDB131 full growth medium at 37°C for 1 and 24 hours (24-48 hours for the second round) before removing them again from the medium (Figure 37). Control medium was incubated without test samples. 100 µl of HMEC-1 cell suspension (at a concentration of $2x10^5$ cells/mL) was seeded in each well of a 96-well plate. The cells were left to grow to confluency for 48-72 hours. At complete confluence (referring to the surface coverage of adherent cells), the growth medium was aspirated and replaced with the conditioned medium from the test samples. The cells were cultured in the conditioned medium to check the cell lividity at three different time points: 0, 24 and 48 hours for the first round (24 and 48 hours for the second round). The biocompatibility was determined visually based on bright field images taken using a Juli™ smart fluorescent cell viewer. The ratio of living and death cells on the image determines the biocompatibility. If the cell culture medium absorbed toxic components of the material, cell lividity would be affected. The tested conditions were compared to cells incubated with unconditioned medium, where there occurs a basal levels of cell debris and cell death.

The test was performed twice on PDMS, Ostemer 324 and Ostemer 220, and once on PDMS+. The results, based on visual comparison, are shown in Table 11
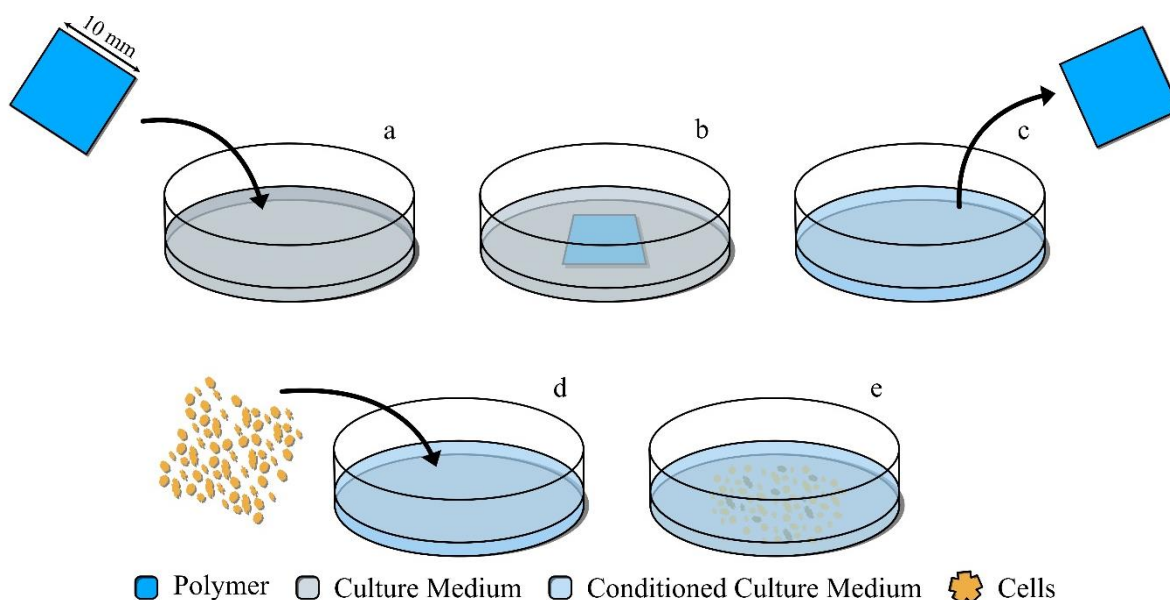

Figure 37: Schematic view of biocompatibility test 1. (a) Polymer membrane added to cell culture medium. (b) Incubated for 1 and 24 hours. (c) Polymer membrane removed. (d) Cells added to culture medium. (e) Cells were cultured for 0, 24 and 48 hours and visually checked for lividity.

Table 11: Biocompatibility: conditioned cell culture medium. Results of round 1 and round 2 of indirect biocompatibility test trough incubation of cell culture medium. There was no difference between the plasma treated and non-plasma treated samples.

Material	Round 1		Round 2	
	Thickness	Result	Thickness	Result
PDMS	70.8 ±1.8 µm	Biocompatible	70.8 ±1.8 µm	Biocompatible
Ostemer 324	76.1 ± 0.1 µm	Biocompatible	76.1 ± 0.1 µm	Biocompatible
Ostemer 220	632µm	Biocompatible	78.8 ± 2.0 µm	Incompatible
PDMS+	-	*Not tested*	73.2 ± 2.1µm	Biocompatible

The images show that during the first round for three materials the cells did not die more than expected for both plasma an non-plasma treated samples (see Appendix D), indicating biocompatibility for PDMS, Ostemer 324 and Ostemer 220. The test is not sufficient to quantify the result. The second round showed a different result (Figure 39). Biocompatibility was again confirmed for PDMS and Ostemer 324. Biocompatibility was also indicated for PDMS+, showing no difference between plasma treated and non-plasma treated samples. However, all samples of Ostemer 220 resulted in a large number of dead cells, indicating a toxicity of the material. The cell death appeared in both plasma and non-plasma treated samples and for each sample, ruling out contamination. No signs of contamination were observed in the cell culture or cell medium. The cell death might be explained by the use of isopropanol and photoresist in the preparation process of the loose membrane samples for Ostemer 220 (see Section 2.1.1.1).

4.1.1.4 Direct Cell Seeding Biocompatibility Test

The second test was a more direct test for biocompatibility, yet still qualitative. The polymer samples were transferred to a 24-well plate (three samples for each condition). The cells were seeded directly on top of the material to determine the interaction of the cells with the material and the cells with each other (Figure 38). 500 µl of cell suspension (at a concentration of $2x10^5$ cells/mL) was added on top of the material samples and the plate was then transferred to the incubator at 37 °C. The medium was changed every 24 hours. The result was determined visually based on bright field images at 4x magnification after 1 and 24 hours after cell seeding (24 and 48 hours for the second testing round) with a Juli[TM] smart fluorescent cell viewer. Biocompatibility is determined visually based on cell adhesion, cell morphology and cell proliferation.

This test was also performed twice on PDMS, Ostemer 324 and Ostemer 220, and once on PDMS+. In round one, the microscopy images show that the cell morphology and proliferation is as expected (appendix D). Additionally, the cells did not die more than expected, indicating PDMS and Ostemer 324 to be biocompatible. Unfortunately, the sample for Ostemer 220 was too thick (632µm) and the surface too rough for sharp imaging. The cells seeded on top of the layer could not be visualized. A new method was used to prepare a thinner Ostemer 220 sample for additional tests (described in Section 2.1.1.1). The Ostemer 324 in the non-plasma treatment even performed as good as PDMS in the plasma treated sample.
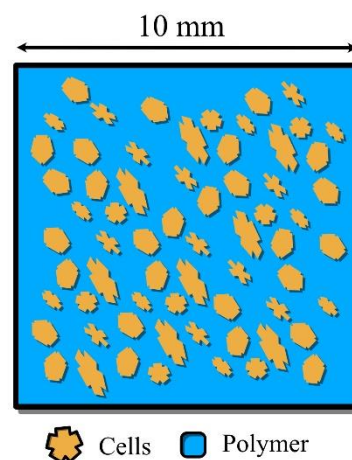

Figure 38: Schematic view of biocompatibility test 2: direct seeding of the cells on a polymer membrane. (Cells not to scale).

Biocompatibility: Conditioned Medium (48h)

PDMS plasma
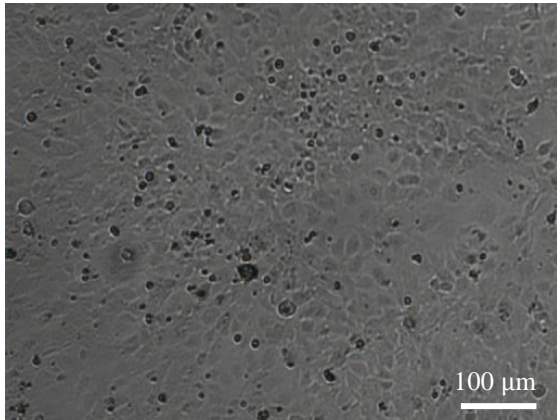
Ostemer 324 plasma
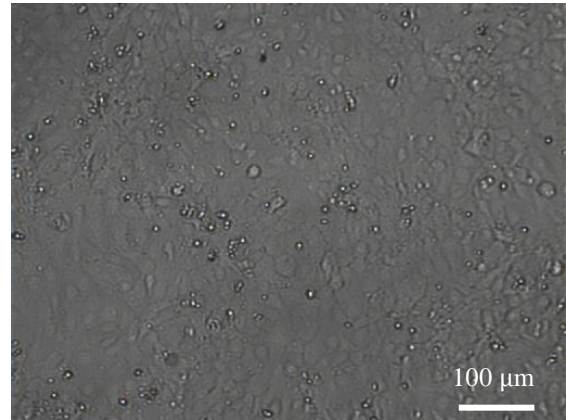
Ostemer 220 plasma
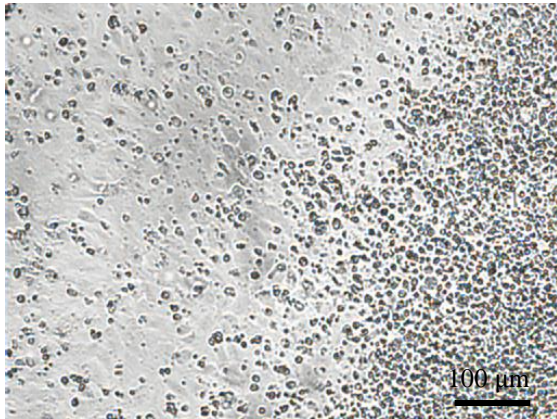
PDMS+ plasma
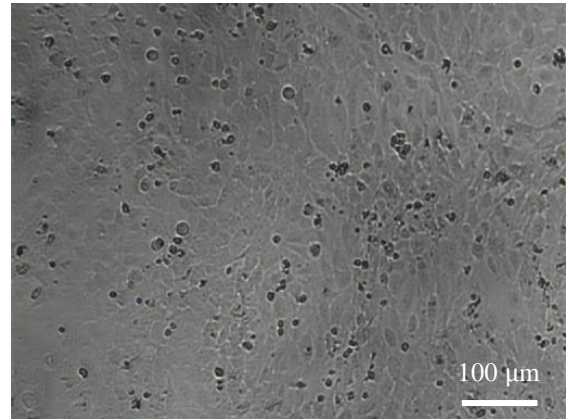
Control
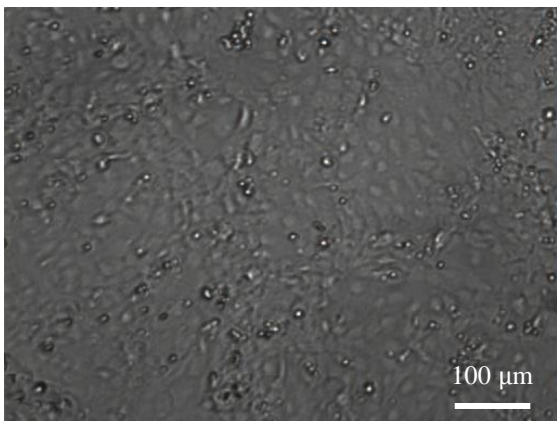
Figure 39: Conditioned medium biocompatibility test round 2. Brightfield imaging at 4x magnification of human dermal microvascular endothelial cells seeded in a 96-well plate with growth medium grown until confluency (48-72h). Then the growth medium was replaced with conditioned medium from the test samples. Images taken 48h after addition of conditioned medium. Images for non-plasma treated samples look similar to the plasma treated samples. The control was performed with unconditioned medium.

The results of round two are shown in Table 12. Round two of direct cell seeding showed an increase in confluence for Ostemer 324 and PDMS+ for both plasma treated and non-plasma treated samples between the 24 hour and 48 hour time point. The 48h confluence for Ostemer 324 (85-95%) and PDMS+ (70-75%) at the non-plasma treated samples where already better than PDMS in the plasma treated sample (50-60%). PDMS was equal for the plasma treated samples at 24 and 28 h (50-60%). The PDMS non-plasma treated sample showed only a 5-10% confluence (Figure 40).

Table 12: Biocompatibility: direct cell Seeding. Results of round 2 of direct cell seeding test for biocompatibility.

Material	Thickness [µm]	24h Confluence	48h Confluence	Result
PDMS	70.8 ±1.8			
Plasma		50-60%	50-60%	Biocompatible
Non-plasma		10%	5-10%	Low compatibility
Ostemer 324	76.1 ± 0.1			
Plasma		70-85%	85-95%	Biocompatible
Non-plasma		70-85%	85-95%	Biocompatible
Ostemer 220	78.8 ± 2.0			
Plasma		0%	0%	Incompatible
Non-plasma		0%	0%	Incompatible
PDMS+	73.2 ± 2.1			
Plasma		50-60%	85-90%	Biocompatible
Non-plasma		50-60%	70-75%	Biocompatible

Conclusion

An indirect biocompatibility test, incubating material samples in cell culture medium, indicated non-toxicity for PDMS, Ostemer 324, and PDMS+. The direct seeding of cells on these materials also showed promising results. Ostemer 324 and PDMS+ appear to have improved biocompatibility compared to PDMS in terms of cell attachment and morphology already in non-plasma treated samples and even better in plasma treated samples. This is very promising for Ostemer 324 and PDMS+, as the previous wettability testing (Chapter 3) indicate that the surface hydrophilicity after plasma treatment is maintained longer compared to PDMS, and therefore the window for desirable cell attachment is longer. Biocompatibility of Ostemer 220 was confirmed with the first conditioned medium test. However, in the second round of testing both direct and indirect tests showed very poor biocompatibility for Ostemer 220 indicated by a large number of dead cells. This might be explained by the preparation method of the samples that included photoresist and isopropanol. Additional testing with other types of cells and more quantitative tests is needed in the future to confirm the biocompatibility of the materials.

Biocompatibility: Direct Cell Seeding (48h)

PDMS plasma: 50-60%

PDMS non-plasma: 5-10%
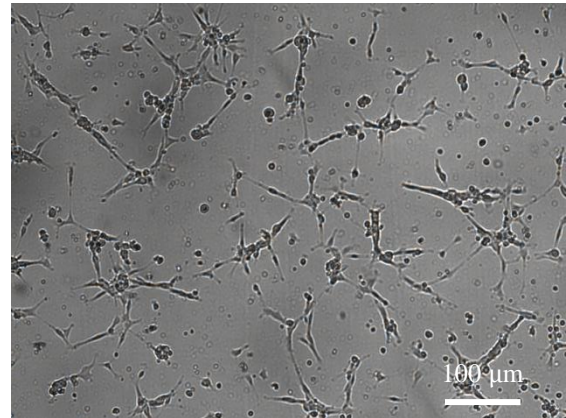
Ostemer 324 plasma: 85-95%
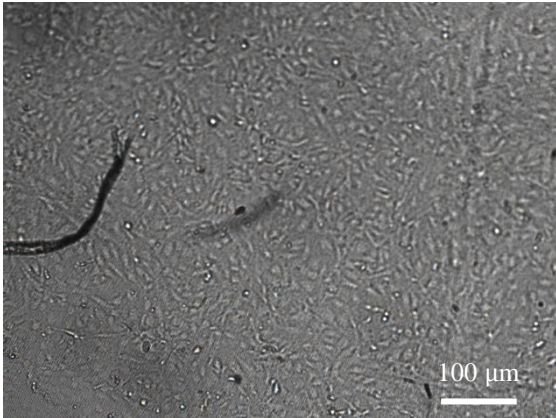
Ostemer 324 non-plasma: 85-95%

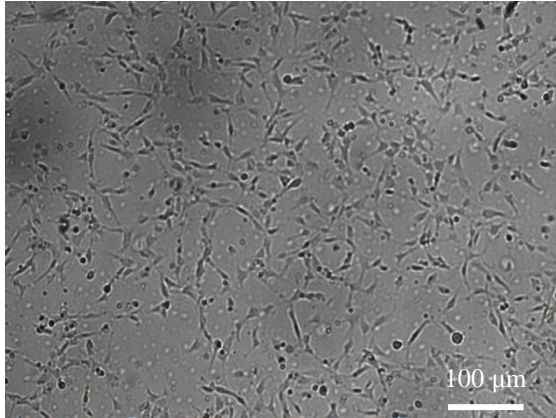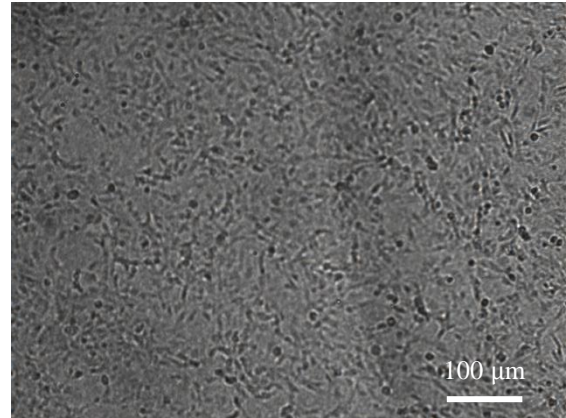### Ostemer 220 plasma: 0%
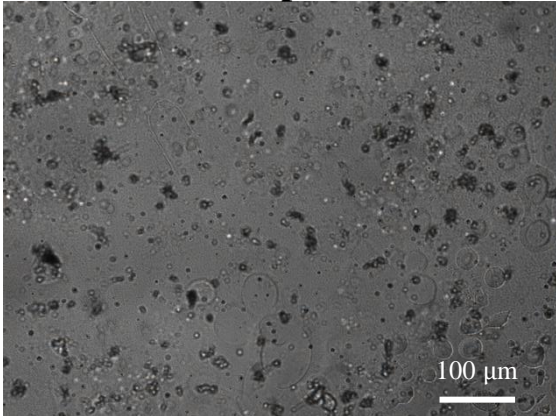
Ostemer 220 non-plasma: 0%
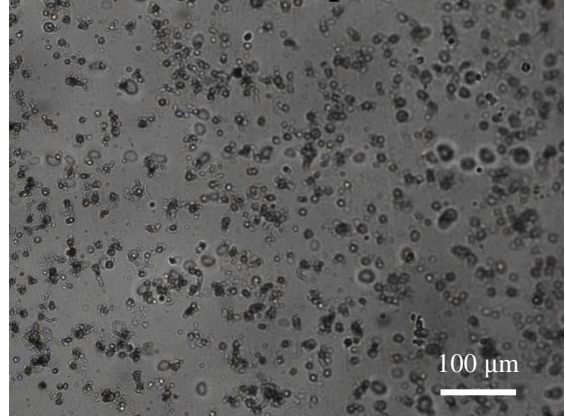
PDMS+ plasma: 85-95%
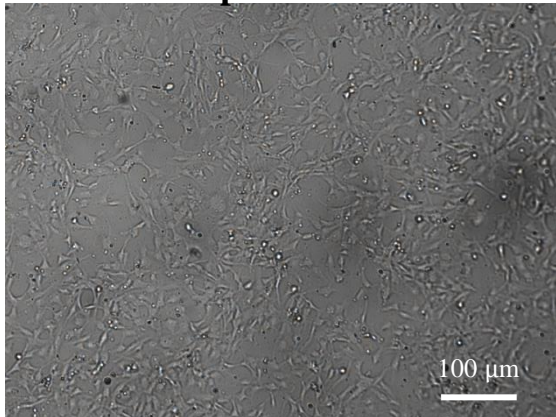
PDMS+ non-plasma: 70-75%
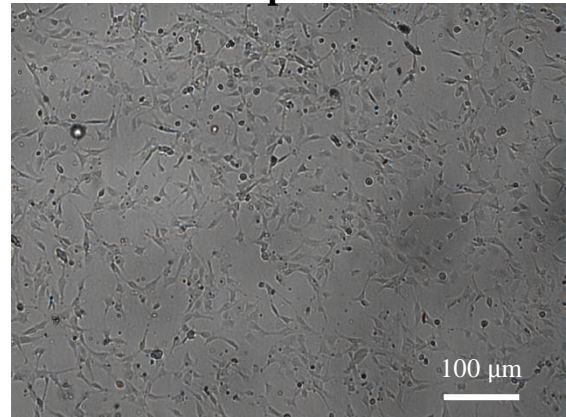
Figure 40: Brightfield imaging at 4x magnification of human dermal microvascular endothelial cells seeded directly on polymer membranes of PDMS, Ostemer 324, Ostemer 220 and PDMS+, 48 hours after seeding.

4.2   Absorption

Absorption is defined as the accumulation of molecules from a liquid into the bulk volume of a material in contact with this liquid, whereas adsorption is defined as the accumulation of molecules on the exposed surface of the material [61]. Previous works have shown that small molecule absorption for OoC polymers reduces the available drug dose inside OoC models [62]. As a consequence, when testing drugs on tissue this can cause misrepresentation of effect and dosage of the drugs. Due to the absorption, part of the drugs can remain inside the material or cross into other microfluidic channels instead of completely reaching the tissue [5], [62]–[64].

In a suitable material, the rate of absorption should be limited or at least known. Predicting the level of absorption in an OoC is not an easy task, as absorption depends on several factors such as medium concentration, fluid velocity, channel size, temperature, experimentation time and diffusion coefficient for the specific drug for the specific material [63]. Due to the influence of these many factors, it is challenging to establish a quantitative value for drug absorption.

Absorption is more pronounced in microfluidic devices because of their size. As the size of channels becomes smaller, the surface-to-volume ratio increases and thus the effect of surface properties increases [39], [65], stressing the importance of finding a material with reduced absorption properties.

4.2.1   Experimental Design

Based on existing literature on material absorption, I developed an absorption test to characterize and compare the polymers tested in this thesis. To measure the absorbance, a fluorescent dye was added to the material, incubated to promote absorption, removed and then the fluorescent intensity remaining in the material was measured as an indicator of absorption.

According to Nianzen Li *et al.*, several dyes can be used to test absorption as they mimic chemical characteristics of commonly used drugs [66]. Characteristics such as molecular weight, hydrophobicity, hydrogen-bond donor atoms and sum of nitrogen and oxygen atoms that affect the absorption of the compound [66]. Besides the compound itself, the properties of the substrate also affect the absorption. Because PDMS is hydrophobic, and has a porous structure, these drug-like compounds penetrate into PDMS. Many variables need to be taken into account when performing an absorption test, for example, as reported in the literature, the diffusion rate of the molecules within the solution, the characteristics of the dye dissolved in a solvent and the possibly changed characteristics of this same dye once absorbed in a material. According to Nianzen Li *et al.* and Toepke *et al.* and Beebe and Brewer *et al.*, Nile Red can be used as the fluorescent dye for such kind of studies [62], [66]–[68]. Nianzen *et al.* do note that the emission spectrum of Nile Red changes in non-polar environment, which is the case once it is absorbed by PDMS, and therefore the solution concentration in the well in relation to the concentration within the material cannot be quantified based on imaging. The fluorescence of the Nile Red dye in the experiment thus needs to be measured only within the material after absorption, which indicates an absorbed amount of molecules, but this amount cannot exactly be quantified based on the solution concentration. Nile Red was readily available and ordered from Sigma Aldrich (mw 318.37).

The intention of the developed absorption test was to mimic the experiment of Toepke *et al.*, where 1 µM solution of Nile Red in dimethyl sulfoxide (DMSO) was put in a microchannel and incubated for 1 minute, and then rinsed with DI water. They made multiple images on different time-points by adding dye to the same channel repeatedly, incrementally increasing the incubation time. The cross-section of the channel showed an absorption halo from the edge of the channel into the material. More papers confirmed they used a solution of Nile red in pure DMSO, or after dissolving in DMSO it was again diluted in phosphor buffered saline. The concentrations of Nile red used in

pure DMSO was 1 μM. Incubation time differed between one minute and 90 minutes. Based on the images of Toepke *et al.*, of incubation of 2 minutes and 6 minutes, and the solution in Yao *et al.*, a 3 minute incubation period was chosen for a 1 μg/mL concentration [67]. The absorption reached over 100 μm in the Toepke experiment, so we expected a result on the same scale. Many experiments in literature were done over time, however we decided to only measure one time-point in our experiment to first check whether the set up would work at all.

4.2.2 Absorption Test

The experimental setup was as follows. Membranes from the polymer, about 70 to 80 μm-thick, were cut in squares of 1 by 1 centimetre. A hole with a diameter of 5 mm was punched in the middle using a biopsy needle (Figure 41a). 60 μl Nile Red, dissolved in DMSO at 1 μg/mL, was added to the hole, incubated for three minutes and subsequently removed and flushed with DI water (Figure 41b and c). A Nikon Eclipse Ti inverted fluorescent microscope with A1R confocal module was used to image the edge of the hole, as shown in Figure 41d. The test was performed on one sample each of PDMS, Ostemer 324, Ostemer 220 and PDMS+. The layer thickness of the materials were 70.8 ± 1.8 μm (800 rpm, 50 sec), 76.1 ± 0.1 μm (500 rpm, 60 sec), 78.8 ± 2.0 (300 rpm 30 sec) and 73.2 ± 2.1 μm (750 rpm, 30 sec) respectively. The absorption test was executed by Dr. J. Capoulade.

Surprisingly, Ostemer 324 and Ostemer 220 were affected by the dye or solution and crumbled and dissolved, making them unsuitable for imaging. The material safety data sheet (MSDS) for Ostemer 324 indicates resistance against DMSO [37], the MSDS for Ostemer 220 does not mention it under resistant chemicals [38]. After contacting the company (Mercene Labs) they confirmed that indeed Ostemer 324 does partly absorb DMSO in the material matrix and that this information should be corrected in the data sheet. PDMS and PDMS+ could be tested and imaged without problems.
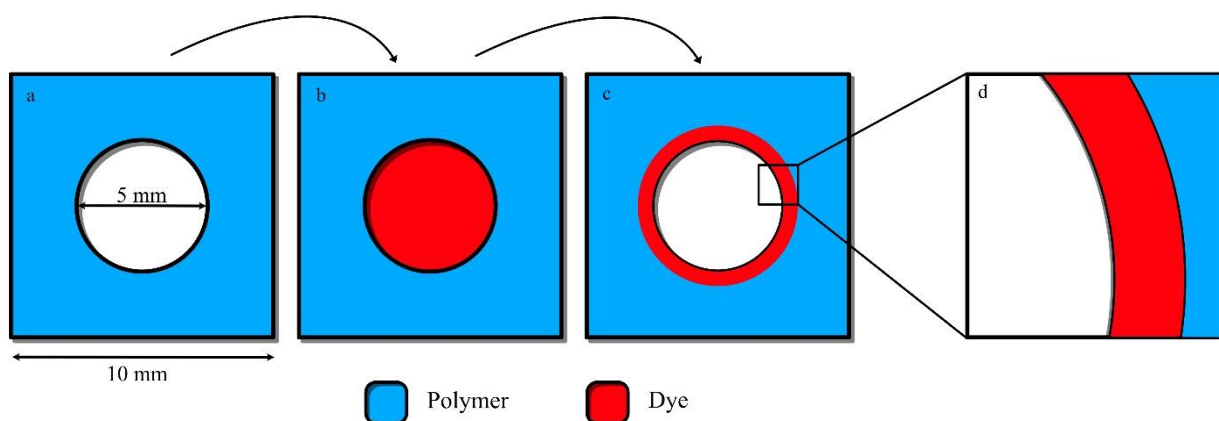
Figure 41: Schematic representation of absorption test. (a) Polymer membrane sample with hole punched in the middle. (b) 60 μl dye is added for 3 minutes. (c) Dye is removed leaving the laterally absorbed molecules within the material. (d) Expected result taken as a stacked image with a confocal fluorescent microscope.

Of both samples (PDMS and PDMS+), 3 images where made on different locations along the edge of the hole. Of each sample, 3 images where taken. Each image is a stack of 31 to 40 images covering the material sample from bottom to top. I averaged these stack images, resulting in a single image of the average intensity of fluorescence within the material indicated by the grey value (Figure 42). Images of PDMS and PDMS+ showed the expected pattern of absorption into the material as predicted in Figure 41. The images show a high intensity of fluorescence at the edge of the material, with a reduction in intensity along the x axis (towards the right in the image). The images were analysed using ImageJ software.

From the averaged images, which were rotated until the material edge was straight, in the y axis, the cross-section was plotted to show a fluorescence intensity profile along the x axis, indicative of the profile of absorption from the edge of the hole inwards into the material along in the xz plane. Figure 43 and Figure 44 show individual measurements of the profile as well as their average. The maxima of the graphs are aligned on the arbitrarily chosen 100µm point. The data as well as the images are normalized based on the background fluorescence of the area without material (grey value of 50). The plots were made from a rectangular selection (see Appendix E), which results in a column average plot, where the x-axis of the graph is the horizontal distance of the selection and the y-axis of the graph shows the averaged pixel intensity indicative of the fluorescent intensity along the z axis of the sample plane. Figure 45 shows both averaged measurements for PDMS and PDMS+ including the standard deviation.
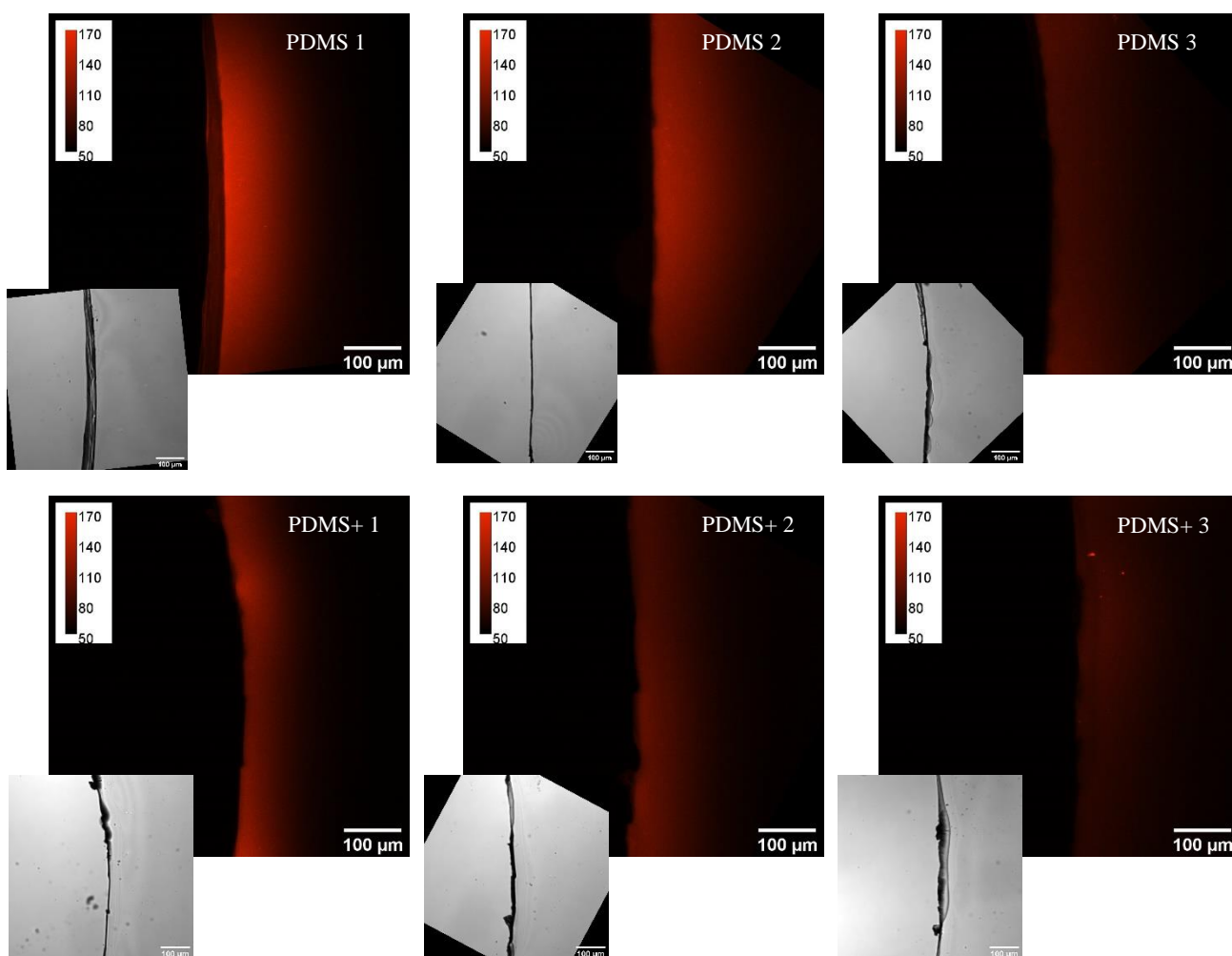
Figure 42: Z-axis projection of each image stack of the averaged fluorescent intensity (grey value). Three measurements for PDMS and three for PDMS+. Including an optical image of the corresponding material edge.

The measurements for PDMS+ are more consistent compared to the measurements for PDMS. The range of values for the PDMS measurements are quite large, and can possibly be explained by a tilt of the sample or tilt of the dye droplet within the well or by a different handling between the samples. Based on the averaged measurements, the maximum value of intensity is higher for PDMS (68.5 ± 28.9 grey value) than for PDMS+ (38.6 ± 10.7 grey value). When we look at the absorbed distance along the x-axis, the graph returns to a grey value of 10 at 196.9 µm from the material edge for PDMS and at 123.0 µm from the edge for PDMS+. Further along the x-axis, and thus deeper for the molecules into the material, the fluorescent intensity gets closer together for both materials. At

Molecule Absorption PDMS

Column average intensity profile x-axis
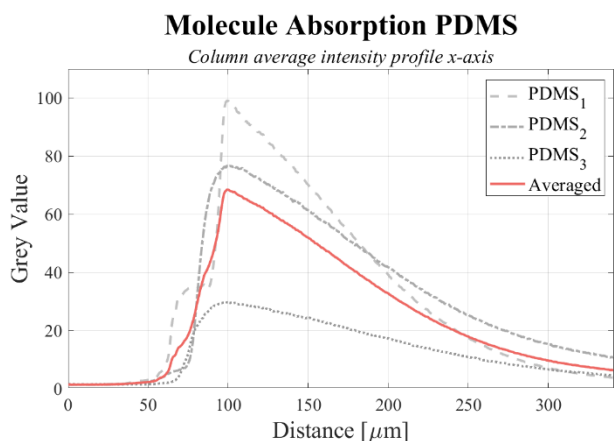
Figure 43: Three separate measurements of grey value for PDMS and the average of these three measurements.

Molecule Absorption PDMS+

Column average intensity profile x-axis

Figure 44: Three separate measurements of grey value for PDMS+ and the average of these three measurements.

200 µm distance from the edge of the material, intensity in PDMS is at 9.6 ± 3.9, while in PDMS+ at 4.3 ± 1.1. The distance travelled by the absorbed molecules, appears to be larger for PDMS than for PDMS+. The intensity does not return to the starting value outside of the material, within the measurement frame. Overall the absorption pattern is quite similar. The measurements for PDMS+ slightly overlap the standard deviation range of the PDMS measurements (Figure 45). The scale of these values compare well to the range of values from Toepke *et al.* at a 2 to 6 minute incubation time.

Molecule Absorption

Column average intensity profile x-axis

Figure 45: Averaged measurements of PDMS and PDMS+ with their corresponding standard deviation.

An error that can be expected in the experiment is the droplet of dye leaking underneath the sample, or even on top of the sample and thereby altering the intensity profile. To check whether this happened, the z-axis profile of the samples was plotted (Figure 46), and showed a larger intensity in the middle of the cross-section compared to the top and the bottom, confirming the dye did not leak. Figure 47 shows images of the sample cross-section of two separate measurements.

Additional measurements could give more clarity on the differences between these materials. Furthermore it would be very interesting to obtain data of absorbance over time, as well as with different dyes to get a better view of the absorption of different drug-like compounds. Another interesting thing to see is what would happen to the absorption profile on longer exposure with the dye, or at higher or lower

Molecule Absorption PDMS

z-axis profile

Molecule Absorption PDMS+

z-axis profile

Figure 46: Z-axis profile of fluorescent intensity for the cross-section of PDMS and PDMS+.

concentrations. Would the absorption reach deeper into the material, would the intensity increase or both. Likely there is a saturation point of absorption where an equilibrium between the solution and the material is reached. Future testing with a different solvent could give an indication of absorption for Ostemer 324 and Ostemer 220.

Figure 47: Cross-section (zx plane) of two individual absorption measurements for PDMS and PDMS+. The cross-section shows the diffusion pattern of absorbed Nile red molecules in the x direction.

The current test was successful for PDMS and PDMS+. PDMS and PDMS+ could, based on their material composition, be expected to have similar results. However the data does show that the dye is absorbed deeper into PDMS and with a higher intensity, compared to PDMS+. This difference could be related to the reduced speed of hydrophobic recovery that was seen in the PDMS+ material after plasma treatment, caused by the additional component or possibly be caused by the increased stiffness of the material.

Conclusion

Reduced absorption of small molecules by PDMS+ could indicate that, at least for a drug compounds with similar properties on which the Nile Red dye was selected, absorption of drugs molecules is less pronounced compared to PDMS. This can improve testing data of drug concentrations in PDMS based OoC platforms.

5 Discussion

The current standard for OoC substrate materials is PDMS. PDMS has many beneficial properties such as biocompatibility, transparency, elasticity and easy prototyping. The main disadvantages of PDMS are its hydrophobicity (reducing cell attachment and cell proliferation), quick hydrophobic recovery (within a few hours) after surface modification and absorption of small molecules, altering drug concentration during testing or causing cross-contamination between channels.

Ostemer 324 is a promising alternative material. The results of fabrication testing show the off-stoichiometric material can be easily spin coated and cured on both Teflon and SiO_2 coated silicon wafers. UV light quickly cures the material, however the additional thermal curing time is 2.5x longer compared to PDMS. Moulding an engineered heart platform turned out to be challenging due to the viscosity of the uncured material and pour adhesion with the mould, but was successful for a few platforms. An additional moulding test where a solvent such as isopropanol is added to the initial Ostemer mixture might make the material less viscous and could potentially improve the moulding process. In such a test we need to make sure that the isopropanol is completely removed at the end of curing and see whether this affected any of the other properties such as stiffness, wettability and biocompatibility.

A degassing test to determine compatibility with processing under vacuum unfortunately showed the material is only compatible for thin layers (9.1 µm-thick). Slightly thicker layers (18.8 µm) already need over an hour to degas in vacuum before the processing parameter is met. After degassing, the processing was performed: etching of Ostemer 324 was successful and resulted in sharp and fully etched holes (600 µm and 4 µm in diameter) through the polymer layer.

The material is 5x stiffer (5.2 MPa) than PDMS (1.1 MPa), which is not necessarily a problem depending on the OoC application. Differences between the measured stiffness and data from the company data sheet can be explained by the sensitivity of the material to its mixing ratio and curing procedure. Curing time of less than 60 seconds was tested and showed no differences. Interesting would be to see how longer curing times, as well as a higher UV light intensity will affect the material.

Ostemer 324 is almost as transparent as PDMS (92% vs 94% transparency in the visible range) and thus compatible for visualization techniques. The transparency of Ostemer 324 does drop to 85% in the UV spectrum range. It is biocompatible in terms of toxicity, cell attachment and cell proliferation. Ostemer 324 showed a larger confluence in a direct cell seeding test for both plasma and non-plasma treated samples (85-95%) compared to the best PDMS condition (plasma, 50-60% confluence). Its increased biocompatibility is very promising. Additional, more quantifiable testing is needed to confirm whether Ostemer 324 is indeed a better cell substrate than PDMS. It would also be interesting to see the interaction of cells in actual OoC platforms such as the EHT platform. Such a test combines the effect of the material surface, hydrophobicity and stiffness on cell adhesion, proliferation and maturation.

Absorption of small molecules is less compared to PDMS according to literature. Our test for small molecule absorption unfortunately failed for Ostemer 324 due to unexpected incompatibility with the used solvent DMSO. Additional testing with a suitable solvent will show a better comparison to PDMS. The gas permeability is reported to be less than in PDMS, which in the case of the EHT platform is not a problem, but could be in other types of designs that include membranes or microchannels. Finally, current costs of Ostemer 324 is about twice as much as PDMS.

The main advantage of Ostemer 324 is its hydrophilicity (CA of 62.2 ± 3.6°) and long window of hydrophobic recovery of 2 to 3 weeks, providing additional preparation time for samples before and during testing. Interesting would be to see whether a possibly stiffer material from longer/more intense UV curing will affect the rate of hydrophobic recovery. Optimization of the plasma treatment could reduce the initially reduced contact angle even more as well as elongate the hydrophobic recovery.

Ostemer 220 performed less well than Ostemer 324, and less well than PDMS. Spin coating the material was already problematic due to poor adhesion between the material and Teflon coated wafers. A new method using an additional photoresist layer between the silicon wafer and polymer made it possible to obtain loose membrane samples by dissolving the photoresist after curing. Curing the material is very quick as it only takes 60 seconds UV curing without additional thermal curing. Moulding the material into engineered heart platforms failed, as due to the poor adherence of the material the platforms in the mould were only partially formed. From the complete mould, only 3 individual micro-pillars were formed and 2 separate wells.

The degassing test was more successful compared to Ostemer 324, but less compared to PDMS. A 12.8 µm layer of cured polymer passed the test immediately. The next thickness tested of 78.8µm failed. Additional testing is needed to find a more precise thickness limit for vacuum processing. Etching the material was successful, with the same procedure as PDMS, sharp round holes were formed and fully etched trough the material.

The uniaxial tensile test showed a similar stiffness (1.4 MPa) compared to PDMS (1.1 MPa). The obtained Young's modulus form the nanoindentation test was in the same range (1.15 ± 1.24 MPa), however due to the poorly formed pillars these measurements have a large variability and can therefore not give a solid indication for the pillar stiffness.

Optical transparency of Ostemer 220 (90%) was close to PDMS (94%) and similar to Ostemer 324 (92%) in the visible spectrum, showing compatibility for imaging.

During the biocompatibility testing Ostemer 220 showed inconsistent results. The first indirect biocompatibility test with conditioned culture medium indicated biocompatibility of the material. The first direct cell seeding test could not be visualized due to thickness of the material. However, the repeated biocompatibility tests with thinner samples both failed (conditioned medium and direct cell seeding) as a large amount of cells died. The only difference between the first and second round, and therefore the most likely explanation for failure is the use of photoresist and isopropanol in the method to obtain loose membrane samples affecting the material and or cells.

Ostemer 220 is unfortunately not very chemically resistant, for example its incompatibility with DMSO caused it to dissolve during the small molecule absorption test. DMSO is also an often used solution in biological applications and is therefore the incompatibility is a great disadvantage. The material is also twice as expensive as PDMS.

Besides the quick curing time, the main advantage of the material is its hydrophilicity (68.3° contact angle). Also the hydrophobic recovery rate is about 5 days and therefore slower than PDMS. The tested plasma treatments were not optimized, but a 3 minute treatment at 20 Watts showed a large reduction to a contact angle of 18.3°.

PDMS+ performed very well compared to PDMS. Besides having to mix the additional component, spinning and curing the material is the same as for PDMS. Moulding the material went without any problems. The thickest tested layer of 175.6 µm passed the degassing test immediately showing compatibility for processing under vacuum conditions. The initial surface wettability is similar to PDMS (105.8° contact angle). After surface oxidation with plasma treatment, the contact angle reduces drastically, again comparable to PDMS. After many similarities, this is where PDMS+ becomes different and improved, as the hydrophobic recovery is about five times longer compared to PDMS. This is consistent with the intention of the modification to improve cell adhesion and cell proliferation. Within the biocompatibility test, the PDMS+ material performed better than PDMS. 48 hours after direct cell seeding, the confluence for PDMS plasma was about 50-60%, while PDMS+ showed a confluence of 85-90%. The non-plasma treated PDMS only showed a 5-10% confluence while PDMS+ again showed a much higher 70-75% confluence. This means that PDMS+ is better for cell adhesion and proliferation in non-plasma treated condition compared to the current standard of PDMS in plasma-treated condition. PDMS+ in plasma condition is comparable to Ostemer 324 in both plasma and non-plasma treatment.

The material was twice as stiff (2.3 MPa) as PDMS, explained by the increased time and temperature of the thermal curing process. The optical transparency was the same (94%). Interestingly, besides the improved hydrophobic recovery also the absorption of small molecules appeared to be reduced compared to non-modified PDMS. The measurements of fluorescent intensity of the absorbed Nile Red dye into the material were very consistent. The maximum intensity value was lower for PDMS+ compared to PDMS (38.6 vs 68.5 grey value). The distance of absorption into the material was shorter as well (123.0 µm PDMS+, 196.9 µm PDMS). Additional and more extensive absorption testing are needed to confirm these results. The measurements for PDMS showed quite a large variability, the measurements were only performed on one sample and on one time point.

Interesting to know would be the stability of the PDMS+ mixture and whether these beneficial properties in terms of hydrophobicity and biocompatibility remain in aged samples as well.

6 Conclusion

Based on testing of important material properties, Ostemer 324 and PDMS+ are potential alternative materials to PDMS for organ-on-chip applications. Table 13 shows a scoring of the tested properties for each material from 1 (poor) to 5 (beneficial). For PDMS+ many of the characteristics are the same as PDMS, the hydrophobic recovery is improved and the absorption is reduced. Ostemer 324 is a very good candidate as well. A few minor disadvantages are the longer curing times and difficulty in moulding. The main advantage is its reduced hydrophobicity and longer window of hydrophilicity due to reduced hydrophobic recovery rate, which in my opinion weighs strongly against these disadvantages, depending on whether the slightly stiffer material is suitable for the desired cells.

Table 13: Scoring of the material properties for each material from 1 to 5. Poor (1) till 5 being suitable (5) for OoC application based on measurements and processing in this thesis.

Property	PDMS	Ostemer 324	Ostemer 220	PDMS+
Spin-coating	5	5	1	5
Curing	4	3	5	4
Moulding	4	1	1	5
Degassing	4	2	3	4
Etching	4	4	4	4
Wettability	1	5	4	3
Stiffness	4	3	4	4
Transparency	5	5	5	5
Biocompatibility	4	5	2	5
Absorption	2	*No result*	*No result*	3
Total	37	33	29	42

6.1 Future Testing

Based on the literature review, Flexaspin and Fluorolink AD1700 were very promising materials. I recommend future testing to include these materials, to see whether they can live up to their expectations on paper.

Theoretically the stiffness of the Ostemers can be adjusted by altering the mixing ratio of the hardener and the base. Additional testing with adjusted mixing ratios is needed to quantify the material stiffness. Longer UV curing time and even more importantly the effect of UV light intensity on the curing of Ostemer 324 and Ostemer 220 is also an interesting parameter to change and see its effect on material stiffness and possibly other properties. Durability testing of moving membranes could be tested as well.

Moulding of the Ostemers was challenging. Increased viscosity and reduced adherence to the mould resulted in problems for degassing of the trapped air bubbles from the mould. Additional testing could include diluting the materials with a solvent such as isopropanol, or using a different surface coating for the mould. During this thesis double PDMS moulding was considered. First, mould the PDMS on an etched silicon wafer. Then, cover this moulded PDMS with a non-adhesive

layer. Then use the moulded PDMS as a negative mould to create a PDMS mould from which the Ostemers could then be moulded. We did not perform this as the Teflon coated mould already improved adhesion between Ostemer 324 and the mould. Covering the PDMS mould with silane would likely not improve on the adhesion either. A flexible mould might improve on removing trapped air.

With regards to the surface modification by plasma treatment, the treatment parameters can be optimized for each material. Furthermore, wettability of the material surface can be tested under different conditions. For the current tests, the samples were stored in air. Additional tests could check wettability after storing the samples in water or liquids resembling culture medium and possibly include checking wettability of a sample after cell culture.

More extensive transparency testing should be performed to check the effects of auto fluorescence and absorption of light by the materials.

Biocompatibility testing can be extended by performing life-dead staining assays on the tested samples to create more accurately quantifiable results. The next step could be to culture cells in the moulded EHT platforms to check their proliferation and maturation. Additional testing with Ostemer 220 should confirm whether or not the material is indeed biocompatible or not. Other biocompatibility parameters such as thrombogenicity, immunogenicity and effect on gene modification is needed for more extensive biocompatibility results. Another interesting test could be a sheer stress test on cell adhesion, where a sheer fluid flow is applied to cells seeded on the materials to quantify their attachment. Different wettability conditions for each sample can quantify the optimal surface contact angle for cell attachment.

My designed absorption test showed to be a partially successful setup. Additional absorption testing with a different solvent can include results for Ostemer 324 and Ostemer 220. To expand on the test, we recommend testing multiple dyes (e.g. rhodamine B) and measure the absorbance over time. These tests can provide more comprehensive data and can check whether there is a point of saturation as well as verify the current results. More complex testing is needed to quantify absorbed concentrations of compounds.

Other properties to be tested for the materials is the gas permeability, specifically oxygen permeability as it is needed to supply cells with oxygen when using moulded micro-channels. A setup where the material membrane separates a chamber into two parts, where the oxygen can be removed from one side, while remaining in the other can be used. Over time, if the material is gas permeable, oxygen levels should restore in the initially oxygen-free chamber. Additional chemical compatibility testing is need for example for DMSO and other solvents used often in biomedical and OoC applications to see whether and how they affect the materials.

Eventually the materials can be applied to other OoC platform designs to test whether they are suitable for components such as micro-channels, moving membranes or incorporation of sensors.

References

[1] "The Drug Development Process | FDA." [Online]. Available: https://www.fda.gov/patients/learn-about-drug-and-device-approvals/drug-development-process. [Accessed: 11-Mar-2022].

[2] P. McGonigle and B. Ruggeri, "Animal models of human disease: Challenges in enabling translation," *Biochem. Pharmacol.*, vol. 87, no. 1, pp. 162–171, 2014.

[3] A. Van De Stolpe and J. Den Toonder, "Workshop meeting report Organs-on-Chips: Human disease models," *Lab Chip*, vol. 13, no. 18, pp. 3449–3470, 2013.

[4] K. Duval *et al.*, "Modeling physiological events in 2D vs. 3D cell culture," *Physiology*, vol. 32, no. 4, pp. 266–277, 2017.

[5] B. J. van Meer *et al.*, "Small molecule absorption by PDMS in the context of drug response bioassays," *Biochem. Biophys. Res. Commun.*, vol. 482, no. 2, pp. 323–328, 2017.

[6] J. D. Caplin, N. G. Granados, M. R. James, R. Montazami, and N. Hashemi, "Microfluidic Organ-on-a-Chip Technology for Advancement of Drug Development and Toxicology," *Adv. Healthc. Mater.*, vol. 4, no. 10, pp. 1426–1450, 2015.

[7] M. Mastrangeli, S. Millet, and J. van den Eijnden-Van Raaij, "Organ-on-chip in development: Towards a roadmap for organs-on-chip," *ALTEX*, vol. 36, no. 4, pp. 650–668, 2019.

[8] A. M. Ghaemmaghami, M. J. Hancock, H. Harrington, H. Kaji, and A. Khademhosseini, "Biomimetic tissues on a chip for drug discovery," *Drug Discov. Today*, vol. 17, no. 3–4, pp. 173–181, 2012.

[9] B. Zhang, A. Korolj, B. F. L. Lai, and M. Radisic, "Advances in organ-on-a-chip engineering," *Nat. Rev. Mater.*, vol. 3, no. 8, pp. 257–278, 2018.

[10] J. E. Sosa-Hernández *et al.*, "Organs-on-a-chip module: A review from the development and applications perspective," *Micromachines*, vol. 9, no. 10, 2018.

[11] L. Vernetti *et al.*, "Functional Coupling of Human Microphysiology Systems: Intestine, Liver, Kidney Proximal Tubule, Blood-Brain Barrier and Skeletal Muscle," *Sci. Rep.*, vol. 7, no. October 2016, pp. 1–15, 2017.

[12] C. Wang, Z. Tang, Y. Zhao, R. Yao, L. Li, and W. Sun, "Three-dimensional in vitro cancer models: A short review," *Biofabrication*, vol. 6, no. 2, 2014.

[13] Y. S. Zhang *et al.*, "From cardiac tissue engineering to heart-on-a-chip: Beating challenges," *Biomed. Mater.*, vol. 10, no. 3, 2015.

[14] A. Eder, I. Vollert, A. Hansen, and T. Eschenhagen, "Human engineered heart tissue as a model system for drug testing," *Adv. Drug Deliv. Rev.*, vol. 96, pp. 214–224, 2016.

[15] M. Dostanić *et al.*, "A Miniaturized EHT Platform for Accurate Measurements of Tissue Contractile Properties," *J. Microelectromechanical Syst.*, vol. 29, no. 5, pp. 881–887, 2020.

[16] F. Martino, A. R. Perestrelo, V. Vinarský, S. Pagliari, and G. Forte, "Cellular mechanotransduction: From tension to function," *Front. Physiol.*, vol. 9, no. JUL, pp. 1–21, 2018.

[17] H. Liu *et al.*, "Microdevice arrays with strain sensors for 3D mechanical stimulation and monitoring of engineered tissues," *Biomaterials*, vol. 172, pp. 30–40, 2018.

[18] P. Zamprogno *et al.*, "Mechanical Properties of Soft Biological Membranes for Organ-on-a-Chip Assessed by Bulge Test and AFM," *ACS Biomater. Sci. Eng.*, 2021.

[19] R. J. Mills *et al.*, "Functional screening in human cardiac organoids reveals a metabolic mechanism for cardiomyocyte cell cycle arrest," *Proc. Natl. Acad. Sci. U. S. A.*, vol. 114, no. 40, pp. E8372–E8381, 2017.

[20] O. J. Abilez *et al.*, "Passive Stretch Induces Structural and Functional Maturation of Engineered Heart Muscle as Predicted by Computational Modeling," *Stem Cells*, vol. 36, no. 2, pp. 265–277, 2018.

[21] J. M. Stein, C. L. Mummery, and M. Bellin, "Engineered models of the human heart: directions and challenges," *Stem Cell Reports*, vol. 16, no. 2020, pp. 1–9, 2020.

[22] E. Giacomelli *et al.*, "Three-dimensional cardiac microtissues composed of cardiomyocytes and endothelial cells co-differentiated from human pluripotent stem cells," *Dev.*, vol. 144, no. 6, pp. 1008–1017, 2017.

[23] J. B. Nielsen, R. L. Hanson, H. M. Almughamsi, C. Pang, T. R. Fish, and A. T. Woolley, "Microfluidics: innovations in materials and their fabrication and functionalization," *Anal. Chem.*, vol. 92, no. 1, pp. 150–168, 2020.

[24] E. K. Sackmann, A. L. Fulton, and D. J. Beebe, "The present and future role of microfluidics in biomedical research," *Nature*, vol. 507, no. 7491, pp. 181–189, 2014.

[25] I. Allijn, M. Ribeiro, A. Poot, R. Passier, and D. Stamatialis, "Membranes for Modelling Cardiac Tissue Stiffness In Vitro Based on Poly(trimethylene carbonate) and Poly(ethylene glycol) Polymers."

[26] E. Berthier, E. W. K. Young, and D. Beebe, "Engineers are from PDMS-land, biologists are from polystyrenia," *Lab Chip*, vol. 12, no. 7, pp. 1224–1237, 2012.

[27] J. Zhou, A. V. Ellis, and N. H. Voelcker, "Recent developments in PDMS surface modification for microfluidic devices," *Electrophoresis*, vol. 31, no. 1, pp. 2–16, 2010.

[28] P. M. Van Midwoud, A. Janse, M. T. Merema, G. M. M. Groothuis, and E. Verpoorte, "Comparison of biocompatibility and adsorption properties of different plastics for advanced microfluidic cell and tissue culture models," *Anal. Chem.*, vol. 84, no. 9, pp. 3938–3944, 2012.

[29] D. Sticker, R. Geczy, U. O. Häfeli, and J. P. Kutter, "Thiol-Ene Based Polymers as Versatile Materials for Microfluidic Devices for Life Sciences Applications," *ACS Appl. Mater. Interfaces*, vol. 12, no. 9, pp. 10080–10095, 2020.

[30] A. Martin, S. Teychené, S. Camy, and J. Aubin, "Fast and inexpensive method for the fabrication of transparent pressure-resistant microfluidic chips," *Microfluid. Nanofluidics*, vol. 20, no. 6, pp. 1–8, 2016.

[31] D. Sticker *et al.*, "Using oxygen-consuming thermoset plastics to generate hypoxic conditions in microfluidic devices for potential cell culture applications," *21st Int. Conf. Miniaturized Syst. Chem. Life Sci. MicroTAS 2017*, no. 2017, pp. 812–813, 2020.

[32] J. X. Shen, S. Youhanna, R. Zandi Shafagh, J. Kele, and V. M. Lauschke, "Organotypic and Microphysiological Models of Liver, Gut, and Kidney for Studies of Drug Metabolism, Pharmacokinetics, and Toxicity," *Chem. Res. Toxicol.*, vol. 33, no. 1, pp. 38–60, 2020.

[33] X. C. Zhou *et al.*, "Thiol-ene-epoxy thermoset for low-temperature bonding to biofunctionalized microarray surfaces," *Lab Chip*, vol. 17, no. 21, pp. 3672–3681, 2017.

[34] C. F. Carlborg, T. Haraldsson, K. Öberg, M. Malkoch, and W. Van Der Wijngaart, "Beyond PDMS: Off-stoichiometry thiol-ene (OSTE) based soft lithography for rapid prototyping of microfluidic devices," *Lab Chip*, vol. 11, no. 18, pp. 3136–3147, 2011.

[35] C. F. Carlborg, F. Moraga, F. Saharil, W. Van Der Wijngaart, and T. Haraldsson, "Rapid permanent hydrophilic and hydrophobic patterning of polymer surfaces via off-stoichiometry thiol-ene (OSTE) photografting," *Proc. 16th Int. Conf. Miniaturized Syst. Chem. Life Sci. MicroTAS 2012*, pp. 677–679, 2012.

[36] D. Sticker, M. Rothbauer, S. Lechner, M. T. Hehenberger, and P. Ertl, "Multi-layered, membrane-integrated microfluidics based on replica molding of a thiol-ene epoxy thermoset for organ-on-a-chip applications," *Lab Chip*, vol. 15, no. 24, pp. 4542–4554, 2015.

[37] N. D. Ostemer, S. Handling, U. V Reaction, and I. Molding, "Ostemer ® 324 Flex."

[38] S. Mercene Labs AB, "Ostemer?220Litho-DATASHEET-," vol. 221, 2017.

[39] X. Zhang and S. J. Haswell, "Materials matter in microfluidic devices," *MRS Bull.*, vol. 31, no. 2, pp. 95–99, 2006.

[40] H. Becker and C. Gärtner, "Polymer microfabrication technologies for microfluidic systems," *Anal. Bioanal. Chem.*, vol. 390, no. 1, pp. 89–111, 2008.

[41] M. Zarchi, S. Ahangarani, and M. Z. Sanjari, "Properties of Silicon Dioxide Film Deposited By PECVD at Low Temperature/Pressure," *Metall. Mater. Eng.*, vol. 20, no. 2, pp. 89–96, Jul. 2014.

[42] W. F. Quirós-Solano *et al.*, "Microfabricated tuneable and transferable porous PDMS membranes for Organs-on-Chips," *Sci. Rep.*, vol. 8, no. 1, Dec. 2018.

[43] N. Gaio, "Organ-on-Silicon," 2019.

[44] S. J. Li, K. Wu, H. Z. Yuan, J. Y. Zhang, G. Liu, and J. Sun, "Formation of wrinkled patterns in metal films deposited on elastic substrates: Tunability and wettability," *Surf. Coatings Technol.*, vol. 362, pp. 35–43, Mar. 2019.

[45] S. J. Yu, Y. P. Du, Y. D. Sun, Q. L. Ye, and H. Zhou, "Wrinkling patterns in metal films sputter deposited on viscoelastic substrates," *Thin Solid Films*, vol. 638, pp. 230–235, Sep. 2017.

[46] A. H. McMillan *et al.*, "Self-sealing thermoplastic fluoroelastomer enables rapid fabrication of modular microreactors," *Nano Sel.*, no. December 2020, pp. 1–18, 2021.

[47] K. Webb, V. Hlady, and P. A. Tresco, "Relative importance of surface wettability and charged functional groups on NIH 3T3 fibroblast attachment, spreading, and cytoskeletal organization," *J. Biomed. Mater. Res.*, vol. 41, no. 3, pp. 422–430, Sep. 1998.

[48] J. H. Lee, S. J. Lee, G. Khang, and H. B. Lee, "The Effect of Fluid Shear Stress on Endothelial Cell Adhesiveness to Polymer Surfaces with Wettability Gradient," *J. Colloid Interface Sci.*, vol. 230, no. 1, pp. 84–90, Oct. 2000.

[49] L. Ikonen, E. Kerkelä, G. Metselaar, M. C. A. Stuart, M. R. De Jong, and K. Aalto-Setälä, "2D and 3D self-assembling nanofiber hydrogels for cardiomyocyte culture," *Biomed Res. Int.*, vol. 2013, 2013.

[50] V. Barbier, M. Tatoulian, H. Li, F. Arefi-Khonsari, A. Ajdari, and P. Tabeling, "Stable modification of PDMS surface properties by plasma polymerization: Application to the formation of double emulsions in microfluidic systems," *Langmuir*, vol. 22, no. 12, pp. 5230–5232, 2006.

[51] A. Alrifaiy, O. A. Lindahl, and K. Ramser, "Polymer-based microfluidic devices for pharmacy, biology and tissue engineering," *Polymers (Basel).*, vol. 4, no. 3, pp. 1349–1398, 2012.

[52] D. P. Dowling, I. S. Miller, M. Ardhaoui, and W. M. Gallagher, "Effect of surface wettability and topography on the adhesion of osteosarcoma cells on plasma-modified polystyrene," *J. Biomater. Appl.*, vol. 26, no. 3, pp. 327–347, 2011.

[53] K. Ren, J. Zhou, and H. Wu, "Materials for microfluidic chip fabrication," *Acc. Chem. Res.*, vol. 46, no. 11, pp. 2396–2406, 2013.

[54] K. Y. Law, "Definitions for hydrophilicity, hydrophobicity, and superhydrophobicity: Getting the basics right," *J. Phys. Chem. Lett.*, vol. 5, no. 4, pp. 686–688, Feb. 2014.

[55] W. D. Niles and P. J. Coassin, "Cyclic olefin polymers: Innovative materials for high-density multiwell plates," *Assay Drug Dev. Technol.*, vol. 6, no. 4, pp. 577–590, 2008.

[56] "Introduction to Fluorescence Microscopy | Nikon's MicroscopyU." [Online]. Available: https://www.microscopyu.com/techniques/fluorescence/introduction-to-fluorescence-microscopy. [Accessed: 04-Mar-2022].

[57] "How Fluorescence Microscopy Works | Thermo Fisher Scientific - NL." [Online]. Available: https://www.thermofisher.com/nl/en/home/life-science/cell-analysis/cell-analysis-learning-center/molecular-probes-school-of-fluorescence/imaging-basics/fundamentals-of-fluorescence-microscopy/how-fluorescence-microscopy-works.html. [Accessed: 04-Mar-2022].

[58] "Fluorescence SpectraViewer." [Online]. Available: https://www.thermofisher.com/order/fluorescence-spectraviewer#!/. [Accessed: 15-Nov-2021].

[59] W. Elshahawy, "Biocompatibility," *Adv. Ceram. - Electr. Magn. Ceram. Bioceram. Ceram.*

Environ., Sep. 2011.

[60] M. Amerian, M. Amerian, M. Sameti, and E. Seyedjafari, "Improvement of PDMS surface biocompatibility is limited by the duration of oxygen plasma treatment," *J. Biomed. Mater. Res. Part A*, vol. 107, no. 12, pp. 2806–2813, Dec. 2019.

[61] T. A. Moore, P. Brodersen, and E. W. K. Young, "Multiple Myeloma Cell Drug Responses Differ in Thermoplastic vs PDMS Microfluidic Devices," *Anal. Chem.*, vol. 89, no. 21, pp. 11391–11398, 2017.

[62] M. W. Toepke and D. J. Beebe, "PDMS absorption of small molecules and consequences in microfluidic applications," *Lab Chip*, vol. 6, no. 12, pp. 1484–1486, 2006.

[63] V. S. Shirure and S. C. George, "Design considerations to minimize the impact of drug absorption in polymer-based organ-on-a-chip platforms," *Lab Chip*, vol. 17, no. 4, pp. 681–690, 2017.

[64] S. B. Campbell, Q. Wu, J. Yazbeck, C. Liu, S. Okhovatian, and M. Radisic, "Beyond Polydimethylsiloxane: Alternative Materials for Fabrication of Organ-on-a-Chip Devices and Microphysiological Systems," *ACS Biomater. Sci. Eng.*, 2020.

[65] K. Domansky *et al.*, "SEBS elastomers for fabrication of microfluidic devices with reduced drug absorption by injection molding and extrusion," *Microfluid. Nanofluidics*, vol. 21, no. 6, pp. 1–12, 2017.

[66] Nianzhen Li, M. Schwartz, and C. Ionescu-Zanetti, "PDMS compound adsorption in context," *J. Biomol. Screen.*, vol. 14, no. 2, pp. 194–202, Feb. 2009.

[67] J. Yao, Y. Guan, Y. Park, Y. E. Choi, H. S. Kim, and J. Park, "Optimization of ptfe coating on pdms surfaces for inhibition of hydrophobic molecule absorption for increased optical detection sensitivity," *Sensors*, vol. 21, no. 5, pp. 1–10, 2021.

[68] B. Brewer, "MNHMT2012-75105," pp. 1–5, 2017.

[69] C. Ding, X. Chen, Q. Kang, and X. Yan, "Biomedical Application of Functional Materials in Organ-on-a-Chip," *Front. Bioeng. Biotechnol.*, vol. 8, no. July, pp. 1–9, 2020.

[70] J. Garra, T. Long, J. Currie, T. Schneider, R. White, and M. Paranjape, "Dry etching of polydimethylsiloxane for microfluidic systems," *J. Vac. Sci. Technol. A Vacuum, Surfaces, Film.*, vol. 20, no. 3, pp. 975–982, 2002.

[71] V. Ozbolat, M. Dey, B. Ayan, A. Povilianskas, M. C. Demirel, and I. T. Ozbolat, "3D Printing of PDMS Improves Its Mechanical and Cell Adhesion Properties," *ACS Biomater. Sci. Eng.*, vol. 4, no. 2, pp. 682–693, 2018.

[72] A. P. Gerratt, I. Penskiy, and S. Bergbreiter, "In situ characterization of PDMS in SOI-MEMS," *J. Micromechanics Microengineering*, vol. 23, no. 4, 2013.

[73] J. Casanova-Moreno, J. To, C. W. T. Yang, R. F. B. Turner, D. Bizzotto, and K. C. Cheung, "Fabricating devices with improved adhesion between PDMS and gold-patterned glass," *Sensors Actuators, B Chem.*, vol. 246, pp. 904–909, 2017.

[74] Y. Li, T. Verbiest, and I. Vankelecom, "Improving the flux of PDMS membranes via localized heating through incorporation of gold nanoparticles," *J. Memb. Sci.*, vol. 428, pp. 63–69, 2013.

[75] A. Vitale, M. Quaglio, S. L. Marasso, A. Chiodoni, M. Cocuzza, and R. Bongiovanni, "Direct photolithography of perfluoropolyethers for solvent-resistant microfluidics," *Langmuir*, vol. 29, no. 50, pp. 15711–15718, 2013.

[76] K. J. Regehr *et al.*, "Biological implications of polydimethylsiloxane-based microfluidic cell culture," *Lab Chip*, vol. 9, no. 15, pp. 2132–2139, 2009.

[77] E. Roy, M. Geissler, J. C. Galas, and T. Veres, "Prototyping of microfluidic systems using a commercial thermoplastic elastomer," *Microfluid. Nanofluidics*, vol. 11, no. 3, pp. 235–244, 2011.

[78] S. Hassan, M. Heinrich, B. Cecen, J. Prakash, and Y. S. Zhang, *Biomaterials for on-chip organ systems*. LTD, 2020.

[79] R. Sivakumar, K. T. L. Trinh, and N. Y. Lee, "Heat and pressure-resistant room temperature

irreversible sealing of hybrid PDMS-thermoplastic microfluidic devicesviacarbon-nitrogen covalent bonding and its application in a continuous-flow polymerase chain reaction," *RSC Adv.*, vol. 10, no. 28, pp. 16502–16509, 2020.

[80] R. Mukhopadhyay, "When PDMS isn't the best," *Anal. Chem.*, vol. 79, no. 9, pp. 3249–3253, 2007.

[81] D. Fuard, T. Tzvetkova-Chevolleau, S. Decossas, P. Tracqui, and P. Schiavone, "Optimization of poly-di-methyl-siloxane (PDMS) substrates for studying cellular adhesion and motility," *Microelectron. Eng.*, vol. 85, no. 5–6, pp. 1289–1293, 2008.

[82] N. Gaio, S. Kersjes, W. Q. Solano, P. Sarro, and R. Dekker, "Versatile and Automated 3D Polydimethylsiloxane (PDMS) Patterning for Large-Scale Fabrication of Organ-on-Chip (OOC) Components," *Proceedings*, vol. 2, no. 13, p. 873, 2018.

[83] A. Vitale, M. Quaglio, M. Cocuzza, C. F. Pirri, and R. Bongiovanni, "Photopolymerization of a perfluoropolyether oligomer and photolithographic processes for the fabrication of microfluidic devices," *Eur. Polym. J.*, vol. 48, no. 6, pp. 1118–1126, 2012.

[84] J. P. Rolland, R. M. Van Dam, D. A. Schorzman, S. R. Quake, and J. M. DeSimone, "Solvent-Resistant Photocurable 'Liquid Teflon' for Microfluidic Device Fabrication," *J. Am. Chem. Soc.*, vol. 126, no. 8, pp. 2322–2323, 2004.

[85] M. Gómez and M. Lazzari, "PFPE-based materials for the fabrication of micro- and nano-optical components," *Microelectron. Eng.*, vol. 97, pp. 208–211, 2012.

[86] R. Bongiovanni, A. Di Meo, A. Pollicino, A. Priola, and C. Tonelli, "New perfluoropolyether urethane methacrylates as surface modifiers: Effect of molecular weight and end group structure," *React. Funct. Polym.*, vol. 68, no. 1, pp. 189–200, 2008.

[87] A. Ghanbari-Siahkali, S. Mitra, P. Kingshott, K. Almdal, C. Bloch, and H. K. Rehmeier, "Investigation of the hydrothermal stability of cross-linked liquid silicone rubber (LSR)," *Polym. Degrad. Stab.*, vol. 90, no. 3, pp. 471–480, 2005.

[88] S. C. Shit and P. Shah, "A review on silicone rubber," *Natl. Acad. Sci. Lett.*, vol. 36, no. 4, pp. 355–365, 2013.

[89] P. S. Nunes, P. D. Ohlsson, O. Ordeig, and J. P. Kutter, "Cyclic olefin polymers: Emerging materials for lab-on-a-chip applications," *Microfluid. Nanofluidics*, vol. 9, no. 2–3, pp. 145–161, 2010.

[90] D. Voicu *et al.*, "Thermoplastic microfluidic devices for targeted chemical and biological applications," *RSC Adv.*, vol. 7, no. 5, pp. 2884–2889, 2017.

[91] C. W. Tsao and D. L. DeVoe, "Bonding of thermoplastic polymer microfluidics," *Microfluid. Nanofluidics*, vol. 6, no. 1, pp. 1–16, 2009.

[92] R. J. Spontak and N. P. Patel, "Thermoplastic elastomers: Fundamentals and applications," *Curr. Opin. Colloid Interface Sci.*, vol. 5, no. 5–6, pp. 333–340, 2000.

[93] E. Roy, J. C. Galas, and T. Veres, "Thermoplastic elastomers for microfluidics: Towards a high-throughput fabrication method of multilayered microfluidic devices," *Lab Chip*, vol. 11, no. 18, pp. 3193–3196, 2011.

[94] A. H. McMillan, E. K. Thomée, A. Dellaquila, H. Nassman, T. Segura, and S. C. Lesher-Pérez, "Rapid fabrication of membrane-integrated thermoplastic elastomer microfluidic devices," *Micromachines*, vol. 11, no. 8, pp. 1–19, 2020.

[95] J. Lachaux *et al.*, "Soft Thermoplastic Elastomer for Easy and Rapid Spin-Coating Fabrication of Microfluidic Devices with High Hydrophilization and Bonding Performances," *Adv. Mater. Technol.*, vol. 4, no. 2, pp. 1–7, 2019.

[96] J. Lachaux *et al.*, "Thermoplastic elastomer with advanced hydrophilization and bonding performances for rapid (30 s) and easy molding of microfluidic devices," *Lab Chip*, vol. 17, no. 15, pp. 2581–2594, 2017.

[97] M. D. Guillemette, E. Roy, F. A. Auger, and T. Veres, "Rapid isothermal substrate microfabrication of a biocompatible thermoplastic elastomer for cellular contact guidance," *Acta Biomater.*, vol. 7, no. 6, pp. 2492–2498, 2011.

[98] M. Geissler, B. Voisin, L. Clime, B. Le Drogoff, and T. Veres, "Thermo-active elastomer composite for optical heating in microfluidic systems," *Small*, vol. 9, no. 5, pp. 654–659, 2013.

[99] L. El Fissi *et al.*, "OSTEMER polymer as a rapid packaging of electronics and microfluidic system on PCB," *Sensors Actuators, A Phys.*, vol. 285, pp. 511–518, 2019.

[100] J. M. Karlsson *et al.*, "High-resolution micropatterning of off-stochiometric thiol-enes (OSTE) via a novel lithography mechanism," *Proc. 16th Int. Conf. Miniaturized Syst. Chem. Life Sci. MicroTAS 2012*, vol. 1600, pp. 225–227, 2012.

[101] D. Sticker *et al.*, "Oxygen Management at the Microscale: A Functional Biochip Material with Long-Lasting and Tunable Oxygen Scavenging Properties for Cell Culture Applications," *ACS Appl. Mater. Interfaces*, vol. 11, no. 10, pp. 9730–9739, 2019.

[102] "Liquid Silicone Rubber (LSR) Parts Injection Molding | SIMTEC." [Online]. Available: https://www.simtec-silicone.com/capabilities/liquid-silicone-rubber/. [Accessed: 31-May-2021].

[103] S. C. H. Thian, J. Y. H. Fuh, Y. S. Wong, H. T. Loh, P. W. Gian, and Y. Tang, "Fabrication of microfluidic channel utilizing silicone rubber with vacuum casting," *Microsyst. Technol.*, vol. 14, no. 8, pp. 1125–1135, 2008.

[104] Y. Xia and G. M. Whitesides, "Soft lithography," *Angew. Chemie - Int. Ed.*, vol. 37, no. 5, pp. 550–575, 1998.

[105] G. S. Fiorini, R. M. Lorenz, J. S. Kuo, and D. T. Chiu, "Rapid Prototyping of Thermoset Polyester Microfluidic Devices," vol. 76, no. 16, pp. 4697–4704, 2004.

[106] M. D. Borysiak, K. S. Bielawski, N. J. Sniadecki, C. F. Jenkel, B. D. Vogt, and J. D. Posner, "Simple replica micromolding of biocompatible styrenic elastomers," *Lab Chip*, vol. 13, no. 14, pp. 2773–2784, 2013.

[107] J. Marczak, P. Slupski, P. Kunicki, and K. Komorowska, "Soft lithography processing of fresnel lens for on-chip applications," *IEEE-NANO 2015 - 15th Int. Conf. Nanotechnol.*, pp. 975–978, 2015.

[108] K. Ren, W. Dai, J. Zhou, J. Su, and H. Wu, "Whole-Teflon microfluidic chips," *Proc. Natl. Acad. Sci. U. S. A.*, vol. 108, no. 20, pp. 8162–8166, 2011.

[109] A. Waldbaur, H. Rapp, K. Länge, and B. E. Rapp, "Let there be chip - Towards rapid prototyping of microfluidic devices: One-step manufacturing processes," *Anal. Methods*, vol. 3, no. 12, pp. 2681–2716, 2011.

[110] Guilhem Velvé Casquillas, Maël Le Berre, Emmanuel Terriac, Fabien Bertholle, Timothée Houssin, and Sebastien Cargou, "PDMS thickness VS spin-coating speed."

[111] W. Y. Zhang, G. S. Ferguson, and S. Tatic-Lucic, "Elastomer-supported cold welding for room temperature wafer-level bonding," *Proc. IEEE Int. Conf. Micro Electro Mech. Syst.*, pp. 741–744, 2004.

[112] "OCA Optical contact angle measuring and contour analysis systems - DataPhysics Instruments." [Online]. Available: https://www.dataphysics-instruments.com/products/oca/. [Accessed: 11-Feb-2022].

Appendix A: Literature Review Chapter 5

5 Material Overview

Based on all the criteria mentioned in chapter 4, the most suitable type of materials for OoC application are polymers. Polymers can be classified in elastomers, thermosets and thermoplastics [53]. Elastomers are crosslinked polymers chains that can be stretched and compressed and afterwards return to their original shape [53]. PDMS is the most famous example [69]. Thermosets, such as SU-9 photoresist and polyamide, crosslink upon heating or radiation exposure. Their shape after the crosslinking cannot be reversed [40]. The polymers in this category are often resistant to solvents and optically transparent. The third category is thermoplastics. Examples are PMMA, PC, polystyrene, polyethylene terephthalate (PET) and polyvinyl chloride (PVC). These polymers can be reshaped after they are initially cured, by reheating the material. Thermoplastics have better solvent compatibility than PDMS, but are incompatible with most organic solvents such as ketones. Thermoplastics are non-gas permeable and very rigid [53]. Another group of polymers are per-fluorinated polymers, such as perfluoro-alkoxy and fluorinated ethylene-propylene (Teflon PFA and FEP). These are inert to chemicals and solvents, optically transparent, soft and moderately permeable to gases. Specific polymers and their properties will be discussed in the next chapter. The upcoming paragraphs will specify the properties of an optimal material for OoC.

In this section, a list of materials and their properties will be discussed, starting with PDMS, followed by several alternatives. At the end of the section, table 1, 2 and 3 present a summary of the data collected in this literature review.

1. Elastomer

1.1 Material: PDMS

PDMS is a crosslinked polymer composed of hydrophobic dimethyl siloxane oligomers. The backbone of the PDMS polymer chain consists of silicon-oxygen-silicon bonds [70]. PDMS is produced by mixing a base with a curing agent in a ratio of for example 10:1 [71]. Commercially available types of PDMS are Sylgard 184 and SE 1700 [71]. Sylgard 184 is the most used silicone in OoC [72].

PDMS has many advantages in the biomedical field. It is biocompatible, transparent, relatively cheap, easy to use, moldable, non-toxic, stable over a wide temperature range and flexible [5], [73]–[75]. The material can be used to create a small number of devices and prototypes. It can also bind to glass, plastic and to itself [24].

Unfortunately, PDMS also has a number of important disadvantages. Different kinds of drugs are soluble in the PDMS material [62]. Moreover, residual un-crosslinked oligomers may leach into the culture medium from the material and incorporate into the cell membrane [24], [26], [76]. This absorption is one of the main disadvantages of PDMS and should be taken into account when performing experiments with the material [76]. Furthermore, PDMS is incompatible with organic solvents, and has limited surface stability after modification, because the surface hydrophobicity recovers over time [26], [77], [75]. The hydrophobicity of PDMS prevents direct cell adhesion and therefore needs surface treatment or coating [78].

PDMS has a high transparency and has a small amount of auto fluorescence [79], [64]. The fluorescence is small enough not to affect conventional microscopy imaging [80].

PDMS is well suited for rapid prototyping, however it is not suitable for mass production due to low speed of casting and curing processes [65]. Possible production methods are replica molding, low cost membrane integrated microfluidic system fabrication [36], patterning with soft lithography [62], spinning and photo patterning through a mask [70]. High throughput production methods such as injection molding, rolling and embossing are less suitable for PDMS [24].

Oxygen and carbon dioxide can diffuse freely through PDMS [53], [62], [80]. This is a beneficial characteristic that allows it to easily supply cells with oxygen and remove the carbon dioxide without needing a perfusion system [64].

PDMS can bind to itself, as well as to silicon substrates by simple surface activation. The strong adhesion makes it possible to use the device under high pressure, as well as high temperature due to its temperature resistance [79]. PDMS binds to itself after plasma-oxygen treatment [80]. Cell adhesion to PDMS is very poor, unless surface modifications or coatings are applied to make the surface hydrophilic [71].

PDMS absorbs organic solvents, evaporates water and both absorbs and adsorbs hydrophobic molecules [62], [80]. Depending on channel size and layer thickness, PDMS can absorb a significant amount of the tested drug and therefore greatly alter the concentration of the solution inside the channel. The effect can be a factor 100 difference between the initial inserted concentration into the channel and the resulting concentration inside the same channel after partial absorption by the material [62]. This is relevant to take into account when you want to determine the proper dosage of medicine, for toxicity and function [61].

PDMS has a hydrophobic surface, due to methyl groups present in the material [71], [81]. Plasma treatment can remove the methyl groups and make the surface more hydrophilic [81]. However, PDMS has the issue of hydrophobic recovery. This is caused by migration of uncured oligomers from the bulk material towards the surface [27], [50]. The shelf live is very short, therefore the most accurate experimentation is done around one hour after preparation of the PDMS [26].

Due to its flexibility, PDMS can be used as a membrane or in pumping mechanisms that mimic mechanical movement of the naturally surrounding tissue such as in the lungs or heart [5], [50]. Moduli of the material are in the order of 1 MPa, depending on mixing ratio of the cross linker agent, curing temperature and baking time [72], [81].

Examples of feature sizes made with PDMS are 15 μm thick membranes and micro pillars with a height of 151 μm [15], [53], [82].

1.2 Material: Perfluoropolyethers (PFPE)

PFPE is a carbon based polyether also classified as a silicone, which is liquid at room temperature and can be photo cured. The polyether contains no hydrogens, is fluorinated, and is similar to liquid Teflon [80]. Some properties are: low surface energy, low modulus (3.9 MPa), high gas permeability, low toxicity and moreover, it is extremely chemically resistant [78], [80], [75], [83], [84]. The material is soft with elastomeric behavior [75]. It is transparent and can be patterned with photolithography, replica molding and spin coating. It is hydrophobic and is appropriate for small feature and pillar production [75], [83], [85], [86].

1.3 Material: Liquid silicone rubber

Not much information is available as liquid silicone rubber (LSR) is not yet widely used for organ on chip application. Some properties include thermal stability, oxidation resistance, low temperature flexibility, low production cost [87] and biocompatibility [88]. LSR can be produced with injection, extrusion and compression molding [88]. Furthermore it absorbs only 1% of moisture after long exposure to water [88] and is suitable for submicron features and 50-100μm channels [87].

2. Thermoplastic

2.1 Material: COC/COP

Cyclic olefin polymer (COP) is a thermoplastic polymer [61], [65]. It is commercially available as Apel, Arton, Topas, Zeonex and Zeonor and it can be bought in pellet form, in solution or in sheets [89].

COP has high chemical resistance, low water absorption, good optical transparency in the near UV range of 250 nm, and has a high gas permeability [90]. The transparency results in high quality fluorescent imaging. It is highly resistant to chemicals and polar solvents such as methanol [89]. However, COP has poor chemical resistance in non-polar organic, aromatic and hydrocarbon solvents such as toluene and hexane [69], [90], [91], [89].

COP can be produced with micro milling, hot embossing, injection molding or nanoimprint lithography [61]. In nanoimprint lithography the material is spin coated for example on silicon or glass [89] and then baked. Then UV photolithography is used with electron beam lithography and deep reactive ion etching to transfer a resist pattern [89].

COP can be bonded with thermal bonding, preferably with material with slightly different glass transition temperature [89]. Plasma activation can improve bonding strength. It has less drug absorption than in PDMS and smaller drug penetration [61]. The depth of penetration of drugs is only 100-300 nm into the surface compared to 5000 nm for PDMS [89].

The water contact angle is between 94 and 136 degrees meaning the material is hydrophobic [55], [89]. Oxygen plasma, UV ozone and chemical coating treatments are possible to modify the material surface. Oxygen plasma reduces the water contact angle to 7 degrees, low pressure plasma to 39 degrees and ozone to 49 degrees [89]. The hydrophobic recovery is slower than in PDMS. The water contact angle has been reported to be maintained at least for 4 weeks [28]. The feature size made with spin coating and plasma etching is on a 7 μm film and resulted in pillars of 4.4 μm wide, 4.9 μm high and a distance between pillars of 1.6 μm [89].

When COP is made from more than one kind of monomer it is a cyclic olefin copolymer (COC) [89]. COC is a thermoplastic polymer, commercially named: Topax or Zeonex/Zeonor [28]. It is hydrophobic, less porous than PDMS, does not significantly absorb water vapor and is biocompatible [80]. It does dissolve in organic solvents [69], [80]. Yet has chemical resistance to polar solvents such as acetone, methanol, and has a low melting point [39]. High quantity production is possible at reasonable pricing [26]. An advantage is that it has no oligomer leaking into the culture medium [32].

3. SEBS

SEBS stands for styrene ethylene/butylene styrene block copolymer [77] and is based on styrene ethylene butylene styrene which is a synthetic thermoplastic elastomer [65], [77]. SEBS is a general term, many compositions of this material exist. Multiple companies make such a compound, such as Flexdym, Versaflex CL30, Zeonor 1060R, Kraton MD6945, Kraton G1657 and Mediprene 500422 [65], [77]. SEBS is a biphasic material, which has combined properties of glassy thermoplastics and soft elastomers. This combination makes it possible that the rubbery material can be processed as a thermoplastic [92]. It is a single macromolecule with thermoplastic segments and rubbery segments covalently bonded [92].

Other properties of SEBS include low cost, transparency, biocompatibility and flexibility [92]. SEBS resists absorption of small hydrophobic molecules. Bonding between SEBS layers or with cells does not require plasma treatments of the surface [65]. Moreover, it is suitable for rapid prototyping using existing methods such as soft lithography, melt extrusion, hot embossing, solvent casting and injection molding [65], [77], [92]. The general wettability is a contact angle of around 97 degrees.

Feature sizes that have been made are a 25μm thick membrane and structures with a height of 30μm [93]. Two specific examples of SEBS are discussed next.

3.1 Material: Flexdym

Flexdym is a thermoplastic elastomer which falls under the SEBS category. The material is optically transparent, as clear as PDMS [94]–[96]. It is flexible (stretches up to a factor 7) and adheres to other materials. Flexdym can be used with hot embossing or extrusion moulding [94]–[96]. Lachaux et al. used a proprietary solution based Flexdym, from Eden microfluidics, and created a film with spin coating. The film thickness ranged from 5 μm to 28 μm depending on the solution used and rotation speed [95]. A channel of 20μm width has been produced, indicating the possible feature size [95]. Oxygen permeability and hydrophobic molecule absorption are less than for PDMS [94], [96]. Flexdym is biocompatible and hydrophilic after plasma treatment for at least 7 days [95]. The contact angle with water is 88°-100° before treatment, and 20° after treatment. The stiffness of the material is 1.15 MPa [96].

The solution based compound for spin coating is not yet commercially available. Questions remain regarding the adhesion with silicon and the effect of oxygen permeability on cells. The main advantage is the reduced absorption of hydrophobic molecules.

3.2 Material: Versaflex CL30

Versaflex is another SEBS polymer, composed of di-block and triblock copolymer types [77]. Versaflex can be treated with plasma oxidation and has a high level of transparency in UV and visible range, slightly less transparent than PDMS [97]. It has 50% transmittance at 295 nm [77]. Moreover, it can be produced by hot embossing and injection moulding [98]. The surface is hydrophobic, with a water contact angle of 106°. After plasma treatment, the angle is 65°. 2 weeks after plasma treatment the contact angels settle to 79° [77]. Finally, it is stretchable with viscoelastic properties [77].

4. Thermoset

4.1 Material: OSTEMER

An OSTEMER is a UV curable, thermoset, off stoichiometric thiol-ene polymer [30], [31]. OSTEMER is made by combining 2 monomers, one with thiol active groups and the other with allyl functional groups [29]. When the thiol and allyl groups are balanced, the material is stoichiometric [29]. In an off-stoichiometric mixture, one of the monomers is in excess, with functional groups of either the allyl or thiol remaining (Figure A1). By adjusting the allyl and thiol concentration, the final material stiffness can be adjusted [34]. This ranges from MPa to GPa, more specifically in a young's modulus range of about 250-1740 MPa [29], [34].

By applying surface modifications, and thus changing the surface density of active thiol groups, the surface can be modified to become stable (longer than 3 months) hydrophilic [29], [35]. The material has a chemical resistance comparable to Teflon and less swelling than PDMS [34]. It is solvent resistant and has low shrinkage stress. Furthermore, it is biocompatible and it bonds to different materials without surface treatment [99]. OSTEMER has very good binding properties, as it can directly covalently bind to other materials and to itself, without the need of techniques that use high pressure and heat that thereby could deform the material [32]. In terms of optical properties, OSTEMER is transparent, has acceptable auto fluorescence and light absorption only below a wavelength of 380 nm [36].

The material can be deposited and patterned with many techniques, such as photo-patternable surface modification, low temperature dry bonding [34], casting, surface grafting, bonding/sealing, dicing [34], direct lithography [100], dry etching, soft lithography and injection moulding [36], [30]. Specifically, the deposition of OSTEMER 322, is performed by initiating curing with UV light, to trigger polymerization between allyl and thiol monomers. The elastic modulus is 3.2 MPa at this point. Curing is then thermally continued, increasing the bonding and creating a stiff material with a 2.3 GPa modulus [36].

An interesting property is that OSTEMER 322 is an oxygen scavenging material. OSTEMER can be used to control oxygen concentration in the tissue and thus culture cells under reduced oxygen concentration [31], [29],[101]. The material has low water vapuor permeability, 0.15 g mm^{-1} per 24 h per m^2 [36]. Water absorption and oxygen permeability are very low compared to PDMS [29]. Finally, The material does not absorb other molecules and there is no oligomer leaking into the culture medium [32], [33].
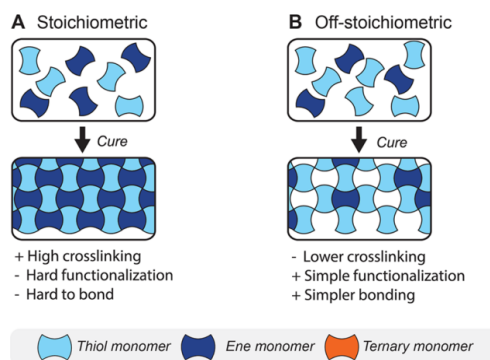

Figure A1: Concept of stoichiometric and off stoichiometric materials [29].

58

5. Overview

Table A1 summarizes the properties of the materials discussed above and compares them to PDMS. Table A2 specifically summarizes which production methods are available for which materials. Finally, in Table A3 the data of each material and property is shown.

Table A1: Advantageous and disadvantageous material properties of PDMS in the first column. The other materials have their material properties indicated as better/equal or worse than PDMS.

	PDMS	PFPE	COP/ COC	LSR	SEBS	Flexdym	Versaflex CL30	Ostemer (322)
Production	~	+	+	+	+	+	+	+
Absorption	-	+	+	+	+	+	+	+
Wettability	-	-	+	-	+	+	+	+
Casting	+	+	+	+	+	+	-	+
Transparency	+	+	+	+	+	+	+	+
Chemical compatibility	-	+	+	+	+	?		+
Adhesion	+	+	+	+		?		+
Min. feature size	+	+	+	+	+	+	+	+
Stiffness	+	+	~	+	+	+	+	+
Gas permeability	+	+	+		-	-	-	-
Cost	+	-	+	+	+	+	+	-

+	Advantage	+	As good as or better than PDMS
-	Disadvantage	-	Worse than PDMS
			Not found
		?	Unknown

Table A2: Production methods suitable for each material.

	PDMS	PFPE	COP/ COC	LSR	SEBS	Flexdym	Versaflex CL30	Ostemer
Soft lithography	+	+	~	+	+	+	+	+
Spin coating	+	+ [75]	- [89]			+ [95]	-	
Photolithography	+	+ [75]	+					
Hot embossing	~		+	+	+	+	+	
Injection molding	~		+	+	+	+	+	+
Etching	+		+		+			+

Table A3: Summary of material properties.

	PDMS	PFPE	COP/COC	LSR	SEBS	FLexdyn	Versaflex CL30	Ostemer (322)
Transparency	High transparency [79], small fluorescence [80]	Low refractive index [83] Extremely transparent [85], [96]	Optical transparency from 300 to 1200 nm range. Auto fluorescence higher than PDMS [89]	Transparent: [102]	More than 85% transmission throughout the entire 400-800 nm visible spectrum.	Transparent, clear as PDMS [95], [96]	High level of transparency in UV and visible range. Slightly less transparent than PDMS. 50% transmittance at 295 nm [77]	Acceptable autofluoresence, transparent in visible region [29], [36].
Production methods	Rapid prototyping, not mass production. soft lithography patterning, molding spin coating.	Uv lithography, replica moling, photolithography [85]. Spin coated + photopolymerization [75].	Micromilling, hot embossing and solvent bonding [61] injection molding and nanoimprint lithography [89].	Injection molding, extrusion, compression molding, curing, casting, soft lithography [87], [88], [103], [104].	Soft thermoplastic lithography, melt extrusion, injection molding and casting [77], [92], [105].	Hot embossing, extrusion molding, spin coating. [94], [96].	Hot embossing [97].	Photopatternable, direct lithography, soft lithography, injection molding [36], [34], [104].
Spin coating	Possible.	Possible [75].	Spin coated and baking [89].			Proprietary [95].		
Gas permeability	Freely permeable [62], Diffusion coefficient oxygen: 2000 to 4000μm^2/s [26]. Water vapor permeability is 1000-6000 μm^2/s [26]. Oxygen permeability: 563.5 Barrer [46].	High gas permeability [84].	High gas permeability [90] .		Gas permeability coefficients 20 to 400 times lower than PDMS [65], [93].	Less than PDMS [94].		Oxygen scavenging material [31].
Adhesion	Binds to itself.		bonded with thermal bonding [89]. Plasma activation can improve bonding strength.			Unknown to silicon.		Binds to itself and other materials without surface modification [33].
Absorption	Absorbs organic solvents and small hydrophobic molecules [61].	Lower than PDMS [83].	Lower than PDMS, smaller drug penetration [61] only 100-300 nm into the surface compared to 5000nm for PDMS. Low water absorption [89].	1% moisture absorption after long exposure [88].	Lower than PDMS [65].	Lower than PDMS [94].	Lower than PDMS [65].	90% lower vapor permeability than PDMS: 0.15 g mm-1 per 24 h per m^2 [29], [36]. 25 times lower absorption or organic molecules than PDMS [33].
Wettability (water contact angle)	Sylgart 184: 104.3° degrees, 30.5° after oxygen plasma treatment [65].	Hydrophobic, 114° [83].	Hydrophobic, 90° [89].	leaking of oligomers [87]. Hydrophobic [88].	Kration G1643, and G1645 97° and 98°. After treatment 78° and 71°. Hydrophobic recovery over the course of a few days [106].	88°-104°. After treatment: 20° for at least 7 days [95], [96].	Hydrophobic, 96.3° [65].	Hydrophilic, between 60° and 80° [29].
Stiffness (young's modulus)	Sylgard 184: 0.8 MPa [34]. 0.5 – 3 MPa [29].	3.9 – 9.4MPa [75].	2.4 GPa [55] Around 1600 to 3400 MPa. [89]	0.5 to 3.5 MPa [102].	Kraton G1643, 13.34 MPa.	1.15 MPa [96].	Stretchable [77], Viscoelastic properties [77].	3.2 MPa to 2.3 GPa [36]. Tunable stiffness, 250 to 1740 MPa [34]. Ostemer 322 – 1000 MPa, Ostemer 324 – 28 MPa, [29].
Feature size	151 μm pillar, 15μm membrane [15], [82]. 50 nm features [107].	100 nm [75].	7μm film, pillars of 4.4μm wide, 4.9μm high and a distance between pillars of 1.6μm [89].	8μm features, 50-100μm channels [87].	30 μm thick membrane (kraton G1645) [65]. 25μm thick membrane, 30μm feature height [93].	Film 5-28 μm. 20 μm channels [95].		200 μm cross sectional channel [30], layer 50 μm, 45 μm high channel [36].
Cost	$95 per kg at 20-kg kit of Sylgard 184 [65].	Cost: 20-40/kg. Comparable or higher than PDMS [108], [109].	Lower than PDMS [109].		9 times less expensive than PDMS [65]. $11 per kg for a 23kg bag of Kraton G1643 [65].		Low cost: $5/Kg [77].	Cost is twice as much as PDMS bulk price [36].
Chemical compatibility	Not resistant to organic solvents [109].	Resistant to organic solvents [109].	Resistant to organic solvents [109].	Excellent solvent compatibility.	Solvent resistant [105].			Resistant to organic solvents and acids [109].
Reusable	No [32].	No [32].	Yes [32].		Yes [64].			Yes [32].

Appendix B: Injection Moulding

PDMS is a widely used material, but not yet suitable for large scale production. The possibility of using it in injection moulding could greatly improve the scale of production, as well as the reproducibility of the products. This chapter discusses a separate project to the previous material characterisation. The goal of this project is to see whether PDMS can be produced on larger scale using the technique of injection moulding. This project is in collaboration with Besi, a developer of equipment and assembly processes for a wide range of applications, including electronics.

Design

Three moulds were designed to fit together. The PDMS was injected in between two of the three moulds to create the designed pattern. The end product was checked to compare to the design, to see if the production was successful.

The company provided the first mask, what will be indicated as the top mould. The accompanying two moulds were designed according to the pattern on the top mould, a six by six matrix of cells. Each cell is 1x1cm in size and has a different design in terms of thickness and shapes of pillars and holes. Our design consisted of two moulds, the wafer mould and the photoresist mould. The wafer mould is a wafer with etched holes made in six-fold. The other mould, the photoresist mould, is a wafer with a patterned layer of photoresist on top, also made six-fold. Each wafer was cut into a square shape. Injection moulding of PDMS (Sylgard-182) was performed with the top mould in combination with a dummy wafer, with the wafer mould and with the photoresist mould.

Figure 49 shows the schematic top view of the three moulds combined. The faded cells do not correspond to cells on our design and hence are marked as not relevant. Figure 48 shows the actual three moulds.

During the production of the photoresist mould by photolithography, the pillars of cells 2.5, 5.5 and 6.4 turned out to be too small and where partly washed off during the production process. Of the six photoresist moulds, half of cell 2.5 remains. Two cells of 5.5 and Two of 6.4. Production of the wafer mould by deep reactive ion etching was successful.

Injection Moulding

Injection moulding of an unprocessed wafer (dummy wafer) in combination with the top mould was successful (Figure 50a). The figure shows the dummy wafer and a layer of PDMS patterned by the top mould. Processing the wafer mould in combination with the top mould failed, as the wafer shattered under the pressure of the clamp. The etched holes possibly compromise the structural integrity of the wafer mould.

Processing the photoresist mould in the injection moulding machine also shattered the photoresist mould. Figure 50b and Figure 51 show the resulting shattered photoresist wafer mould with a layer of PDMS on top. The topside of the PDMS layer shows the pattern of the top mould. It appears the photoresist structures react with the PDMS, resulting in poor curing of the material. It is unclear what exactly causes this reaction.

Initial results show formation of micron scale structures appears possible using injection moulding for PDMS. Further investigation and testing is required to improve on the clamping procedure to prevent breaking the mould, to improve PDMS curing on the photoresist interface and to visualize the cross-section of the resulting structures to see whether they are properly formed. The resulting cross-section can be compared with Figure 52, which shows a schematic cross-section of the planned design for each cell.
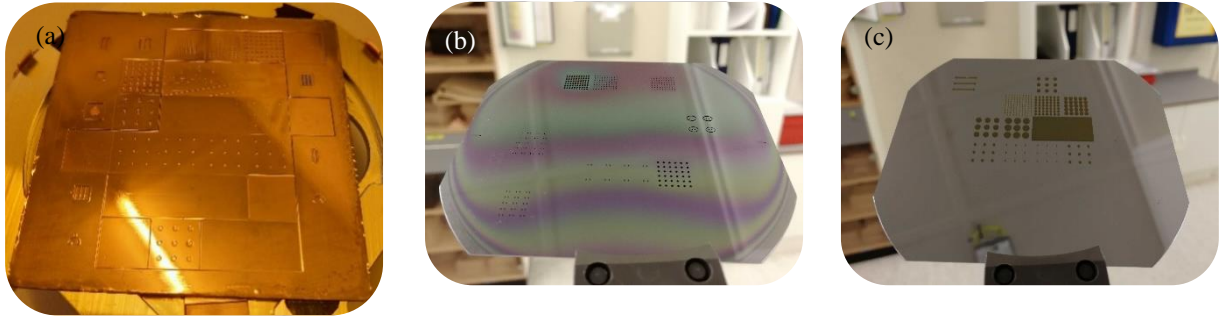
Figure 48: The three moulds used in the Besi experiment. (a) Besi top mould. (b) Wafer mould. (c) Photoresist mould.
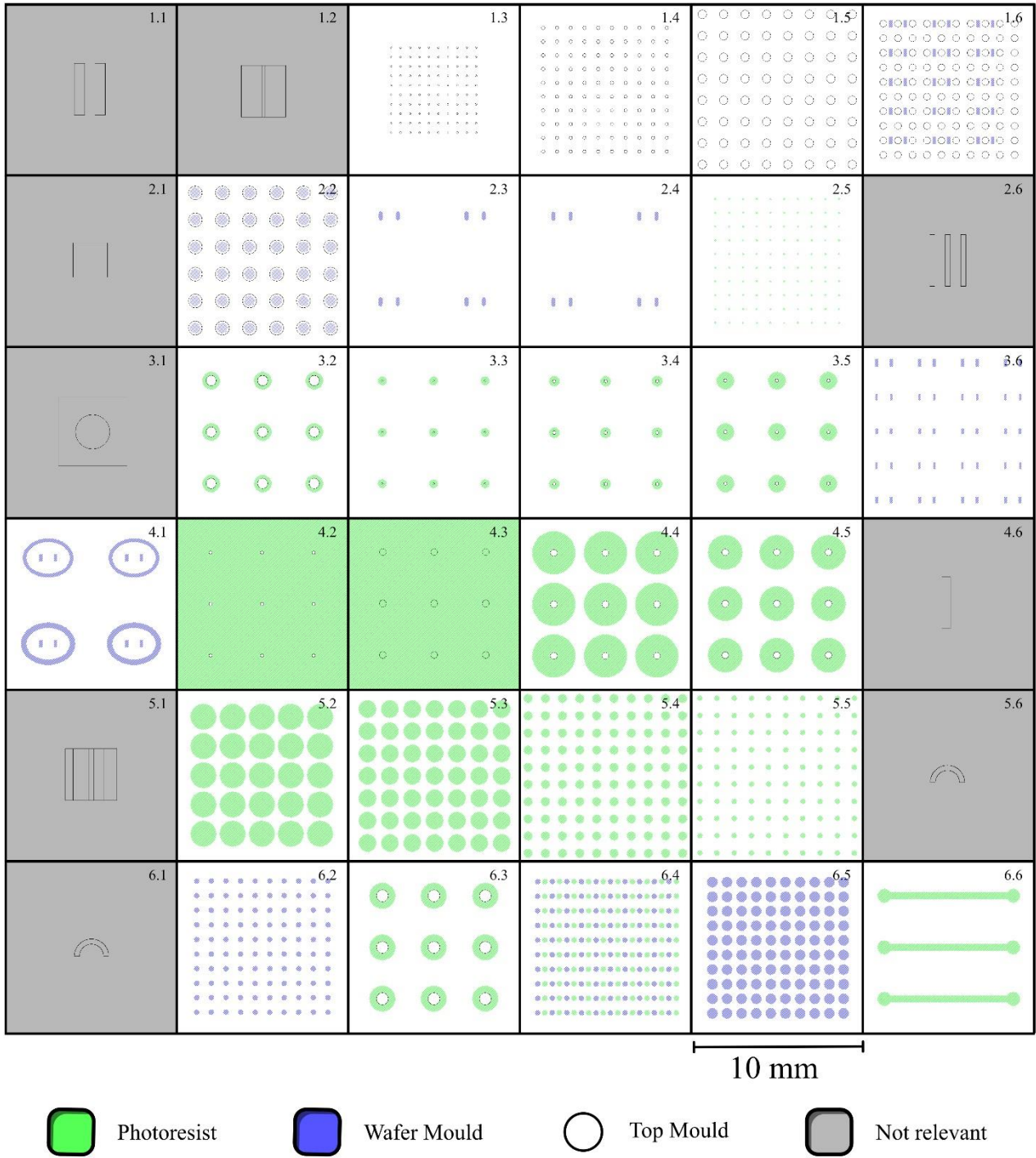

Figure 49: Schematic combined design of 3 moulds used in the injection moulding experiment. Top mould, photoresist mould and wafer mould. The wafer mould and photoresist mould are in actuality not used at the same time.
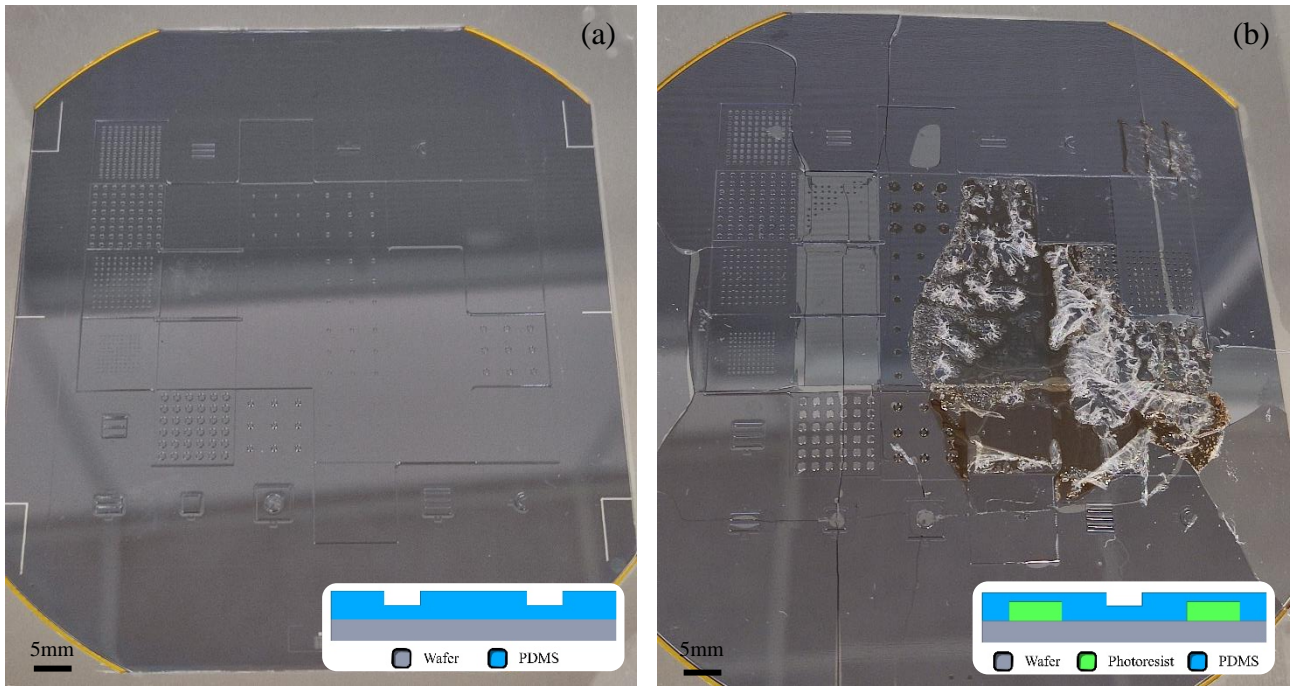
Figure 50: (a) Injection moulded PDMS on a flat silicon wafer visualizing the pattern of the top mould. (b) Injection moulded PDMS on the photoresist wafer mould, visualizing the pattern of the top mould. The wafer shattered under the pressure of the procedure. PDMS cured poorly on the photoresist structures. A schematic cross-section is included for both samples.
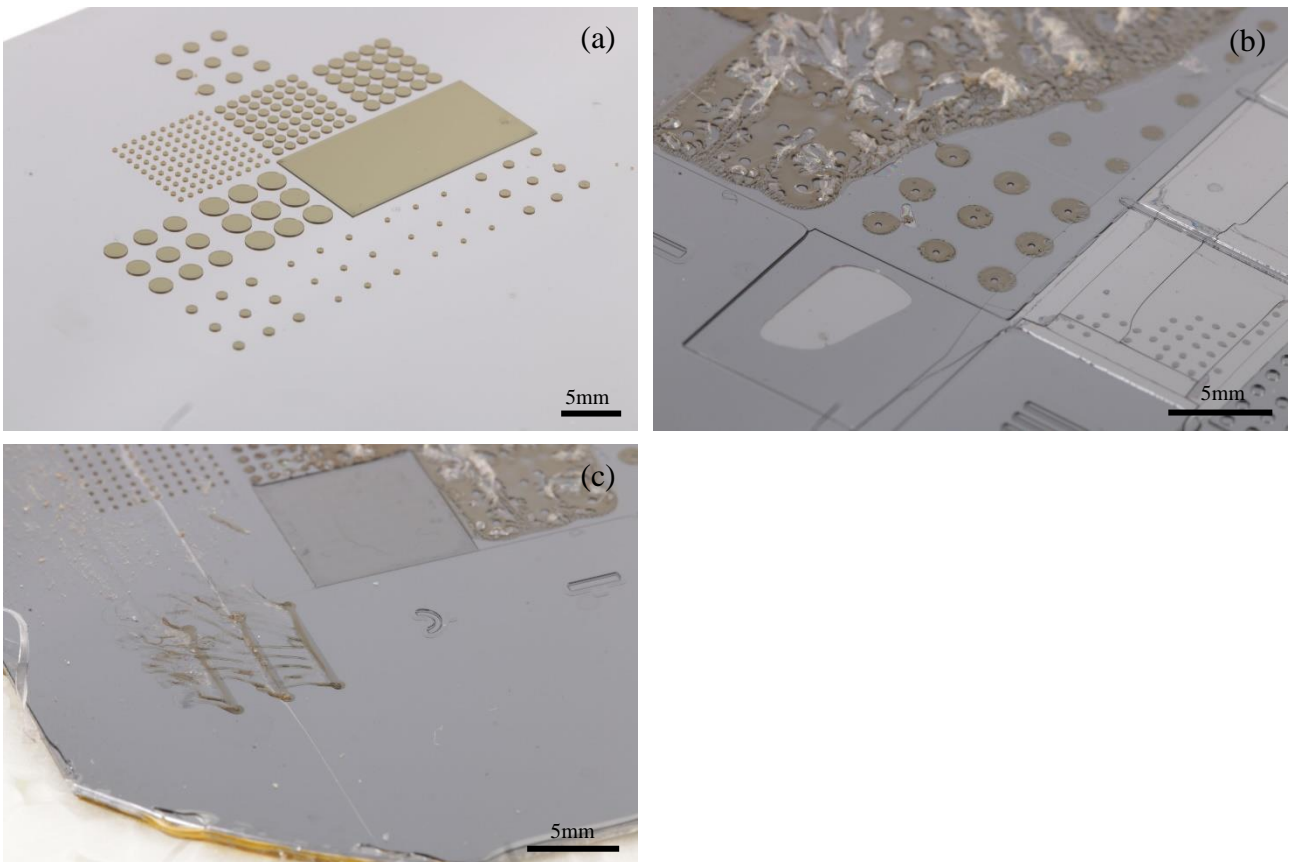
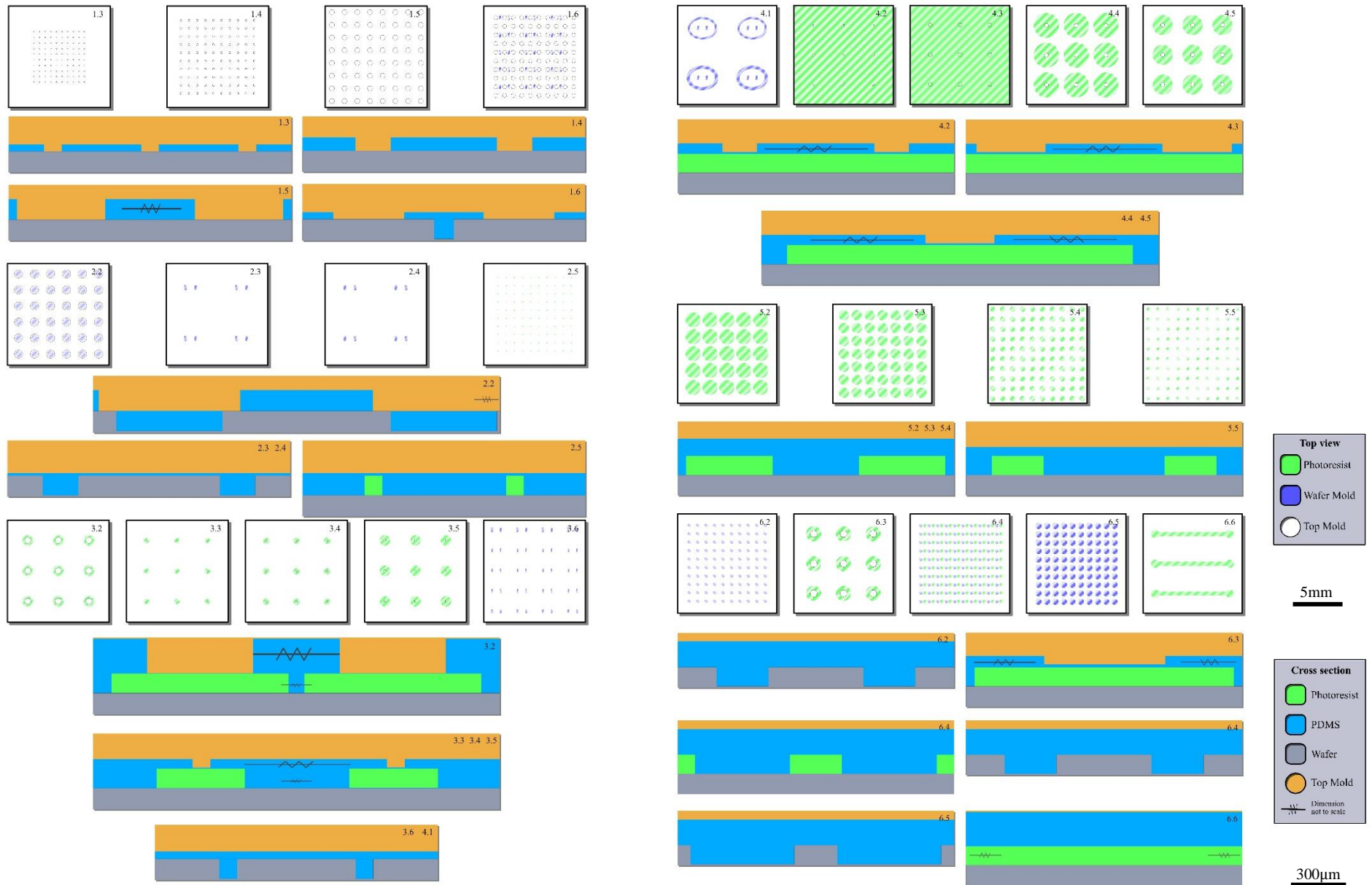*Figure 51: Close up images of (a) photoresist mould, (b and c) photoresist mould with a patterned layer of injection moulded PDMS.*

Figure 52: Illustration of combined mould design as presented in Figure 49 with the corresponding designed cross-section for each cell. The top view is to scale where the scale bar indicates 5 mm. The illustrated cross sections are to scale where the scale bar indicates 300 µm.

64

Appendix C: SEM of Aluminium on Polymer

Figure 53 shows the wrinkle pattern of a 250nm aluminium layer sputtered on top of a polymer layer as a result of material deformation during the sputtering process, explained in Section 2.1.3.2.
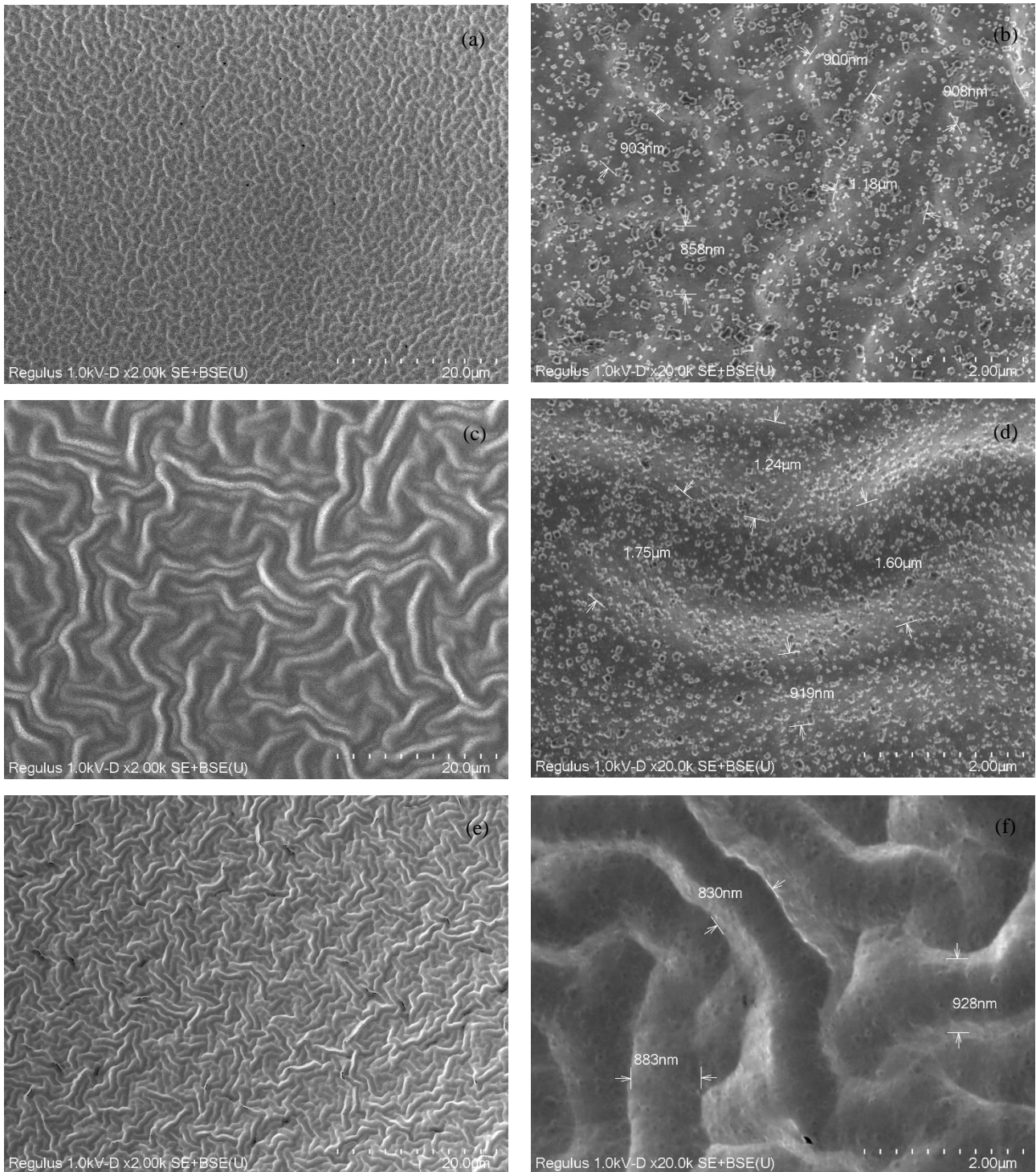
Figure 53: 250nm Aluminium sputtered on top of a polymer layer imaged by scanning electron microscopy at 2000x and 20.000x magnification. (a-b) 9.1μm layer Ostemer 324, (c-d) 6.7μm layer of Ostemer 220 and (e-f) 10.7μm layer PDMS+.

Appendix D: Biocompatibility Testing

Table 14 and Table 15 show an overview of both biocompatibility tests for round 1 and round 2 of testing as described in chapter4.1.1.3 and 4.1.1.4. Additional images are shown in figure x.

Table 14: Test 1: Conditioned Medium: overview of conditioned medium test round 1 and round 2.

		Round 1	**Round 2**
Step			
1	Disinfection of the samples in 70% ethanol	10 mins	10 mins
2	Rinsing of the samples in DI water	10 mins	10 mins
3	Plasma treatment on half of the samples	3 mins 20 watt	6 mins 20 watt
4	Preparation of endothelial cells		
5a	Material sample incubation in cell medium	1h, 24h	24-48h
5b	Cell seeding 96 well plate until confluency	48-72h	48-72h
6	Culture medium replaced with conditioned medium in 96 well plate	48h	48h
7	Imaged at	0h, 24h, 48h	24h, 48h

Table 15: Test 2: Direct Cell Seeding: overview of direct cell seeding test round 1 and round 2.

		Round 1	**Round 2**
Step			
1	Disinfection of the samples in 70% ethanol	10 mins	10 mins
2	Rinsing of the samples in DI water	10 mins	10 mins
3	Plasma treatment on half of the samples	3 mins 20 watt	6 mins 20 watt
4	Preparation of endothelial cells		
5	Cell seeding on material surface	24h	48h
6	Culture medium replaced	-	Every 24h
7	Imaged at	1h, 24h	24h, 48h

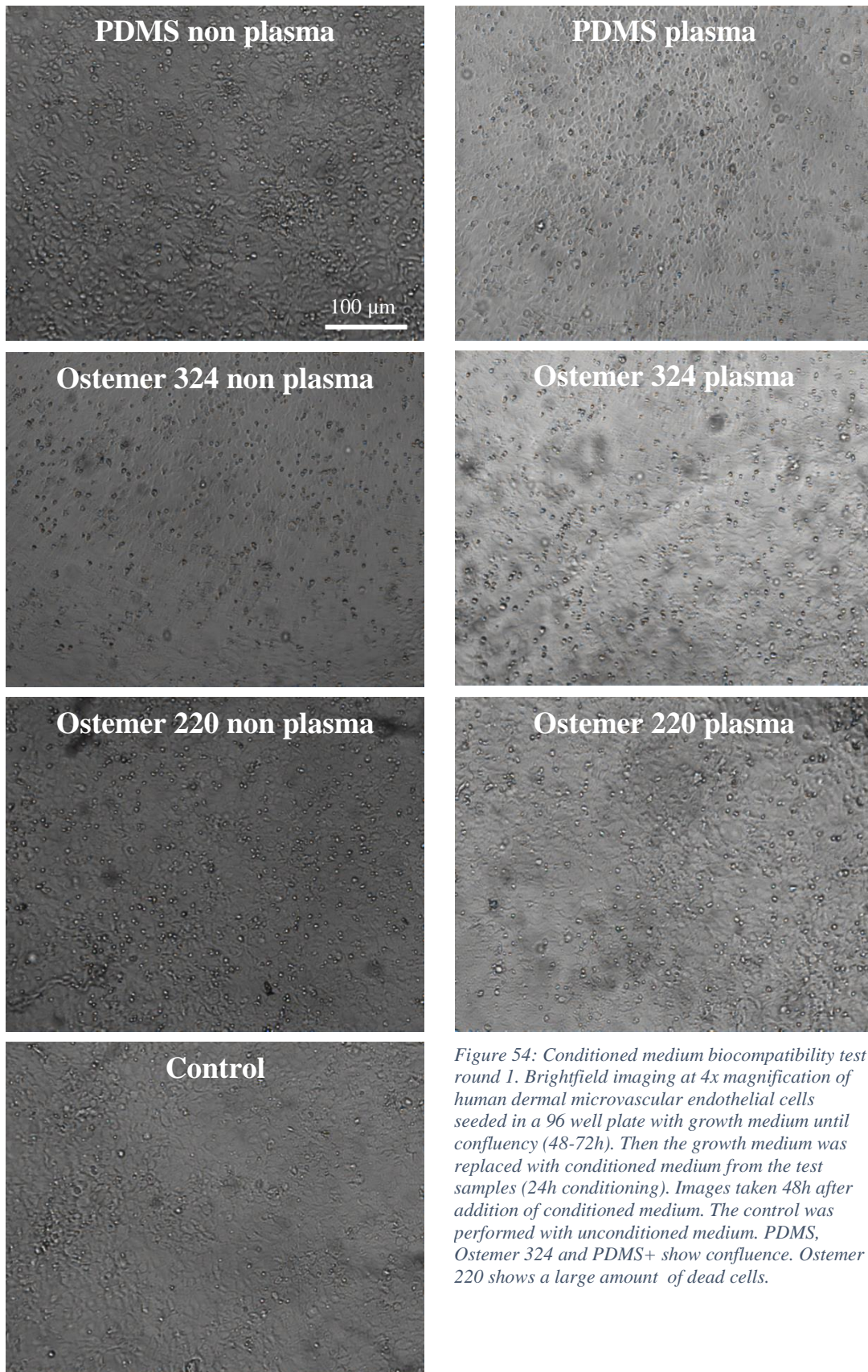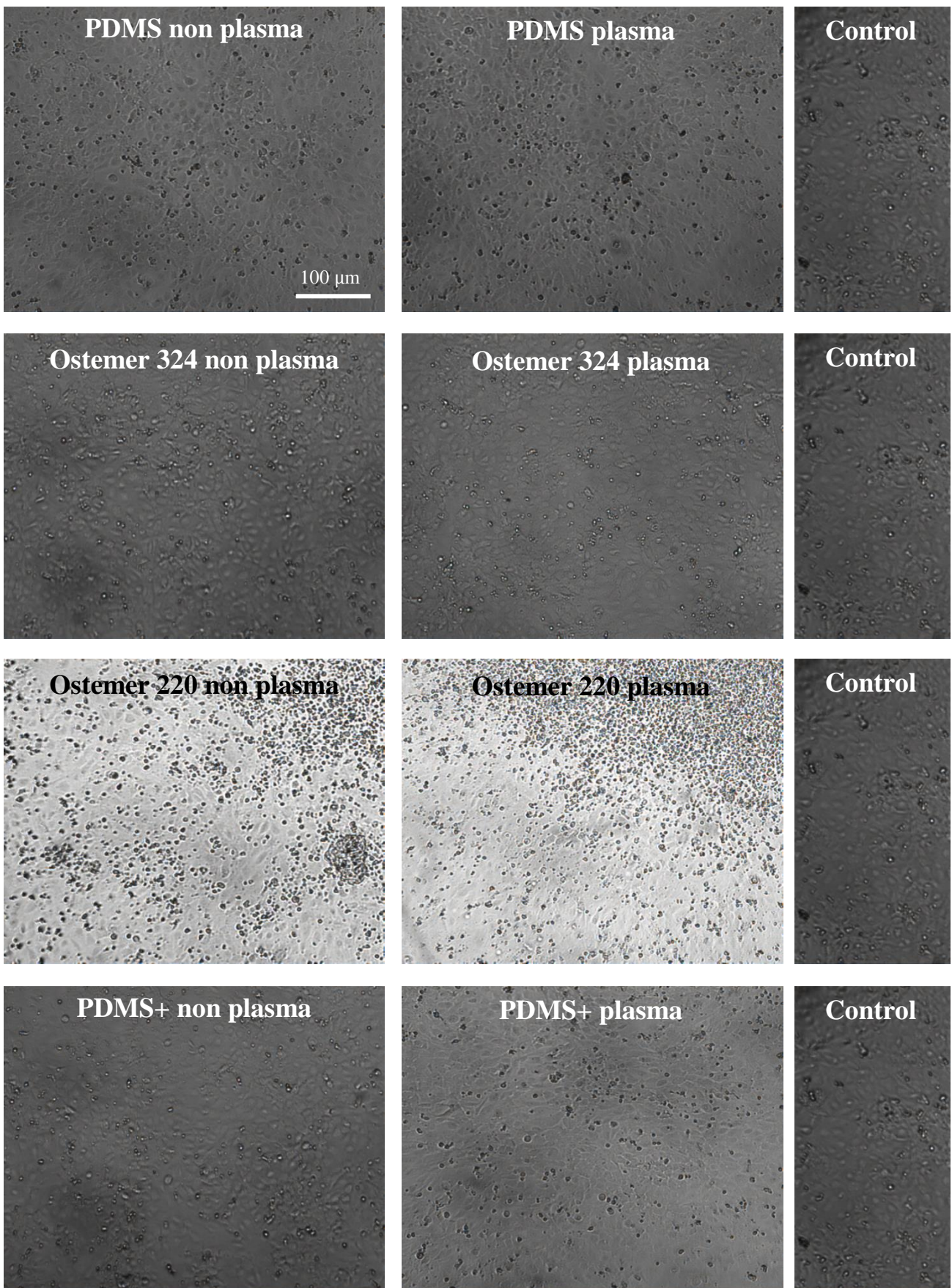# 1.1: Biocompatibility: Conditioned Medium

Figure 54: Conditioned medium biocompatibility test round 1. Brightfield imaging at 4x magnification of human dermal microvascular endothelial cells seeded in a 96 well plate with growth medium until confluency (48-72h). Then the growth medium was replaced with conditioned medium from the test samples (24h conditioning). Images taken 48h after addition of conditioned medium. The control was performed with unconditioned medium. PDMS, Ostemer 324 and PDMS+ show confluence. Ostemer 220 shows a large amount of dead cells.

1.2: Biocompatibility: Direct Cell Seeding (at 24h)
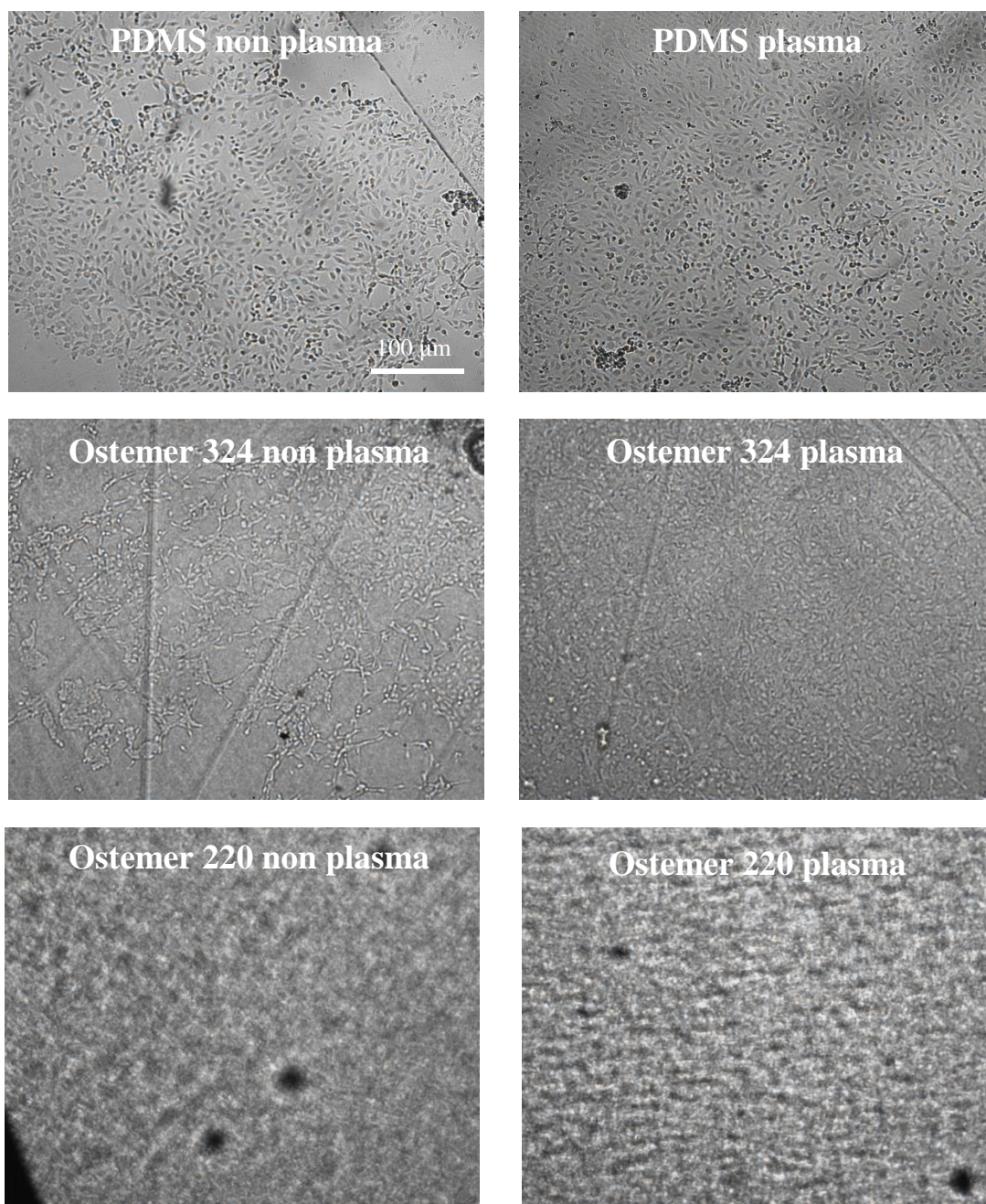
Figure 55: Round 1 of testing direct cell seeding on three materials. The sample for Ostemer 220 could not be imaged due to the thickness of the material. PDMS and Ostemer 324 show cell confluence.

2.1: Biocompatibility: Conditioned medium (at 48h)

Figure 56: Conditioned medium biocompatibility test round 2. Brightfield imaging at 4x magnification of human dermal microvascular endothelial cells seeded in a 96 well plate with growth medium until confluency (48-72h). Then the growth medium was replaced with conditioned medium from the test samples. Images taken 48h after addition of conditioned medium. The control was performed with unconditioned medium. PDMS, Ostemer 324 and PDMS+ show confluence. Ostemer 220 shows a large amount of dead cells.

2.2: Biocompatibility: Direct Cell Seeding (at 24h)
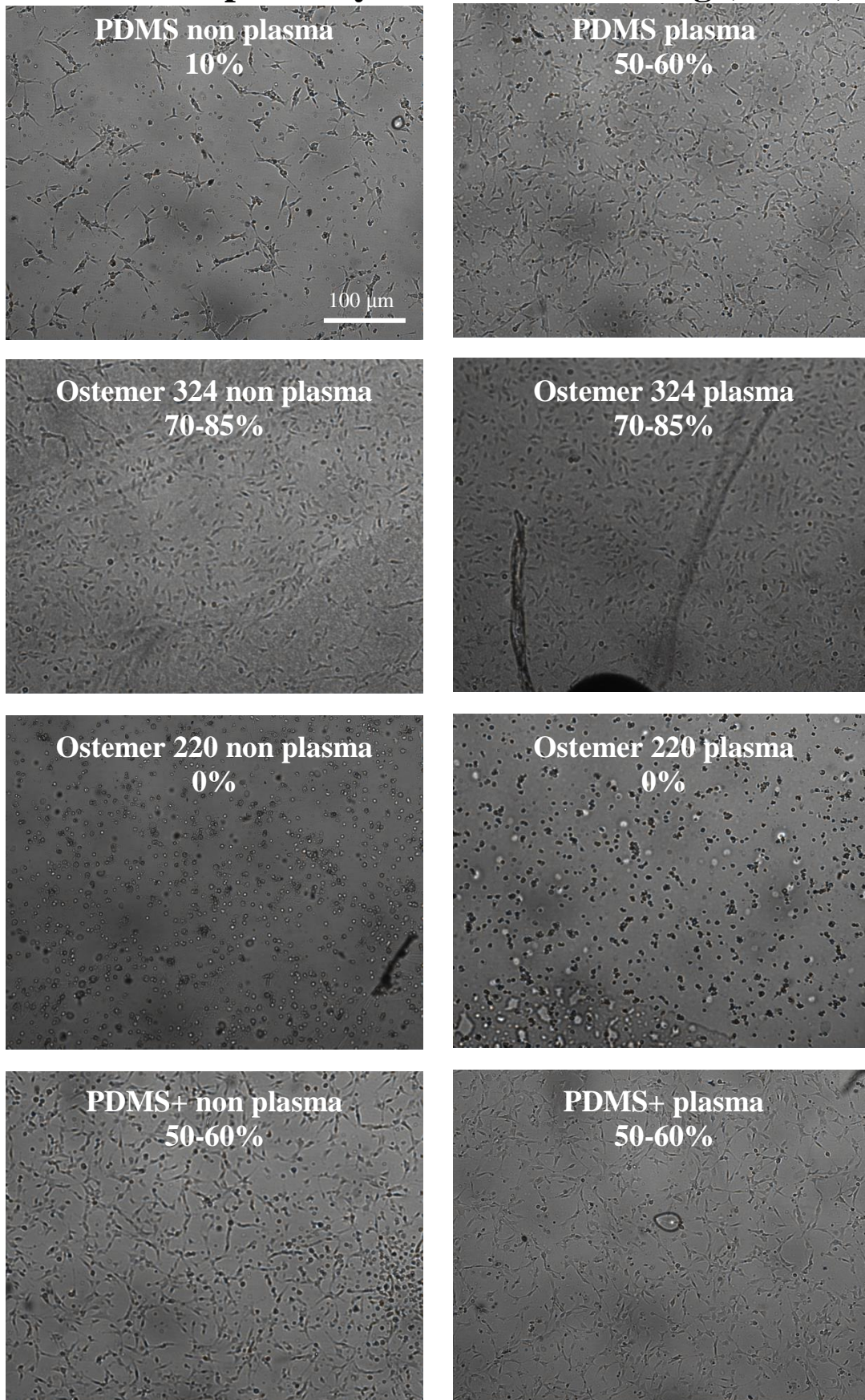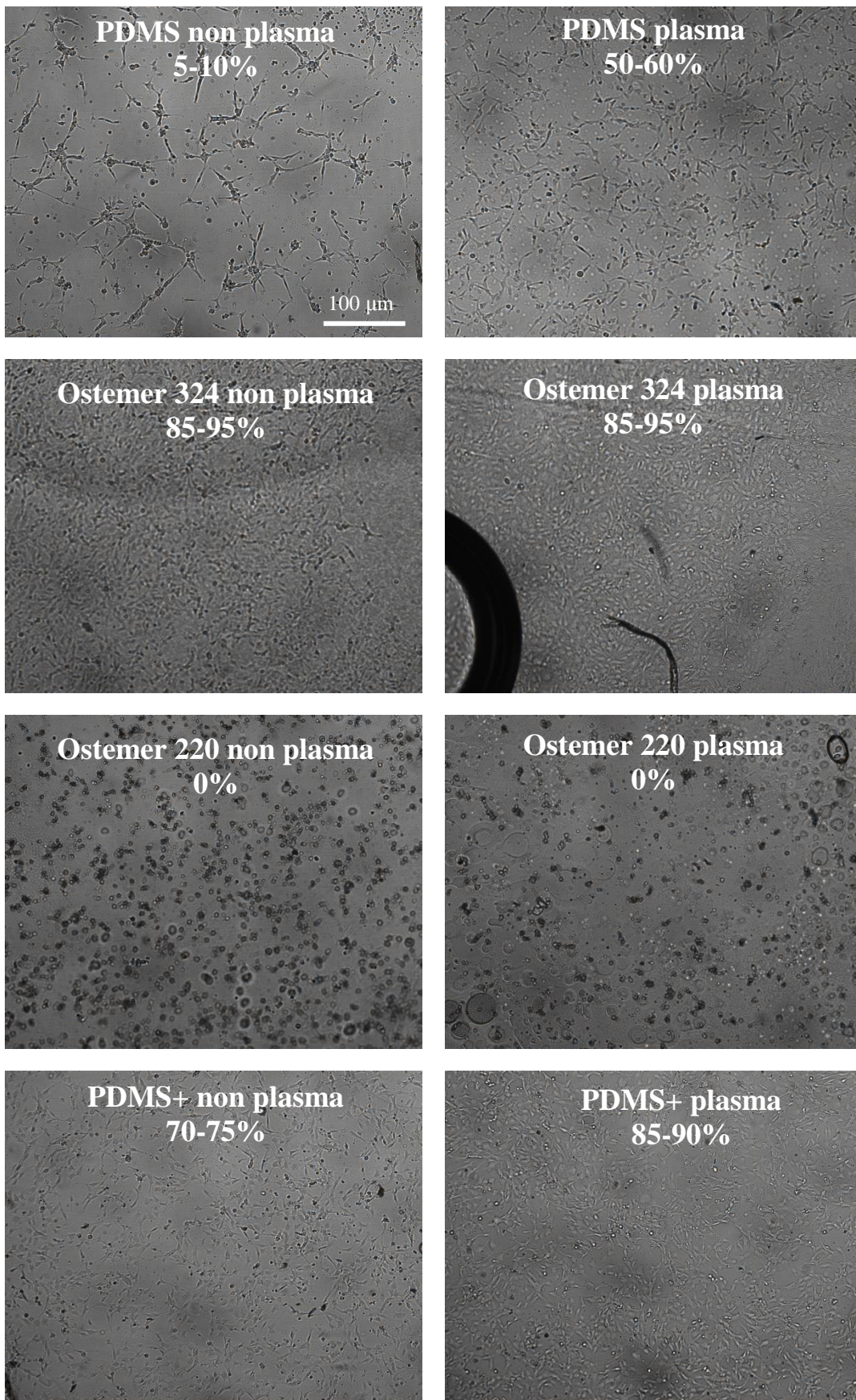

Figure 57 Brightfield imaging at 4x magnification of the second round of testing human dermal microvascular endothelial cells seeded directly on polymer membranes of PDMS, Ostemer 324, Ostemer 220 and PDMS+, 24 hours after seeding. Confluence indicated in percentage.

2.2: Biocompatibility: Direct Cell Seeding (at 48h)

Figure 58: Brightfield imaging at 4x magnification of the second round of testing human dermal microvascular endothelial cells seeded directly on polymer membranes of PDMS, Ostemer 324, Ostemer 220 and PDMS+, 48 hours after seeding. Confluence indicated in percentage.

Appendix E: Selection Area Absorption Data

Figure 59 shows the rectangular selection from each averaged stack of images from which the column average intensity profile was determined as shown in 4.2.2.
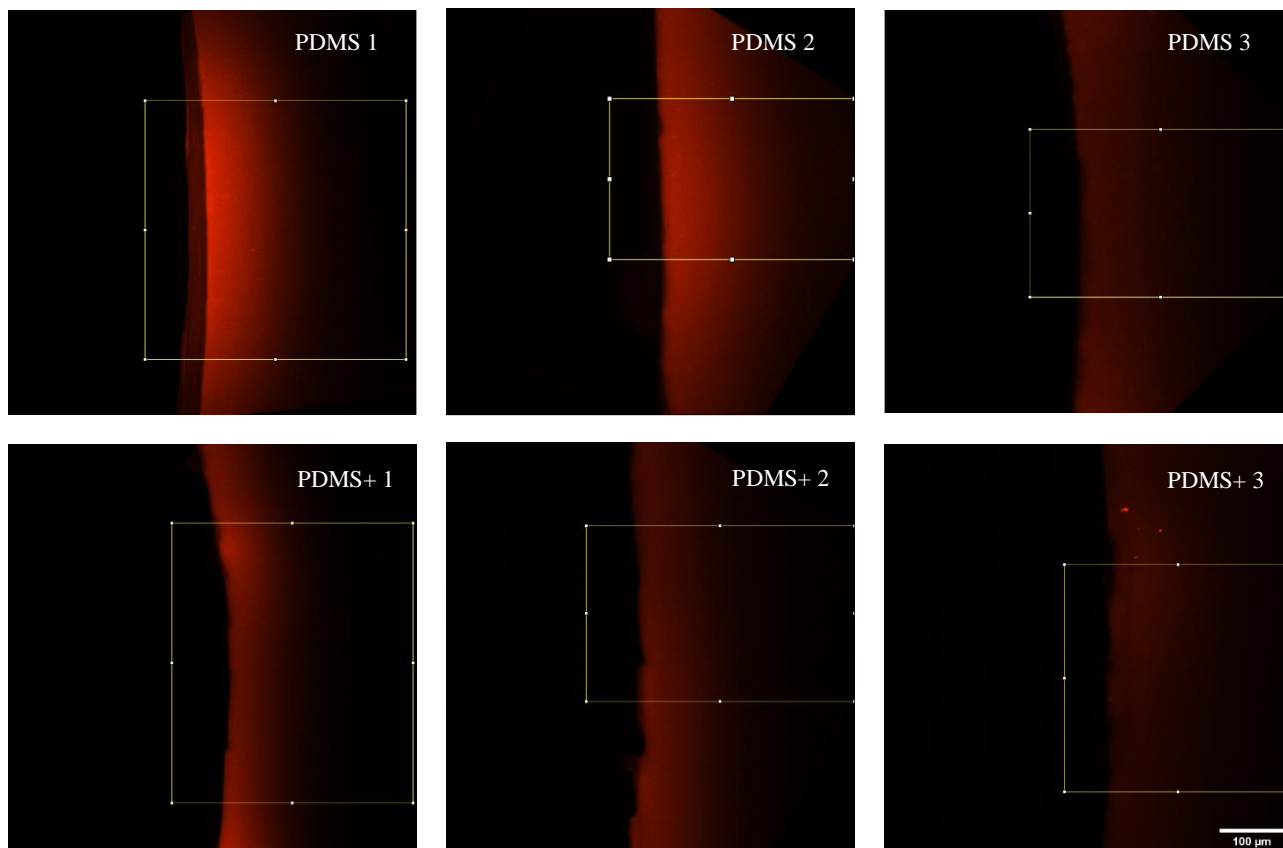

Figure 59: Z-axis projection of each image-stack of the averaged fluorescent intensity (grey value). Three measurements for PDMS and three for PDMS+. Including the rectangular selection from which the column average intensity profile was determined.